Transport-Theory-Equivalent Diffusion Coefficients for Node-Homogenized Neutron Diffusion Problems in CANDU Lattices

Amin Patel

A THESIS SUBMITTED IN PARTIAL
FULFILLMENT OF THE REQUIREMENTS
FOR THE DEGREE OF

Master of Science
in
The Faculty of Science

Modelling & Computational Science

UNIVERSITY OF ONTARIO INSTITUTE OF
TECHNOLOGY (UOIT)

Supervisor:	Dr. Eleodor Nichita, Faculty of Energy Systems and Nuclear Science
Examining Board:	Dr. Lixuan Lu, Dr. Anthony Waker
External Examiner:	Dr. Benjamin Rouben

Abstract

Calculation of the neutron flux in a nuclear reactor core is ideally performed by solving the neutron transport equation for a detailed-geometry model using several tens of energy groups. However, performing such detailed calculations for an entire core is prohibitively expensive from a computational perspective. Full-core neutronic calculations for CANDU reactors are therefore performed customarily using two-energy-group diffusion theory (no angular dependence) for a node-homogenized reactor model. The work presented here is concerned with reducing the loss in accuracy entailed when going from Transport to Diffusion. To this end a new method of calculating the diffusion coefficient was developed, based on equating the neutron balance equation expressed by the transport equation with the neutron balance equation expressed by the diffusion equation. The technique is tested on a simple twelve-node model and is shown to produce transport-like accuracy without the associated computational effort.

Keywords: Applied Reactor Physics, Transport Theory, Diffusion Theory, Diffusion Coefficients, CANDU, Natural Uranium, Nuclear Reactors, PHWR

Dedication

To my brother Faisal (1978-1996), who wanted to be a doctor and work for NASA

You aimed for the celestial bodies
I got entangled with these neutrons
These resonances can make one forget
But that's alright you know
I hear they got fancy neutron stars up there.

Acknowledgements

I express appreciation towards my thesis supervisor, Dr. Eleodor Nichita, for his patience, and willingness to work on refining the original ideas that were put forth during the early stages of this research. He has the “knack”, a beautiful mind, if I may.

I would like to thank my fellow colleague Fawaz Ali for his friendship and support; it was a long journey, but graduate school was an experience in the truest sense. Wish you the best in all of your future endeavours. To Dr. Buono, my professors and fellow graduate school colleagues: This would not have happened without your mentoring and help.

I shall always cherish the conversations I had with Dr. Brian Ikeda during those long and excruciating nights of research work; I would drop by his office and see the idiom “burning the midnight oil” put into practice. It was always comforting to have talked with Brian during those strange moments of scientific epiphany.

Special thanks to Yolande Akl, Raducu Gheorghe and all the wonderful folks at the Canadian Nuclear Safety Commission (CNSC) who provided me with a rare and wonderful opportunity to get an appreciation for the “big picture”.

One’s research is always an infinitesimal drop in the ocean of knowledge. This thesis is dedicated to my family.

> *For, He it is who has made you inherit the earth, and has raised some of you by degrees…so that He might try you by means of what He has bestowed upon you….He is indeed much-forgiving, a dispenser of grace. (6:165 سُوْرَةُ الأَنعَام)*

Table of Contents

Page

List of Figures and Tables

Figures

Tables

List of Acronyms

CANDU	CANada Deuterium Uranium
PHWR	Pressurized Heavy Water Reactor
CP	Collision Probabilities
MCFD	Mesh Centered Finite Differences

Nomenclature

Density	n	Neutrons per unit volume
Flux	$\Phi = nv$	Neutrons per unit of surface area and time
Macroscopic cross-section	Σ	1/cm
Mean Free Path	$1/\Sigma$	cm
k-effective	k	

Thesis Roadmap

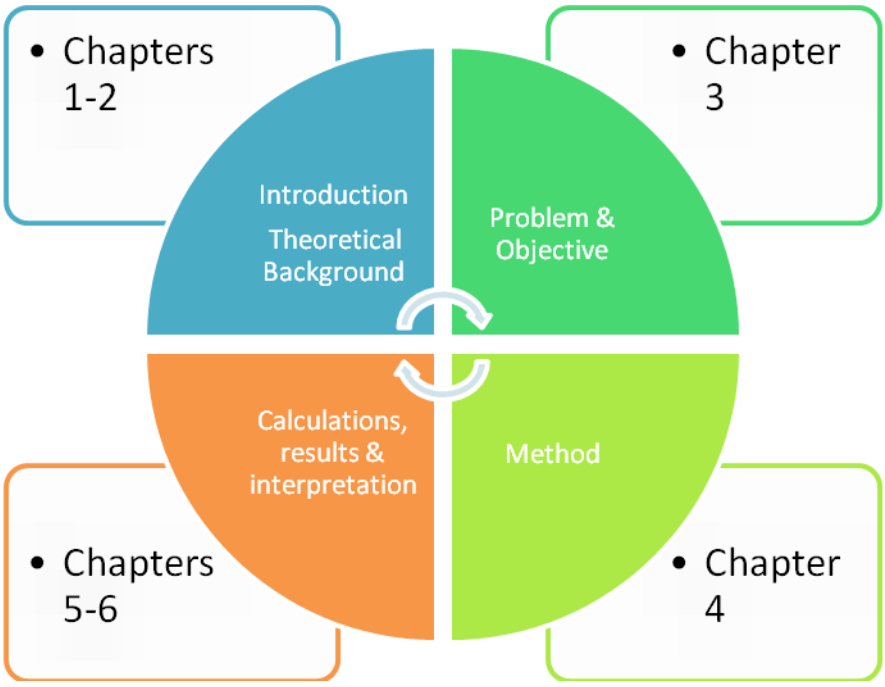

1.0 INTRODUCTION

"The movement of neutrons can be treated as a transport process"

CANDU reactors consist of a horizontal, non-pressurized, calandria vessel which contains the heavy-water moderator. The calandria is penetrated axially by fuel channels consisting of two concentric tubes separated by a gas gap: an inner tube called the pressure tube, and an outer tube called the calandria tube. The pressure tubes hold the fuel bundles, which are cooled by the flow of coolant at high temperature and pressure. The coolant flows in opposite directions in adjacent channels. For a CANDU 6 reactor, there are 380 fuel channels, each holding twelve 37-element fuel bundles, approximately 50-cm long each. The distance between channels (lattice pitch) is 28.575 cm.

The heat generation rate is directly determined by the neutron flux. Calculation of the (angle-dependent) neutron flux in the core is ideally performed by solving the neutron transport equation (linear Boltzmann equation) for a detailed-geometry model using several tens of energy groups. However, performing such detailed calculations for an entire core is prohibitively expensive from a computational perspective. Full-core neutronic calculations for CANDU reactors are therefore performed customarily using two-energy-group diffusion theory (no angular dependence) for a node-homogenized reactor model. A node consists usually of a parallelepiped one lattice pitch by one lattice pitch (one lattice cell) by one bundle length. Such a two-group node-homogenized model represents the last step in a succession of approximations (in decreasing order of accuracy):

1. many-energy-group heterogeneous transport
2. two-energy-group heterogeneous transport
3. two-energy-group node-homogenized transport
4. two-energy-group node-homogenized diffusion.

Numerical calculations reveal that the largest error is incurred when going from approximation 3 to approximation 4. The work presented here is concerned with reducing the loss in accuracy entailed by going from approximation 3 to approximation 4 by appropriately adjusting the values of the diffusion coefficients. To that end a new method of calculating the diffusion coefficient was developed, based on equating the neutron balance equation expressed by the transport equation with the neutron balance equation expressed by the diffusion equation.

The technique is tested on a simple twelve-node model and is shown to produce transport-like accuracy without the associated computational overhead. While the emphasis is on reducing the numerical discrepancy when moving from approximation 3 to approximation 4, the difference between approximation 4 and approximation 1 has also been included (Chapter 5-6) for completeness.

The scope of computations (Figure 1.1, adapted from [1]) is restricted to steady state problems (postulating constant neutron distribution) and is sufficient to establish the efficacy of the proposed method. Non-steady state problems are normally reserved for post-accident design scenarios and fuel management is a distinct research area of its own.

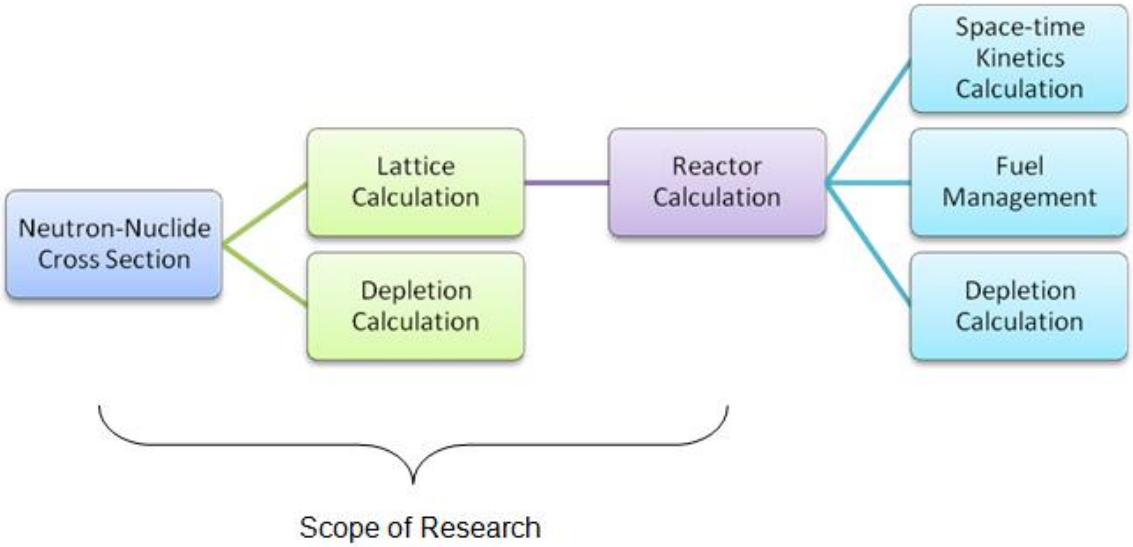

Figure 1.1 – Problem scope

As is standard practice with multi-parameter averaging methods, fine representation of neutron energy serves as the starting point, which is then replaced by a rather coarse energy representation of neutron density. Experience shows that with care (and competence!), averaging calculations can be sufficient for reactor design. Nonetheless, with increase in the physical heterogeneity of cores, reducing gaps between successive transport approximations has become imperative. This work represents a much needed step in this direction, lest design and regulatory demands outpace modeling capabilities.

In terms of “other possibilities”, highly detailed transport-theory-based full-reactor-core calculations are beginning to be attempted using deterministic codes such as UNIC from Argonne National Laboratory in the US and some Monte Carlo codes, such as MCNP, developed at Los Alamos National Laboratory, also in the US. To be applicable to full-core calculations, these codes need to be run on large parallel architectures, nearing 1E6 processors and the wall-clock time for such

calculations is still of the order of days to weeks, making them impractical for day-to-day design and analysis tasks.

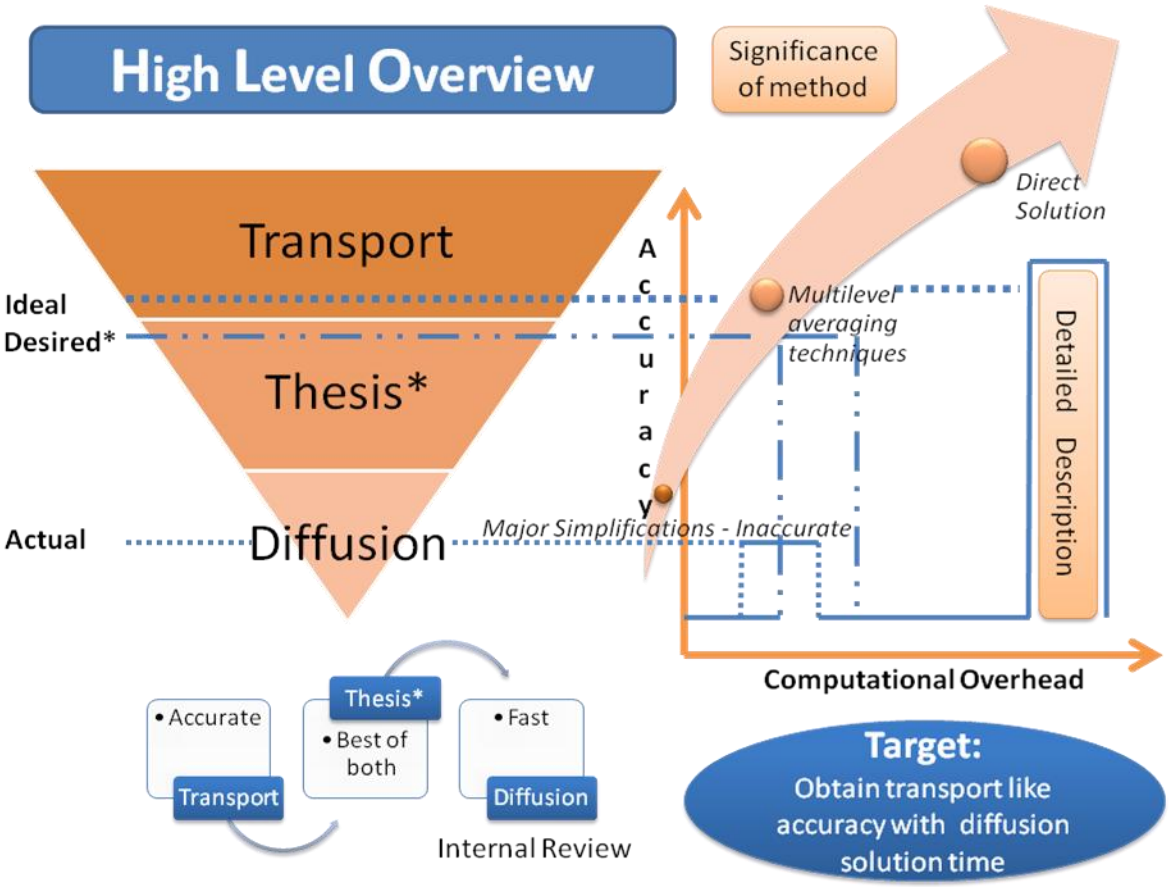

Figure 1.2 – Research Premise

The premise of this research (Figure 1.2) is that if computational gains can be made by improving methods without using parallelization and expensive computer architectures then perhaps deterministic methods (such as multi-parameter-averaging techniques) represent a rewarding area of research.

2.0 THEORETICAL BACKGROUND

In this chapter we present the theoretical aspects of neutron transport and diffusion. We start (in Section 1) by presenting the derivation of the differential and integral forms of the transport [linear Boltzmann] equation. The differential form shall be converted to the integral form, the two being equivalent from a mathematical point of view.

Analytical solutions to the steady-state continuous-energy differential and integral can be obtained under highly restrictive conditions but are of little use for practical applications. Instead, one can use numerical methods.

The discretization of the energy variable leads to the multigroup approximation (derived in Section 2.1.3). After presenting the multigroup energy treatment, the reader is then introduced to the spatial and angular discretization of the transport equation. Given the cost of using direct and detailed transport solutions, the practice of using multi-parameter averaging techniques (i.e. energy condensation and homogenization) is then formally introduced to the reader. For completeness a brief point on the alternative “probabilistic” Monte Carlo approach is made.

With requisite theoretical background having been covered in the transport domain, the next stop for the reader shall be the diffusion equation. By then this brief coverage of transport and its approximation, diffusion, shall be sufficient to embark on “the statement of the problem” (Chapter 3).

2.1 Continuous-energy differential transport equation

The integro-differential (or simply “differential”) form of the neutron transport equation is highly complicated as it involves both derivatives

and integrals of the flux. The starting point of the transport equation [1] is a balance relation for neutrons in a finite volume.

Note: Ω is a vector quantity

Defining control volume C; bounded by surface ∂C (Fig. 2.1)

Consider particles located in C traveling in direction Ω (within a $d^2\Omega$ interval), with a speed equal to V_n (within a dV_n interval).

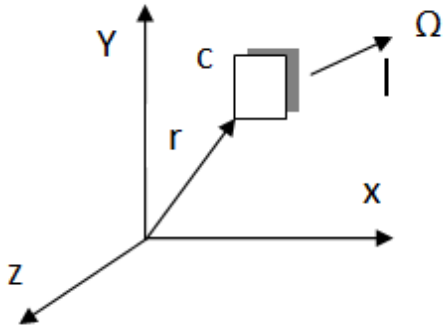

Figure 2.1 - Particle balance in a control volume

The number of particles in domain C with speeds around V_n and travel direction around omega.

$$\int_C \left[n(r,V_n,\Omega,t) dV_n d^2\Omega \right] d^3r \qquad 2.1$$

Defining the following:

Change in the number of particles in C during Δt

$$d^3\mathrm{A} = \int_C d^3r [n(r,V_n,\Omega,t+\Delta t) - n(r,V_n,\Omega,t)] dV_n d^2\Omega \qquad 2.2$$

Net number of particles streaming out of C during Δt obtained by integrating the outward particle current over ∂C

$$d^3\mathrm{B} = \int_{\partial C} d^2r(\Omega \cdot N)\phi(r,V_n,\Omega,t)dV_n d^2\Omega\Delta t \qquad 2.3$$

N is the unit vector, normal to ∂C, and pointing outside ∂C at point r.

Using divergence theorem to transform Eq. (2.3) into

$$d^3\mathrm{B} = \int_{C} d^3r\nabla \cdot \Omega\phi(r,V_n,\Omega,t)dV_n d^2\Omega\Delta t \qquad 2.4$$

Number of collisions in C during Δt is

$$d^3C = \int_{C} d^3r\left[\Sigma(r,V_n)[V_n n(r,V_n,\Omega,t)dV_n d^2\Omega\right]\Delta t \qquad 2.5$$

The coefficient capital sigma Σ is called the total macroscopic cross section and has units of cm^{-1}.

Definition of Macroscopic Cross Section (Σ)

$$\Sigma^x(r,V_n) = \sum_{i=1}^{n} N_i(r)\sigma_i^x(V_n)$$

N_i = number density for nuclide species i

n =number of different nuclides

N_i =atom (number) density of nuclide i

σ_i^x =microscopic cross section of reaction x for nuclide i

Assume macroscopic total cross section Σ is independent of Ω and t.

Number of new particles created in C during Δt is

$$d^3D = \int_{C} d^3r\left[Q(r,V_n,\Omega,t)dV_n d^2\Omega\right]\Delta t \qquad 2.6$$

Where $Q(r,V_n,\Omega,t)$ is the neutron source density.

The particle balance is written

$$d^3\mathrm{A} = -d^3\mathrm{B} - d^3C + d^3D \tag{2.7}$$

The integral over the control volume can be discarded from the four terms (by taking the limit C->0), leading to

$$\frac{n(r,V_n,\Omega,t+\Delta t) - n(r,V_n,\Omega,t)}{\Delta t} = -\nabla\cdot\Omega\phi(r,V_n,\Omega,t) - \Sigma(r,V_n)[V_n n(r,V_n,\Omega,t)] + Q(r,V_n,\Omega,t) \tag{2.8}$$

Taking the limit as $\Delta t \to 0$ and introducing the angular flux, $\phi(r,V_n,\Omega,t) = n(r,V_n,\Omega,t).V_n$ as the dependent variable, we obtain the differential form of the transport equation.

$$\frac{1}{V_n}\frac{\partial}{\partial t}(r,V_n,\Omega,t) + \nabla\cdot\Omega\phi(r,V_n,\Omega,t) + \Sigma(r,V_n)\phi(r,V_n,\Omega,t) = Q(r,V_n,\Omega,t) \tag{2.9}$$

Using the identity $\nabla\cdot wf(r) = w\cdot\nabla f(r)$, Eq (2.9) can be rewritten as

$$\frac{1}{V_n}\frac{\partial}{\partial t}(r,V_n,\Omega,t) + \Omega\cdot\nabla\phi(r,V_n,\Omega,t) + \Sigma(r,V_n)\phi(r,V_n,\Omega,t) = Q(r,V_n,\Omega,t) \tag{2.10}$$

In steady-state conditions, the equation reduces to

$$\Omega\cdot\nabla\phi(r,V_n,\Omega) + \Sigma(r,V_n)\phi(r,V_n,\Omega) = Q(r,V_n,\Omega) \tag{2.11}$$

Equation (2.10) is the basic formulation of the linear Boltzmann equation.

2.1.1 Continuous-energy integral form of the transport equation

The characteristic form of the transport equation

Expressing the streaming operator $\Omega.\cdot\nabla\phi$ over the characteristic, a straight line of direction Ω corresponding to the particle trajectory, yields what is referred to as the characteristic form of the transport equation.

At each time of its motion, the particle is assumed to be at distance s from a reference position r on its characteristic, so that its actual position is $r+s\Omega$ at time $t+s/V_n$.

The streaming operator can be transformed using the following derivation.

We write

$$\frac{d}{ds}=\frac{dx}{ds}\frac{\partial}{\partial x}+\frac{dy}{ds}\frac{\partial}{\partial y}+\frac{dz}{ds}\frac{\partial}{\partial z}+\frac{dt}{ds}\frac{\partial}{\partial t} \qquad 2.12$$

With

$$ds\Omega=dr=dxi+dyj+dzk \qquad 2.13$$

Taking the dot product of $ds\Omega=dr=dxi+dyj+dzk$ with **i**, we obtain $ds\Omega\cdot i=dx$. Similarly $ds\Omega\cdot j=dy$ and $ds\Omega\cdot k=dz$. After substitution into Eq. (2.12), we obtain

$$\frac{d}{ds}=(\Omega\cdot i)\frac{\partial}{\partial x}+(\Omega\cdot j)\frac{\partial}{\partial y}+(\Omega\cdot k)\frac{\partial}{\partial z}+\frac{1}{V_n}\frac{\partial}{\partial t}=\Omega\cdot\nabla+\frac{1}{V_n}\frac{\partial}{\partial t} \qquad 2.14$$

Substituting Eq. (2.14) into Eq. (2.10), we obtain the backward characteristic form of the transport equation:

$$\frac{\partial}{\partial s}\phi(r+s\Omega,V_n,\Omega,t+s/V_n)+\Sigma(r+s\Omega,V_n)\phi(r+s\Omega,V_n,\Omega,t+s/V_n) = Q(r+s\Omega,V_n,\Omega,t-s/V_n) \quad 2.15$$

Equation (2.15) can also be written in the forward form as

$$-\frac{\partial}{\partial s}\phi(r-s\Omega,V_n,\Omega,t-s/V_n)+\Sigma(r-s\Omega,V_n)\phi(r-s\Omega,V_n,\Omega,t-s/V_n) = Q(r-s\Omega,V_n,\Omega,t-s/V_n) \quad 2.16$$

The integral form of the transport equation

For a given value of the source density $Q(r,V_n,\Omega,t)$, integrating the angular flux along its characteristic gives the integral transport equation.

Introducing an integrating factor $e^{-\tau(s,V_n)}$ where the optical path (τ) is defined as a function of the macroscopic total cross section $\Sigma(r,V_n)$ using

$$\tau(s,V_n)=\int_0^s ds'\Sigma(r-s',V_n) \quad 2.17$$

We compute the following relation:

$$\frac{\partial}{\partial s}\left[e^{-\tau(s,V_n)}\right]\phi(r-s\Omega,V_n,\Omega,t-s/V_n) = e^{-\tau(s,V_n)}\left[\begin{array}{l}-\Sigma(r-s\Omega,V_n)\\ \times\phi(r-s\Omega,V_n,\Omega,t-s/V_n)+\frac{\partial}{\partial s}\phi(r-s\Omega,V_n,\Omega,t-s/V_n)\end{array}\right] \quad 2.18$$

Using the identity

$$\frac{d}{ds}\int_0^s ds' g(s') = g(s) \qquad 2.19$$

Substitution of Eq. (2.16) into Eq. (2.19) leads to

$$-\frac{\partial}{\partial s}\left[e^{-\tau(s,V_n)}\right]\phi(r - s\Omega, V_n, \Omega, t - s/V_n) = e^{-\tau(s,V_n)}Q(r - s\Omega, V_n, \Omega, t - s/V_n) \qquad 2.20$$

Equation (2.20) can be integrated between 0 and ∞, so that

$$-\int_0^\infty ds \frac{\partial}{\partial s}\left[e^{-\tau(s,V_n)}\right]\phi(r - s\Omega, V_n, \Omega, t - s/V_n) = \int_0^\infty ds e^{-\tau(s,V_n)}Q(r - s\Omega, V_n, \Omega, t - s/V_n) \qquad 2.21$$

or

$$\phi(r, V_n, \Omega, t) = \int_0^\infty ds e^{-\tau(s,V_n)}Q(r - s\Omega, V_n, \Omega, t - s/V_n) \qquad 2.22$$

Equation (2.22) is the integral form of the transport equation for the infinite-domain case.

A particle from source $Q(r', V_n, \Omega)$ will travel with an exponential attenuation factor in direction Ω and contribute to the flux at point r.

If the domain is finite, it is possible to integrate only over the s values corresponding to a value of r' inside the domain. In this case, the integral form of the transport equation is written

$$\phi(r,V_n,\Omega,t) = e^{-\tau(s,V_n)}\phi(r-b\Omega,V_n,\Omega,t-b/V_n) \quad 2.23$$
$$\int_0^b ds e^{-\tau(s,V_n)} Q(r-s\Omega,V_n,\Omega,t-s/V_n)$$

Where $\phi(r-b\Omega,V_n,\Omega,t-b/V_n)$ can be assimilated to a boundary flux.

The integral form of the transport equation is generally limited to isotropic sources in the laboratory frame, so that

$$Q(r,V_n,\Omega,t) = \frac{1}{4\pi} Q(r,V_n,t) \quad 2.24$$

2.1.2 Boundary conditions

Boundary ∂V surrounds domain V

We introduce $N(r_s)$, the outward normal at $r_s \in \partial V$. Solution of the transport equation in V requires the knowledge of the angular flux $\phi(r_s,V_n,\Omega,t)$ for $\Omega \cdot N(r_s) < 0$.

The incoming flux *j* is related to the outgoing flux via the albedo boundary condition. Written as

$$\phi(r_s,V_n,\Omega,t) = \beta\phi(r_s,V_n,\Omega',t) \text{ with } \Omega \cdot N(r_s) < 0 \quad 2.25$$

Ω' being the direction of the outgoing particle. For vacuum and reflective boundary conditions the albedo β is equal to zero and one, respectively.

Specular reflection is when

$$\Omega \cdot N(r_s) = -\Omega' \cdot N(r_s) \text{ and } (\Omega \times \Omega') \cdot N(r_s) = 0 \quad 2.26$$

A white boundary condition is a reflective boundary condition where particles striking the boundary turn back to V with an isotropic angular distribution.

$$\phi(r_s, V_n, \Omega, t) = \beta \frac{\int_{\Omega' \cdot N(r_s) > 0} d^2\Omega' [\Omega' \cdot N(r_s)] \phi(r_s, V_n, \Omega', t)}{\int_{\Omega' \cdot N(r_s) > 0} d^2\Omega' [\Omega' \cdot N(r_s)]} \quad \text{with } \Omega \cdot N(r_s) < 0 \tag{2.27}$$

Where β is the albedo.

When white boundary conditions are used, Eq (2.27) simplifies to

$$\phi(r_s, V_n, \Omega, t) = \frac{\beta}{\pi} \int_{\Omega' \cdot N(r_s) > 0} d^2\Omega' [\Omega' \cdot N(r_s)] \phi(r_s, V_n, \Omega', t) \quad \text{with } \Omega \cdot N(r_s) < 0 \tag{2.28}$$

In a periodic lattice where the flux on one boundary is equal to the flux on another parallel boundary we have the periodic boundary condition:

$$\phi(r_s, V_n, \Omega, t) = \phi(r_s + \Delta r, V_n, \Omega, t) \tag{2.29}$$

Where Δr is the lattice pitch.

A non-physical condition corresponding to the nonexistence of particles on ∂V is referred to as the zero-flux boundary condition.

2.1.3 Multigroup transport equation

The energy variable is discretized using what is known as a multigroup treatment. The maximum energy of neutrons for the problem of interest is denoted by E_0. A new variable u is then defined called the lethargy $u = \ln(E_0 / E)$. E_0 is called the reference energy and is normally taken as being above 10 MeV, which is a sufficiently large value to encompass all neutrons present in a nuclear reactor.

The lethargy is zero for the neutrons of energy E_0 and increases as neutrons slow down.

We divide the energy domain $0 \le E \le E_0$ into G groups W_g, so that

$Wg = \{u; u_{g-1} \le u < u_g\} = \{E; E_g < E < E_{g-1}\}; g = 1, G$ where $u_g = \ln(E_0 / E_g)$ and $u_0 = 0$. 2.30

Before proceeding, we will note that the angular flux is, in fact, a distribution with respect to neutron speed, lethargy or energy and hence:

$$\phi(u, r, \Omega)du = \phi(V_n, r, \Omega)dV_n = \phi(E, r, \Omega)dE \quad 2.31$$

The group values of the flux, cross section, differential cross section and source density are defined as

$$\phi_g(r, \Omega) = \int_{u_{g-1}}^{u_g} du \phi(r, u, \Omega) \quad 2.32$$

$$\phi_g(r) = \int_{u_{g-1}}^{u_g} du \phi(r, u) \quad 2.33$$

$$\left(\Sigma(r)\phi\ (r)\right)_g = \int_{u_{g-1}}^{u_g} du\Sigma(r,u)\phi(r,u) \qquad 2.34$$

$$\left(\Sigma_{s,l}(r)\phi\ (r)\right)_{g\leftarrow h} = \int_{u_{g-1}}^{u_g} du \int_{u_{h-1}}^{u_h} du'\Sigma_{s,l}(r,u\leftarrow u')\phi(r,u') \qquad 2.35$$

And

$$\left(Q(r,\Omega)\right)_g = \int_{u_{g-1}}^{u_g} duQ(r,u,\Omega) \qquad 2.36$$

The multigroup cross-section components are defined in such a way as to preserve the values of the reaction rates. We write

$$\Sigma_g(r) = \frac{1}{\phi_g(r)}\left(\Sigma(r)\phi(r)\right)_g \qquad 2.37$$

$$\Sigma_{s,l,g\leftarrow h}(r) = \frac{1}{\phi_h(r)}\left(\Sigma_{s,l}(r)\phi(r)\right)_{g\leftarrow h} \qquad 2.38$$

And

$$\nu\Sigma_{f,j,g}(r) = \frac{1}{\phi_g(r)}\nu\Sigma_{f,j}(r)\phi(r)_g \qquad 2.39$$

The transport equation for neutrons can be written in multigroup form, leading to a set of G-coupled integro-differential equations.

Multigroup steady-state transport equation

The multigroup and differential form of the steady-state transport equation in group g is written

$$\Omega\cdot\nabla\phi_g(r,\Omega) + \Sigma_g(r)\phi_g(r,\Omega) = Q_g(r,\Omega) \qquad 2.40$$

The characteristic form of Eq. (2.40) is

$$\frac{d}{ds}\phi_g(r+s\Omega,\Omega)+\Sigma_g(r+s\Omega)\phi_g(r+s\Omega,\Omega) = Q_g(r+s\Omega,\Omega) \quad 2.41$$

Integral infinite-domain:

$$\phi_g(r,\Omega)=\int_0^{\infty} ds e^{-\tau_g(s)} Q_g(r-s\Omega,\Omega) \quad 2.42$$

Finite domain:

$$\phi_g(r,\Omega)=e^{-\tau g(b)}\phi_g(r-b\Omega,\Omega)+\int_0^{s} ds e^{-\tau_g(s)} Q_g(r-s\Omega,\Omega) \quad 2.43$$

Optical path in group g is

$$\tau_g(s)=\int_0^{s} ds' \Sigma_g(r-s'\Omega) \quad 2.44$$

We have obtained an eigenproblem taking the form of a set of coupled differential equations.

2.2 Numerical methods for neutron transport equation

Monte Carlo

Monte Carlo is a stochastic "probabilistic" method that relies on the use of random number generators. The life of a large number of neutrons is simulated from emission until death. While uncertainties cannot be reduced to zero, it has the advantage of easy implementation wherein the Boltzmann equation is not represented explicitly, and no multilevel averaging technique is required when representing the geometry and energy distribution within a reactor core.

The number of simulations required for a "run" can be quite high at times, and as such it necessitates the parallelization of computations via additional processing muscle.

The Collision Probability Method

Probabilistic Monte Carlo methods are extremely expensive, and time consuming for practical applications. The Collision Probability method is very robust and in wide use for solving the transport equation. The integral transport equation is the starting point for the Collision Probability method. The Collision Probabilities method offers the geometrical advantages of Monte Carlo, with the efficiency of deterministic methods.

Assuming isotropic sources, spatial discretization of the integral transport equation in multigroup form leads to the Collision Probability method. When dealing with unstructured meshes this method is advantageous. In the case of an infinite lattice of identical cells, Collision Probabilities can be defined over an infinite domain. Collision Probabilities can also be defined over a finite domain, requiring that boundary conditions be added to close the domain.

Integrating Eq. (2.42) over the solid angles to obtain integrated flux $\phi_g(r)$:

$$\phi_g(r) = \int_{4\pi} d^2\Omega \phi_g(r,\Omega) = \frac{1}{4\pi} \int_{4\pi} d^2\Omega \int_0^\infty ds e^{-\tau_g(s)} Q_g(r - s\Omega) \qquad 2.45$$

The optical path $\tau_g(s)$ given by Eq (2.44).

Introducing the change of variable $r' = r - s\Omega$ with $d^3r' = s^2 d^2\Omega ds$. We obtain

$$\phi_g(r) = \frac{1}{4\pi}\int_{\infty} d^3r' \frac{e^{-\tau_g(s)}}{s^2} Q_g(r') \qquad 2.46$$

With $s = |r - r'|$.

When dealing with identical cells (or an infinite lattice) repeating themselves with periodic boundary conditions or in a symmetric fashion, the above form of Transport is used.

Let us now partition the unit cell into regions V_i.

Symbol V_i^{∞} is used to represent the infinite set of regions V_i belonging to all the cells in the lattice.

Suppose the sources of secondary neutrons are uniform and equal to $Q_{i,g}$ on each region V_i.

After multiplication by $\Sigma_g(r)$ and integration over each region V_i, Eq. (2.46) can be written

$$\int_{V_j} d^3r \Sigma_g(r)\phi_g(r) = \frac{1}{4\pi}\int_{V_j} d^3r \Sigma_g(r)\sum_i Q_{i,g}\int_{V_i\infty} d^3r' \frac{e^{-\tau_g(s)}}{s^2} \qquad 2.47$$

If q is exclusively a scattering and fission source (both proportional to the flux).

$$Q_{i,g} = \sum_h \Sigma_{s0,i,g\leftarrow h}\phi_{i,h} + \frac{1}{k_{eff}} Q_{i,g}^{fiss} \qquad 2.48$$

With the fission source in Eq. (2.48) defined as

$$Q_{i,g}^{fiss} = \chi_g \sum_h \nu\Sigma_{f,j,h}\phi_{i,h} \qquad 2.49$$

Where χ_g is the fission spectrum and $\Sigma_{f,j,h}$ is the macroscopic fission cross section of nuclide j for neutrons in group h.

The equations become homogeneous and the problem becomes an eigenvalue problem:

$$\int_{V_j} d^3r\Sigma_g(r)\phi_g(r) = \frac{1}{4\pi}\int_{V_j} d^3r\Sigma_g(r)\sum_i\left[\sum_h \Sigma_{s0,i,g\leftarrow h}\phi_{i,h} + \frac{1}{k_{eff}}\chi_g\sum_h \nu\Sigma_{f,j,h}\phi_{i,h}\right]\bullet$$

$$\int_{V_i\infty} d^3r' \frac{e^{-\tau_g(s)}}{s^2}$$

Equation (2.47) can be simplified to

$$V_j\Sigma_{j,g}\phi_{j,g} = \sum_i Q_{i,g}V_iP_{ij,g} \qquad 2.50$$

Where

$$\phi_{j,g} = \frac{1}{V_j}\int_{V_j} d^3r\phi_g(r) \qquad 2.51$$

$$\Sigma_{j,g} = \frac{1}{V_j\phi_{j,g}}\int_{V_j} d^3r\Sigma_g(r)\phi_g(r) \qquad 2.52$$

And

$$p_{ij,g} = \frac{1}{4\pi V_i} \int_{V_i^{\infty}} d^3r' \int_{V_j} d^3r \Sigma_g(r) \frac{e^{-\tau_g(s)}}{s^2} \qquad 2.53$$

When neutrons are born isotropically and uniformly in any of the regions V_i of a lattice, undergoing their first collision in region V_j of a unit cell, the collision probability is $p_{ij,g}$.

Reduced CPs can be defined from Eq (2.53), if the total cross section $\Sigma_g(r)$ is constant and equal to $\Sigma_{j,g}$ in region V_j:

$$p_{ij,g} = \frac{P_{ij,g}}{\Sigma_{j,g}} = \frac{1}{4\pi V_i} \int_{V_i^{\infty}} d^3r' \int_{V_j} d^3r \frac{e^{-\tau_g(s)}}{s^2} \qquad 2.54$$

Reduced CPs generally remain finite in the limit where $\Sigma_{j,g}$ tends to be zero. This ensures the correct behaviour of the collision probability theory in cases where some regions of the lattice are voided.

Reciprocity and conservation properties:

$$p_{ij,g} V_i = p_{ji,g} V_j \qquad 2.55$$

And

$$\sum_j p_{ij,g} \Sigma_{j,g} = 1; \forall i \qquad 2.56$$

Using the reciprocity property, Eq. (2.50) can be further simplified to

$$\phi_{i,g} = \sum_j Q_{j,g} p_{ij,g} \qquad 2.57$$

In the case of a domain surrounded by a surface ∂D, collision probability techniques can also be applied.

Free path lengths are restricted to finite lengths defined inside ∂D and Eq. (2.53) is used as the basic integral transport equation.

2.3 Further approximations to the neutron transport equation

2.3.1 Group Condensation

The usual number of energy groups necessary for a detailed representation of neutron transport is a few tens. This can still present serious computation-time challenges so oftentimes the number of energy groups is reduced to only a few (2-4) by grouping many fine groups g into a larger group, G. The process is called group condensation.

Calculation of Condensed Macroscopic Cross Sections for Each Region

$$\Phi_G = \sum_{g \in G} \varphi_g \qquad 2.58$$

$$\overline{\Sigma}_G = \frac{\sum_{g \in G} \Sigma_g \varphi_g}{\Phi_G} \qquad 2.59$$

The condensed Flux is the sum (not the average) of several fine-group fluxes.

Overbar denotes average over several fine energy groups

For each region r we then have:

$$\phi_{rG} = \sum_{g \in G} \varphi_{rg} \tag{2.60}$$

$$\overline{\Sigma}^{x}_{rG} = \frac{\sum_{g \in G} \Sigma^{x}_{rg} \varphi_{rg}}{\Phi_{rG}} \tag{2.61}$$

The coarse-group flux is called the few-group flux

2.3.2 Homogenization

To further reduce the size of the computational problem, oftentimes, larger regions of the reactor, called nodes, are “homogenized”, a process by which macroscopic cross sections are volume averaged using flux weighting to preserve the integral reaction rate.

Flux and Cross Section Homogenization

$$V_R = \sum_{r \in R} V_r \tag{2.62}$$

$$\hat{\Phi}_{RG} = \frac{\sum_{r \in R} V_r \Phi_{rg}}{V_R} \tag{2.63}$$

$$\hat{\Phi}_{RG} = \frac{\sum_{r \in R} \overline{\Sigma}^{x}_{rG} \Phi_{rg} V_r}{\hat{\Phi}_{RG} V_R} \tag{2.64}$$

The hat denotes average over regions.

Homogenized and condensed (collapsed) flux and cross sections

$$\hat{\Phi}_{RG} = \frac{\sum_{r \in R} V_r \sum_{g \in G} \varphi_{rg}}{V_R} \tag{2.65}$$

$$\hat{\Phi}_{RG} = \frac{\sum_{r \in R} \sum_{g \in G} \Sigma^{x}_{rG} \varphi_{rg} V_r}{\overline{\Phi}_{RG} V_R} \tag{2.66}$$

2.3.3 Diffusion Approximation

Diffusion Equation

In practice, for full-core calculations one uses the diffusion equation using a small number of energy groups, with homogeneous properties in each nodes. Just like the transport equation, the diffusion equation expresses the neutron balance but does not account for the angular dependence of the flux. Diffusion is not always applicable, especially near boundaries, absorbers and sources.

Certain approximations used in deriving the diffusion equation include assuming the angular flux to being linearly anisotropic, having a slow change in flux in space. Other assumptions include having isotropic sources. As such the diffusion approximation yields proper fluxes at the core (i.e. fuel pins) but not in places where properties change significantly (i.e. boundaries).

In deriving the diffusion equation, use of Fick's Law has been made. The law expresses that the net neutron current shall be along the direction of greatest decrease in neutron flux.

Consider an arbitrary volume V of neutrons (one speed and monoenergetic) as a starting point. Using the condition of continuity [3], the total number of neutrons in our arbitrary volume is:

$$\frac{d}{dt}\int_V n(r,t)dV = \text{production rate - absorbtion rate - leakage rate.} \qquad 2.67$$

The total rate of production of neutrons:

$$\text{production rate} = \int_V s(r,t)dV \qquad 2.68$$

The rate of absorption in terms of the neutron flux:

$$\text{absorption rate} = \int_V \Sigma_a \phi(r,t) dV \qquad 2.69$$

The net rate of flow of neutrons outward through *dA*

$$\textit{leakage}\ \text{rate} = \int_A J(r,t).n\, dA \qquad 2.70$$

Inserting equations (2.68), (2.69), (2.70) into (2.67)

$$\frac{d}{dt}\int_V n(r,t)dV = \int_V s(r,t)dV - \int_V \Sigma_a \phi(r,t)dV - \int_A J(r,t).n\, dA \qquad 2.71$$

Transforming the surface integral to a volume integral using the divergence theorem

$$\int_A J(r,t).n\, dA = \int_V divJ(r,t).dV \qquad 2.72$$

Equation (2.71) turns into:

$$\frac{d}{dt}\int_V n(r,t)dV = \int_V s(r,t)dV - \int_V \Sigma_a \phi(r,t)dV - \int_V divJ(r,t).dV \qquad 2.73$$

Since integrands are the same in equation (2.73)

$$\frac{n(r,t)}{dt} = s(r,t) - \Sigma_a \phi(r,t) - divJ(r,t) \qquad 2.74$$

Equation (2.74) is called the equation of continuity
When sources are independent of time:

$$divJ(r,t) + \Sigma_a \phi(r,t) - s(r) = 0 \qquad 2.75$$

Equation (2.75) is the steady-state equation of continuity

Fick's Law:

Fick's law can be derived in a number of ways. In what follows, we will follow a derivation based on the integral transport equation.

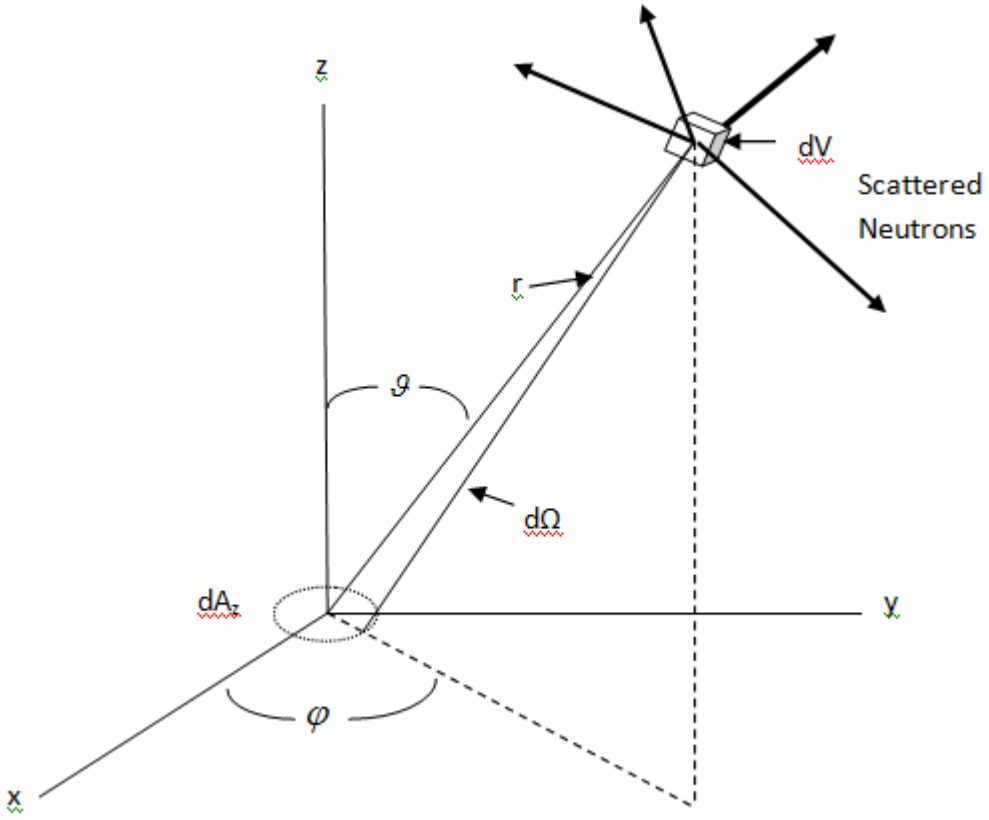

Figure 2.2 – Diagram for Fick's Law

Fraction of the total solid angle subtended by dA_z at dV :

$$\frac{dA_z \cos\vartheta}{4\pi r^2} \qquad 2.76$$

Number of neutrons scattered per second in dV which head toward dA_z :

$$\frac{\Sigma_s \phi(r) \cos\vartheta dA_z dV}{4\pi r^2} \qquad 2.77$$

The number of neutrons which does reach dA_z per second

$$\frac{e^{-\Sigma_t r}\Sigma_s \phi(r) \cos\vartheta dA_z dV}{4\pi r^2} \qquad 2.78$$

The total number of neutrons which flow downward through dA_z per second

$$\frac{\Sigma_s dA_z}{4\pi}\int_{\varphi=0}^{2\pi}\int_{\vartheta=0}^{\pi/2}\int_{r=0}^{\infty} e^{-\Sigma_t r}\phi(r)\cos\vartheta\sin\vartheta dr d\vartheta d\varphi \qquad 2.79$$

The number of neutrons passing per second in the negative z-direction *(can be shown for x and y as well)* through a unit area

$$J_z^- = \frac{\Sigma_s}{4\pi}\int_{\varphi=0}^{2\pi}\int_{\vartheta=0}^{\pi/2}\int_{r=0}^{\infty} e^{-\Sigma_t r}\phi(r)\cos\vartheta\sin\vartheta dr d\vartheta d\varphi \qquad 2.80$$

If $\phi(r)$ varies slowly with position, expanding in Taylor's series

$$\phi(r) = \phi_0 + x\left(\frac{d\phi}{dx}\right)_0 + y\left(\frac{d\phi}{dy}\right)_0 + z\left(\frac{d\phi}{dz}\right)_0 + ..., \qquad 2.81$$

x, y, and z in spherical coordinates:

$$x = r\sin\vartheta\cos\varphi \quad y = r\sin\vartheta\sin\varphi \quad z = r\cos\vartheta \qquad 2.82$$

Inserting equation (2.81) into (2.80)

$$J_z^- = \frac{\Sigma_s}{4\pi}\int_{\varphi=0}^{2\pi}\int_{\vartheta=0}^{\pi/2}\int_{r=0}^{\infty} e^{-\Sigma_t r}\left[\phi_0 + \left(\frac{d\phi}{dz}\right)_0 r\cos\vartheta\right]\cos\vartheta\sin\vartheta dr d\vartheta d\varphi \qquad 2.83$$

Giving:

$$J_z^- = \frac{\Sigma_s\phi_0}{4\Sigma_t} + \frac{\Sigma_s}{6\Sigma_t^2}\left(\frac{d\phi}{dz}\right)_0 \qquad 2.84$$

$$J_z^+ = \frac{\Sigma_s\phi_0}{4\Sigma_t} - \frac{\Sigma_s}{6\Sigma_t^2}\left(\frac{d\phi}{dz}\right)_0 \qquad 2.85$$

Net flow of neutrons

$$J_z = J_z^+ - J_z^- = -\frac{\Sigma_s}{3\Sigma_t^2}\left(\frac{d\phi}{dz}\right)_0 \qquad 2.86$$

Vector J:

$$J = iJ_x + jJ_y + kJ_z = -\frac{\Sigma_s}{3\Sigma_t^2}\, grad\phi \qquad 2.87$$

Fick's Law:

$$J = -D\, grad\, \phi \qquad 2.88$$

Where:

$$D = \frac{\Sigma_s}{3\Sigma_t^2} \qquad 2.89$$

Inserting equation (2.88) into (2.75)

$$div\, D\, \text{grad}\, \phi - \Sigma_a\phi + s = \frac{dn}{dt} \qquad 2.90$$

Since flux is given by $\phi = nv$:

$$\nabla\cdot\left(D\nabla\phi\right) - \Sigma_a\phi + s = \frac{1}{\text{v}}\frac{d\phi}{dt} \qquad 2.91$$

If flux is independent of time:

$$\nabla\cdot\left(D\nabla\phi\right) - \Sigma_a\phi + s = 0 \qquad 2.92$$

Equation (2.92) is the steady state, one-group, diffusion equation. It can be extended to its multigroup form:

$$\nabla\cdot\left(D_g\nabla\phi_g\right) - \Sigma_{ag}\phi_g + s_g = 0$$

2.3.4 Finite-difference discretization of the multigroup diffusion equation

The mesh-centered finite-difference method is often implemented in reactor physics codes for solving the neutron diffusion equation. The basic idea is to solve a Partial Differential Equations's spatial and time derivatives using finite differences. Once a mesh is chosen, spatial integration of parallelepipeds is carried out using constant nuclear properties.

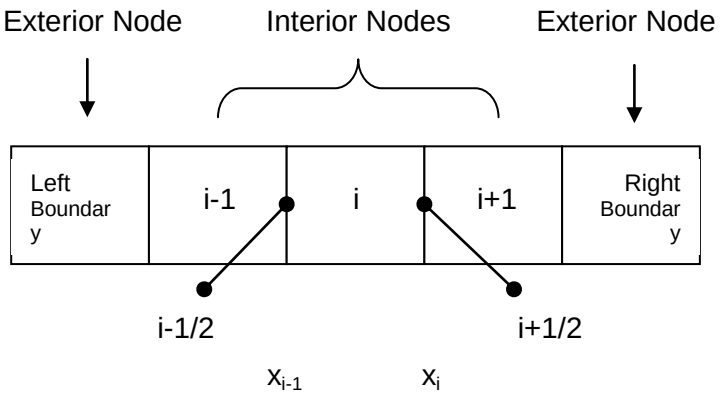

Figure 2.3 – Mesh Indexing

Where the non-constant mesh size is denoted by h_i

$$h_i = x_i - x_{i-1}$$

Where h is defined as the difference between the center of a mesh, and the center of a previous mesh.

Continuity of Currents:

Assuming that the flux, as well as the current is continuous at the interface between two mesh boxes:

$$D_i\left(\frac{d\Phi}{dx}\right)^{-}_{i+1/2} = D_{i+1}\left(\frac{d\Phi}{dx}\right)^{+}_{i+1/2} \quad 2.93$$

Evaluating the double derivative:

Using the center difference approximation

$$\left(\frac{d^2\Phi}{dx^2}\right)_i = \frac{1}{h_i}\left[\left(\frac{d\Phi}{dx}\right)^{-}_{i+1/2} - \left(\frac{d\Phi}{dx}\right)^{+}_{i-1/2}\right] \quad 2.94$$

One needs to evaluate $\left(\frac{d\Phi}{dx}\right)^{-}_{i+1/2}$ and $\left(\frac{d\Phi}{dx}\right)^{+}_{i-1/2}$

Interior Meshes:
Approximating

$$\left(\frac{d\Phi}{dx}\right)^{-}_{i+1/2} \approx \frac{\Phi_{i+1/2} - \Phi_i}{h_i/2} \quad \text{(backward difference)} \quad 2.95$$

$$\left(\frac{d\Phi}{dx}\right)^{+}_{i+1/2} \approx \frac{\Phi_{i+1} - \Phi_{i+1/2}}{h_{i+1}/2} \quad \text{(forward difference)} \quad 2.96$$

Substituting (2.95) and (2.96) into (2.93) we get

$$\frac{2D_i}{h_i}(\Phi_{i+1/2} - \Phi_i) = \frac{2D_{i+1}}{h_{i+1}}(\Phi_{i+1} - \Phi_{i+1/2}) \quad 2.97$$

where isolating for $\Phi_{i+1/2}$ gives

$$\Phi_{i+1/2} = \frac{h_{i+1}D_i\Phi_i - h_iD_{i+1}\Phi_{i+1}}{h_{i+1}D_i + h_iD_{i+1}} \quad 2.98$$

Substituting (2.98) into (2.95) we get

$$\left(\frac{d\Phi}{dx}\right)^{-}_{i+1/2} = \frac{2D_{i+1}(\Phi_{i+1} - \Phi_i)}{h_{i+1}D_i + h_iD_{i+1}} \quad 2.99$$

Similarly we get:

$$\left(\frac{d\Phi}{dx}\right)^{+}_{i-1/2} = \frac{2D_{i-1}(\Phi_i - \Phi_{i-1})}{h_iD_{i-1} + h_{i-1}D_i} \quad 2.100$$

Recasting (2.99) and (2.100)

$$\left(\frac{d\Phi}{dx}\right)^{-}_{i+1/2} = \frac{-h_i}{D_i} a_{i,i+1}(\Phi_{i+1} - \Phi_i) \qquad 2.101$$

Where $a_{i,i+1} = \frac{-D_i}{h_i} \frac{2D_{i+1}}{h_{i+1}D_i + h_i D_{i+1}}$ 2.102

$$\left(\frac{d\Phi}{dx}\right)^{+}_{i-1/2} = \frac{-h_i}{D_i} a_{i,i-1}(\Phi_i - \Phi_{i-1}) \qquad 2.103$$

Where $a_{i,i-1} = \frac{-D_i}{h_i} \frac{2D_{i-1}}{h_i D_{i-1} + h_{i-1} D_i}$ 2.104

Substituting (2.101) and (2.103) into (2.94) we get:

$$\left(\frac{d^2\Phi}{dx^2}\right)_i = \frac{1}{h_i}\left[\frac{-h_i}{D_i} a_{i,i+1}(\Phi_{i+1} - \Phi_i) - \frac{-h_i}{D_i} a_{i,i-1}(\Phi_i - \Phi_{i-1})\right] \qquad 2.105$$

$$\left(\frac{d^2\Phi}{dx^2}\right)_i = \frac{-h_i}{h_i D_i}\left[a_{i,i+1}(\Phi_{i+1} - \Phi_i) - a_{i,i-1}(\Phi_i - \Phi_{i-1})\right] \qquad 2.106$$

$$\left(\frac{d^2\Phi}{dx^2}\right)_i = \frac{-1}{D_i}\left[a_{i,i+1}(\Phi_{i+1} - \Phi_i) - a_{i,i-1}(\Phi_i - \Phi_{i-1})\right] \qquad 2.107$$

If D term is assumed to be constant

$$a_{i,i+1} = \frac{-D_i}{h_i} \frac{2D_i}{h_{i+1}D_i + h_i D_i} \qquad 2.108$$

$$a_{i,i+1} = \frac{-D_i}{h_i} \frac{D_i}{D_i} \frac{2}{h_{i+1} + h_i} \qquad 2.109$$

$$a_i^{x+} = a_{i,i+1} = \frac{-D_i}{h_i} \frac{2}{h_{i+1} + h_i} \qquad 2.110$$

If D term is assumed to be constant

$$a_{i,i-1} = \frac{-D_i}{h_i}\frac{2D_i}{h_i D_i + h_{i-1} D_i} \tag{2.111}$$

$$a_{i,i-1} = \frac{-D_i}{h_i}\frac{D_i}{D_i}\frac{2}{h_i + h_{i-1}} \tag{2.112}$$

$$a_i^{x-} = a_{i,i-1} = \frac{-D_i}{h_i}\frac{2}{h_i + h_{i-1}} \tag{2.113}$$

Changing Notation (Simpler Notation) Refer to (2.110) & (2.113)

$$\left(\frac{d^2\Phi}{dx^2}\right)_i = \frac{-1}{D_i}\left[a_i^{x+}(\Phi_{i+1} - \Phi_i) - a_i^{x-}(\Phi_i - \Phi_{i-1})\right] \tag{2.114}$$

Expanding

$$\left(\frac{d^2\Phi}{dx^2}\right)_i = \frac{-1}{D_i}\left[a_i^{x+}\Phi_{i+1} - a_i^{x+}\Phi_i - a_i^{x-}\Phi_i + a_i^{x-}\Phi_{i-1}\right] \tag{2.115}$$

$$\left(\frac{d^2\Phi}{dx^2}\right)_i = \frac{-1}{D_i}\left[a_i^{x+}\Phi_{i+1} - (a_i^{x+} + a_i^{x-})\Phi_i + a_i^{x-}\Phi_{i-1}\right] \tag{2.116}$$

Substituting (2.110) & (2.113) into above equation [D's cancel out]:

Interior Nodes 2.117

$$\left(\frac{d^2\Phi}{dx^2}\right)_i$$
$$= \frac{2}{h_i}\frac{1}{h_{i+1} + h_i}\Phi_{i+1}$$
$$-\left(\frac{2}{h_i}\frac{1}{h_{i+1} + h_i} + \frac{2}{h_i}\frac{1}{h_i + h_{i-1}}\right)\Phi_i + \frac{2}{h_i}\frac{1}{h_i + h_{i-1}}\Phi_{i-1}$$

Boundary Meshes:

The solutions must satisfy boundary conditions of the type:

$$\gamma_{boundary} = \left(\frac{\vec{J}\hat{n}}{\Phi}\right)_{boundary} \tag{2.118}$$

Let $\beta = \frac{1}{D}\left(\frac{\vec{J}\hat{n}}{\Phi}\right)$ 2.119

Hence $\gamma = D\beta$ 2.120

The outward current-to-flux ratio:

$$\gamma^{xu} = \frac{u\vec{J}_b^u}{\Phi_b^u} = \frac{u\vec{J}_{b+u/2}^{(-u)}}{\Phi_b^u} \quad 2.121$$

In the above, "u" is the sign of the outward normal to the external boundary. It is -1 for the left boundary and +1 for the right boundary. Applying finite-differencing technique to the boundary node:

$$\left(\frac{d\Phi}{dx}\right)_{b+u/2}^{-u} = u\frac{\Phi_{b+u/2}^{u} - \Phi_b}{h_b/2} \quad 2.122$$

Boundary current:

$$J_{b+u/2}^{(-u)} = u\frac{-D_b\left(\Phi_{b+u/2}^{u} - \Phi_b\right)}{h_b/2} \quad 2.123$$

Boundary condition is now written:

$$\gamma^u = \frac{-D_b\left(\Phi_{b+u/2}^{u} - \Phi_b\right)}{\frac{h_b}{2}\Phi_{b+u/2}^{u}} \quad 2.124$$

$$\Phi_{b+u/2} = \frac{2D_b\Phi_b}{h_b\gamma^- + 2D_b} \quad 2.125$$

Substituting (2.125) into (2.122), the first derivative of the flux for the boundary becomes 2.126

$$\left(\frac{d\Phi}{dx}\right)_{b+u/2}^{-u} = \frac{\Phi_b}{\frac{D_b}{\gamma^u} + \frac{h_b}{2}} = \frac{-h_b}{D_b}a_b^u\Phi_b$$

$$a_b^u = \frac{-1}{h_b\left(\frac{1}{\gamma^u} + \frac{h_b}{2D_b}\right)} \quad 2.127$$

Setting $\gamma = D\beta$ in (2.124)

$$\beta^u = \frac{-\left(\Phi^{\mathrm{u}}_{b+\mathrm{u}/2} - \Phi_b\right)}{\frac{h_b}{2}\Phi^{\mathrm{u}}_{b+\mathrm{u}/2}} \qquad 2.128$$

Hence we get

$$a_b^u = \frac{-1}{h_b\left(\frac{1}{D_b\beta^u} + \frac{h_b}{2D_b}\right)} \qquad 2.129$$

$$a_b^u = \frac{-D_b}{h_b\left(\frac{1}{\beta^u} + \frac{h_b}{2}\right)} \qquad 2.130$$

Hence the second-order partial derivative for a boundary mesh can now be expressed as

$$\left(\frac{d^2\Phi}{dx^2}\right)_b = -\frac{1}{D_b}\left[a_{b-u}^{-u}\Phi_{b-u} - (a_b^{-u} + a_b^u)\Phi_b\right] \qquad 2.131$$

The D term cancels out when substituting (2.130) in (2.131)

Left Boundary

$$\left(\frac{d^2\Phi}{dx^2}\right)_i = \frac{2}{h_i}\frac{1}{h_{i+1}+h_i}\Phi_2 - \left(\frac{2}{h_i}\frac{1}{h_{i+1}+h_i} + \frac{2}{h_i}\frac{1}{\left(\frac{h_i(\Phi_{i-1/2})}{(\Phi_i - \Phi_{i-1/2})} + h_i\right)}\right)\Phi_i \qquad 2.132$$

$$\left(\frac{d^2\Phi}{dx^2}\right)_1 = \frac{2}{h_1}\frac{1}{h_2+h_1}\Phi_2 - \left(\frac{2}{h_1}\frac{1}{h_2+h_1} + \frac{2}{h_1}\frac{1}{\left(\frac{h_1(\Phi_{1-1/2})}{(\Phi_1 - \Phi_{1-1/2})} + h_1\right)}\right)\Phi_1 \qquad 2.133$$

Right Boundary

$$\left(\frac{d^2\Phi}{dx^2}\right)_i = \frac{2}{h_i}\frac{1}{h_i + h_{i-1}}\Phi_{i-1} - \left(\frac{2}{h_i}\frac{1}{h_i + h_{i-1}} + \frac{2}{h_i}\frac{1}{\left(\frac{h_i(\Phi_{i+1/2})}{(\Phi_i - \Phi_{i+1/2})} + h_i\right)}\right)\Phi_i \qquad 2.134$$

$$\left(\frac{d^2\Phi}{dx^2}\right)_n = \frac{2}{h_n}\frac{1}{h_n + h_{n-1}}\Phi_{n-1} - \left(\frac{2}{h_n}\frac{1}{h_n + h_{n-1}} + \frac{2}{h_n}\frac{1}{\left(\frac{h_n(\Phi_{n+1/2})}{(\Phi_n - \Phi_{n+1/2})} + h_n\right)}\right)\Phi_n \qquad 2.135$$

3.0 STATEMENT OF THE PROBLEM AND OBJECTIVE

"Each problem that I solved became a rule which served afterwards to solve other problems" (Rene Descartes)

As explained previously, in order to reduce the computation time, a number of successive approximations are made to the fine-geometry, many-group transport equation. These approximations are expected to introduce errors. To estimate the magnitude of the errors introduced by each approximation step, a geometrically small test model was developed, one for which detailed transport calculations as well as approximate calculations can be performed and results compared.

3.1 Test Model

A test model consisting of twelve regions in a row is used. Eleven of the nodes are fuel nodes (corresponding to different burnups) and one node is the reflector node, as shown in Fig. 3.1. Boundary conditions are of the reflective type on the W side and of the vacuum type on the E side.

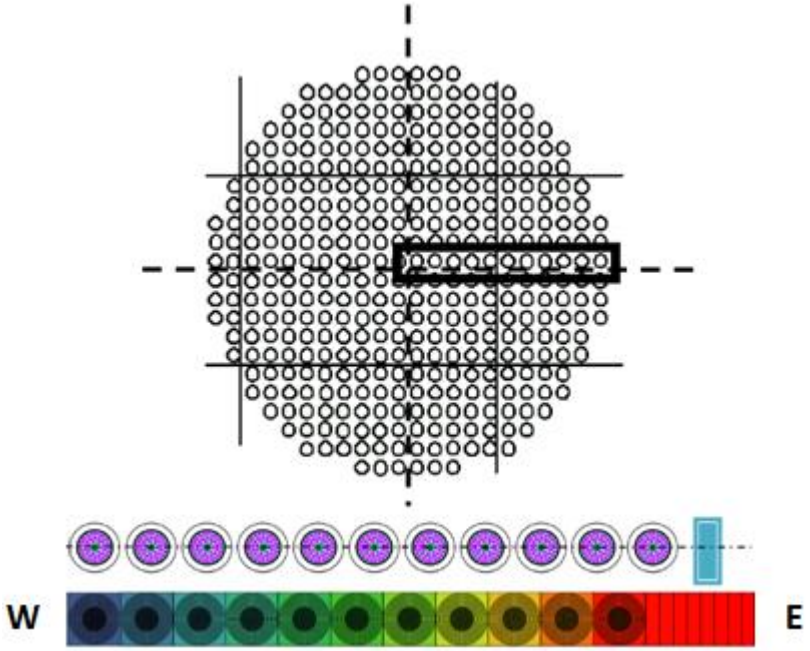

Figure 3.1 – Test Model

Each node is divided into 8 computational meshes. Transport calculations are performed using the Collision Probability (CP) method as implemented in the code DRAGON. Diffusion calculations are performed using Black-Stallion, a finite-differences diffusion code.

A standardized input for a 37-element CANDU natural uranium bundle was used for generating the cross section parameters for natural uranium fuel. Neutronics evaluation was performed using the code DRAGON and the IAEA-WLUP (WIMS Library Update Project) 69-group microscopic cross section library. Calculations were performed for different fuel configurations. Irradiated fuel was simulated using depleted Uranium fuel (0.4% U235). The fast and thermal flux were calculated for both 69 (detailed geometry) and 2 energy group (detailed and coarse) simulations. Comparison of transport results (DRAGON 3.05) with Diffusion was based on Black-Stallion.

Data generated by DRAGON is parsed and cross sections are interfaced with Black-Stallion through the use of a custom written script.

Extensive testing of DRAGON and Black-Stallion was carried out and repeated after integrating enhancements to Black-Stallion as well after having incorporated use of cross sections generated by DRAGON. Validation includes comparison with analytical solutions as well as benchmarking of Black-Stallion. For the validation cases, the results are in full agreement between DRAGON, Black-Stallion and “back-of-the-envelope” analytical calculations.

3.2 Configurations

Three configurations were studied:

i. Simple case with uniform fresh fuel

ii. Intermediate case incorporating varied burnup

iii. Extreme case incorporating abrupt shift in burnup

These tests were designed to highlight the discrepancy that arises when moving from Transport to Diffusion under different fuel loading scenarios. Under such arrangements the shift from detailed to coarse geometry along with a reduced number of energy groups was studied. The resulting observation is that the major source of inaccuracy is transitioning from homogenized transport to homogenized diffusion; energy groups not being an issue. The extreme case illustrates the discrepancy between transport and diffusion in a manner that permits us to generalize the above observation (Refer Figures 3.21-3.26).

3.3 DRAGON representation of the model

DRAGON transport code can handle exact (or almost exact) representations of core geometry [2]. As a general rule, physics data libraries (an input to the transport code) are context-independent, however the same does not hold true for neutron cross sections which are dependent on burnup and spatial geometrical parameters. The methodology and approach to generation of cross sections was to use a multi-fuel-region model, having already tested a single-fuel-region model during the initial stages.

CANDU-6 lattice cell contains 37-element natural-uranium bundle and pressurized heavy-water coolant in a pressure tube enclosed within a calandria tube. A region of unpressurized heavy water (moderator) at relatively low temperature surrounds the calandria tube (Figure 3.2).

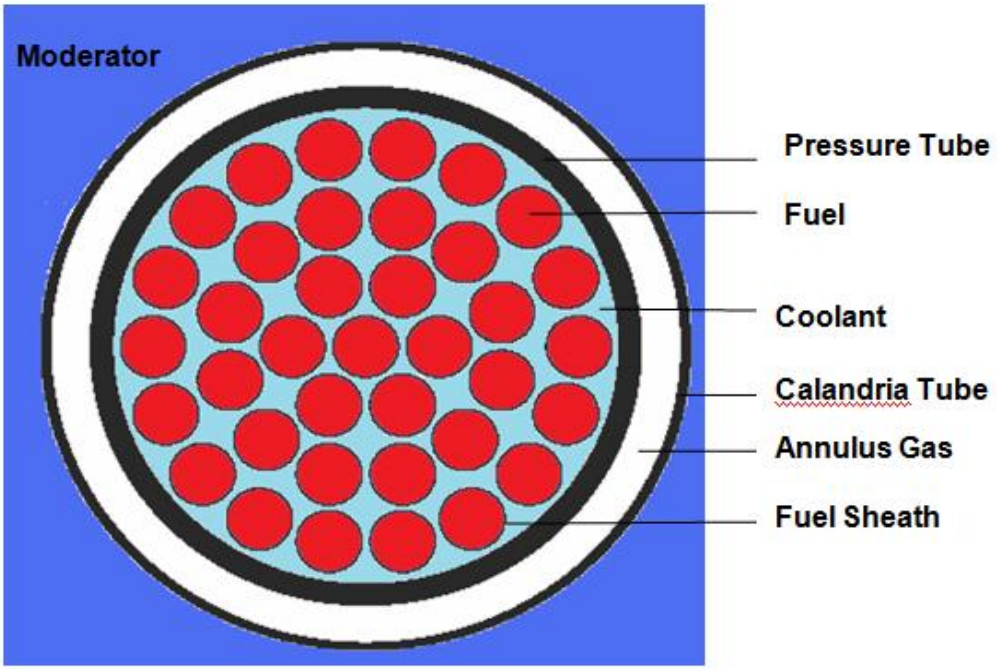

Figure 3.2 – Lattice Cell Elements

Eleven detailed fuel regions (each comprised of a lattice cell) were modelled (Figure 3.3), the right most fuel region being bounded by a reflector region. Different configurations were designed by varying the position of fresh and depleted fuel cells.

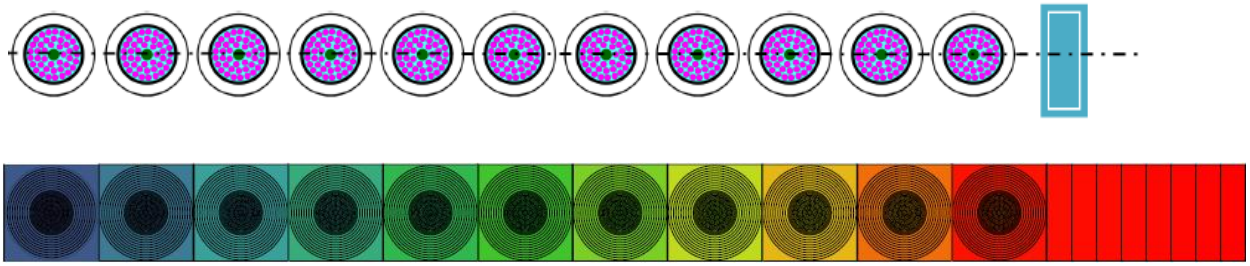

Figure 3.3 – Model with Fuel and Reflector

In place of a time and resource intensive full core simulation, the transport model takes advantage of symmetry and as such is representative of flux (or power) profile that is seen in a full core model. The lattice cell (Figure 3.4) was modelled with a length of 28.575 cm in both the X and Y direction. This includes the coolant, moderator,

cladding material, and a gap. The reflector has a length of 60 cm. Fuel parameters for the model have been reproduced in Table 3.1

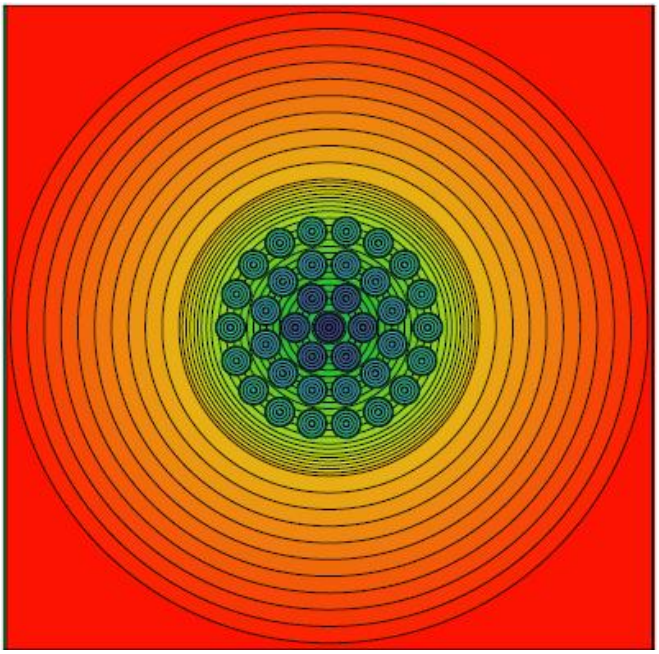

Figure 3.4 - Lattice Cell representation in DRAGON

The fuel cell was split in a x-y pattern (Figure 3.5) as opposed to a radial one.

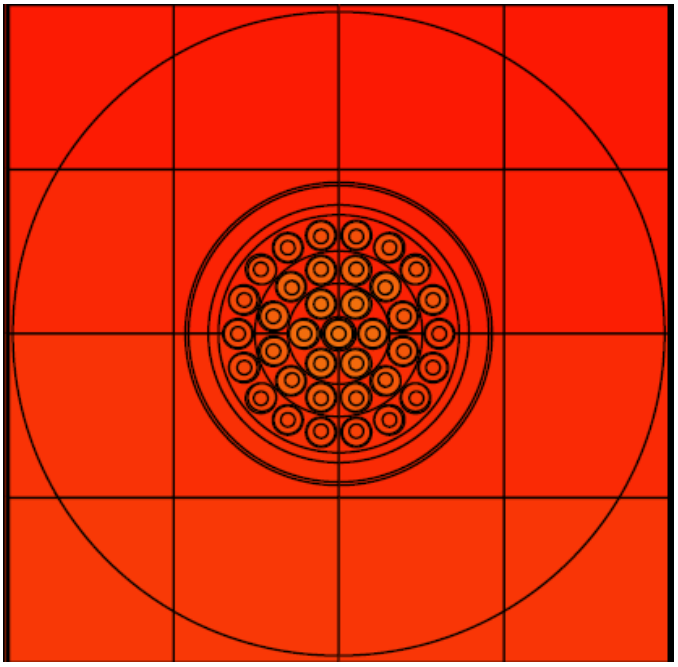

Figure 3.5 – Mesh Splitting

In terms of boundary conditions (Figure 3.6), a reflective boundary condition was chosen in the X-, Y- and Y+ direction whereas a void boundary was chosen in the X+ direction. When a surface has zero re-entrant angular flux it is referred to as a void boundary.

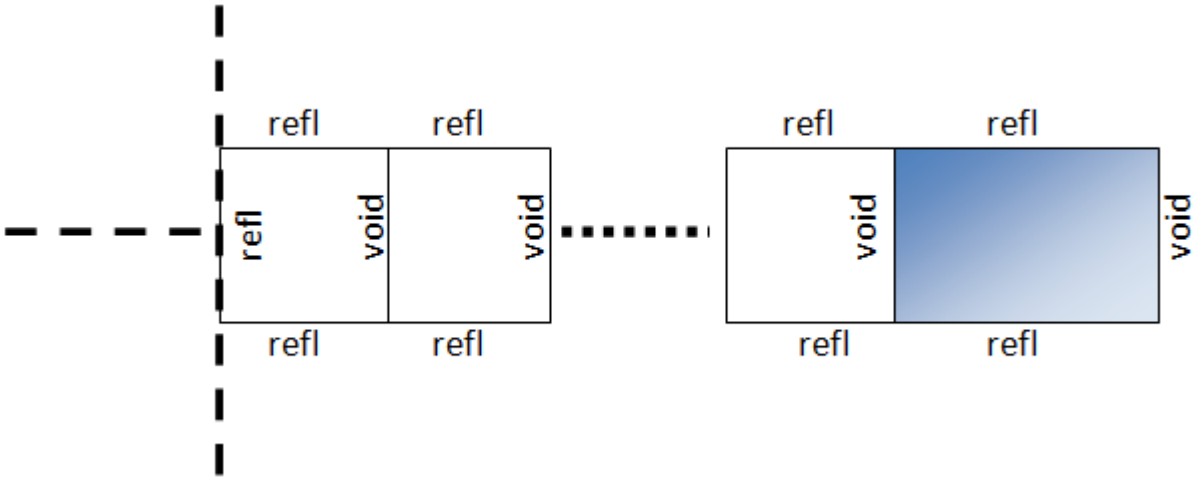

Figure 3.6 – Boundary Conditions

In order to obtain the flux at the interfaces, two tiny vertical mesh strips were created in each lattice cell. The flux at the interface is the average of the flux in the tiny strips between two adjacent nodes. The reflector (Figure 3.7) also has two tiny vertical mesh strips at both ends.

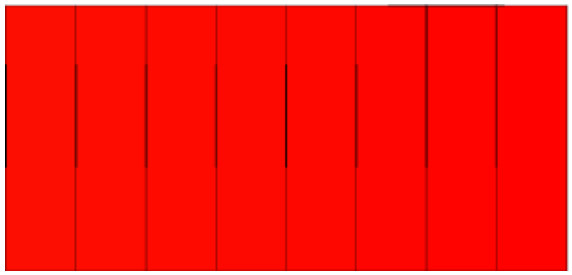

Figure 3.7 – Reflector (Heavy Water)

Fuel material	Natural UO_2
Initial uranium compositions	weight percent
234U	0.0054
235U	0.7110
238U	99.2836
Fuel density	10 g/cm3
Fuel temperature	1100 K
Element radius	0.6 cm
Number of fuel pins	37
Inner fuel ring radius (6)	1.4 cm
Middle fuel ring radius (12)	2.8 cm
Outer fuel ring radius (18)	4.3 cm
Cladding material	Zr
Cladding radius	0.6 cm
Pressure tube	Zr
Inner radius	5.1 cm
Outer radius	5.6 cm
Calandria tube	Zr
Inner radius	6.4cm
Outer radius	6.6 cm
Coolant	D2O
Atom purity	99.75 %
Density	0.8 g/cm3

Temperature	550 K
Moderator	D2O
Atom purity	99.91 %
Density	1.1 g/cm3
Temperature	350K
Fuel channel square pitch	28.575 cm

Table 3.1 – Fuel Properties

3.3.1 Diffusion Model (two-group, node homogenized)

A model with eleven fuel regions plus one reflector region (Figure 3.8) was implemented in BLACK STALLION. Cross-sections from DRAGON representing coarse geometry were utilized.

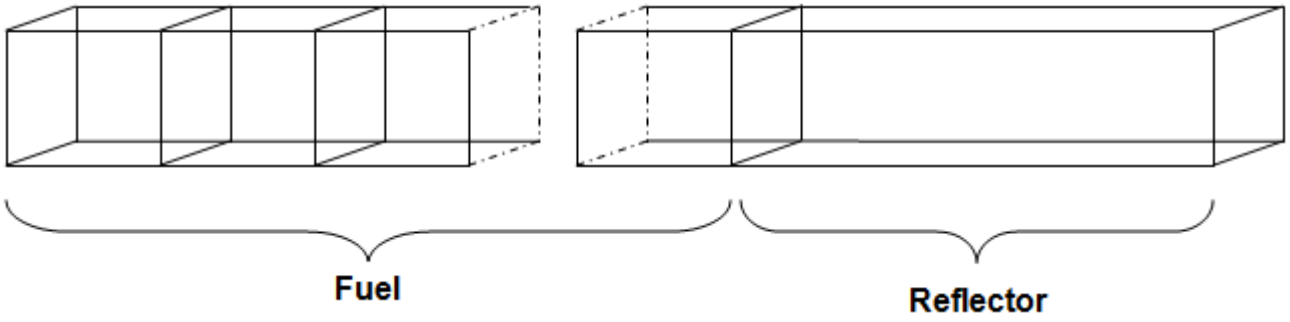

Figure 3.8 – Diffusion Model Depiction

3.4 Comparison of Different Approximations

3.4.1 Configuration I

Fast Flux

Fast Flux	1	2	3	4	5	6
69 gr. Detailed Transport	2.90E+02	2.86E+02	2.78E+02	2.66E+02	2.50E+02	2.30E+02
2 gr. Detailed Transport	2.94E+02	2.89E+02	2.81E+02	2.68E+02	2.51E+02	2.31E+02
2 gr. Homo. Transport	3.01E+02	2.96E+02	2.86E+02	2.72E+02	2.54E+02	2.32E+02
2 gr. Homo. Diffusion	2.86E+02	2.82E+02	2.74E+02	2.62E+02	2.47E+02	2.28E+02

Fast Flux	7	8	9	10	11	12
69 gr. Detailed Transport	2.07E+02	1.81E+02	1.51E+02	1.19E+02	7.97E+01	5.81E+00
2 gr. Detailed Transport	2.07E+02	1.80E+02	1.50E+02	1.18E+02	7.84E+01	5.61E+00
2 gr. Homo. Transport	2.05E+02	1.76E+02	1.44E+02	1.09E+02	6.66E+01	5.20E+00
2 gr. Homo. Diffusion	2.07E+02	1.82E+02	1.55E+02	1.25E+02	8.63E+01	5.91E+00

Table 3.2 – Configuration I, Fast Flux

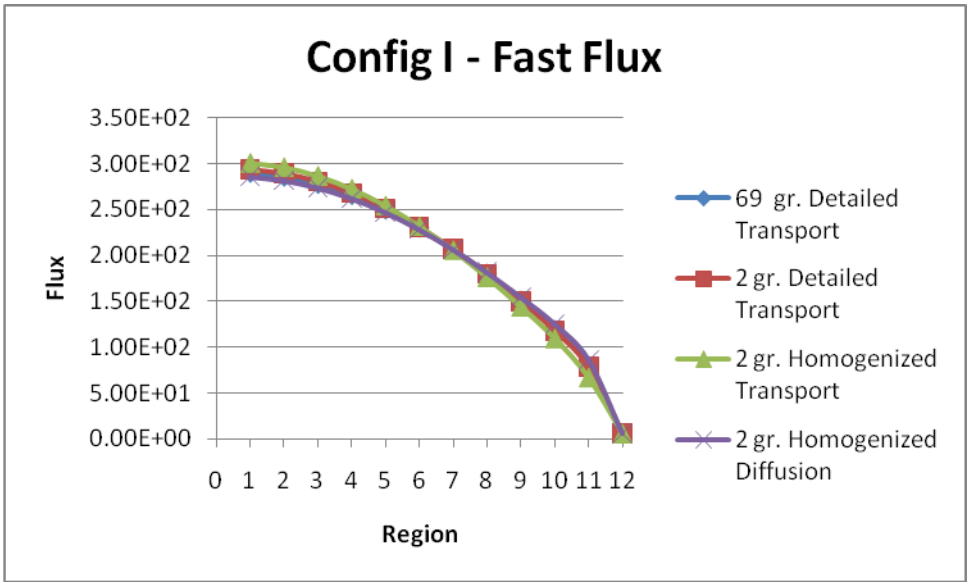

Figure 3.9 – Configuration I, Fast Flux

Error (%)

Nodes	1	2	3	4	5	6
Transport vs. Diffusion %	-4.92	-4.71	-4.32	-3.66	-2.71	-1.36
Nodes	7	8	9	10	11	12
Transport vs. Diffusion %	0.53	3.31	7.5	14.7	29.61	13.6

Root Mean Square (%)

10.93 %

Table 3.3 – Configuration I, Fast Flux, Error

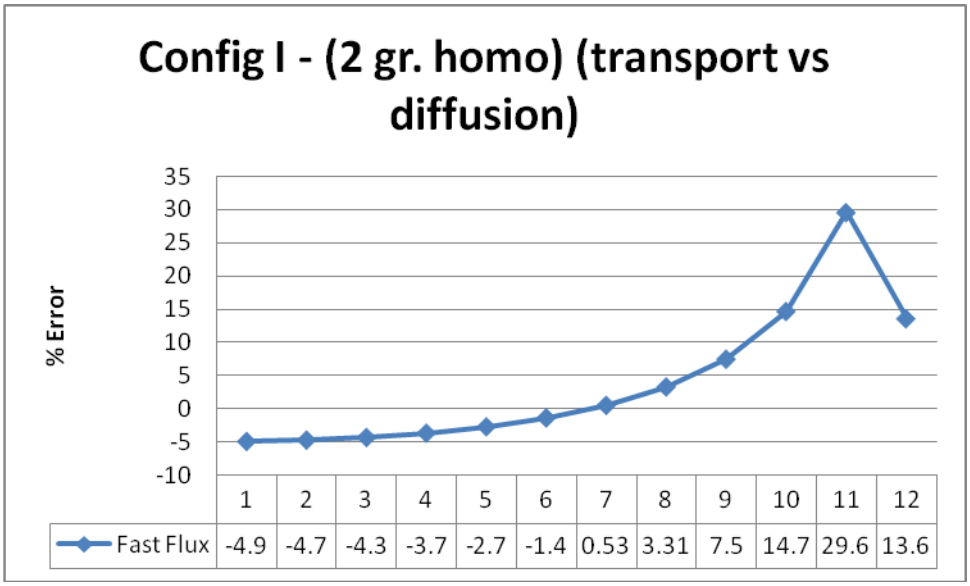

Figure 3.10 – Configuration I, Fast Flux, Error

Thermal Flux

Thermal Flux	1	2	3	4	5	6
69 gr. Detailed Transport	6.57E+02	6.47E+02	6.29E+02	6.02E+02	5.66E+02	5.22E+02
2 gr. Detailed Transport	6.48E+02	6.39E+02	6.20E+02	5.91E+02	5.54E+02	5.09E+02
2 gr. Homo. Transport	6.65E+02	6.54E+02	6.33E+02	6.02E+02	5.62E+02	5.12E+02
2 gr. Homo. Diffusion	6.33E+02	6.25E+02	6.07E+02	5.82E+02	5.48E+02	5.06E+02

Thermal Flux	7	8	9	10	11	12
69 gr. Detailed Transport	4.69E+02	4.09E+02	3.43E+02	2.70E+02	1.99E+02	1.15E+02
2 gr. Detailed Transport	4.56E+02	3.97E+02	3.31E+02	2.60E+02	1.92E+02	1.10E+02
2 gr. Homo. Transport	4.54E+02	3.89E+02	3.18E+02	2.41E+02	1.68E+02	8.92E+01
2 gr. Homo. Diffusion	4.58E+02	4.03E+02	3.42E+02	2.77E+02	2.19E+02	1.38E+02

Table 3.4 – Configuration I, Thermal Flux

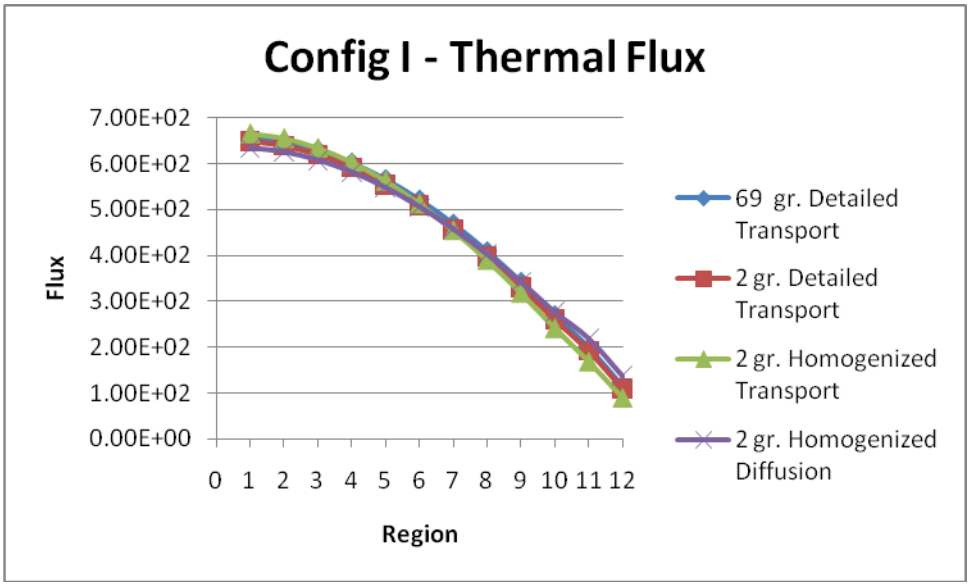

Figure 3.11 – Configuration I, Thermal Flux

Error (%)

Nodes	1	2	3	4	5	6
Transport vs. Diffusion %	-4.71	-4.51	-4.1	-3.44	-2.49	-1.14
Nodes	7	8	9	10	11	12
Transport vs. Diffusion %	0.76	3.52	7.74	14.82	30.31	54.31

Root Mean Square (%)

18.80 %

Table 3.5 – Configuration I, Thermal Flux, Error

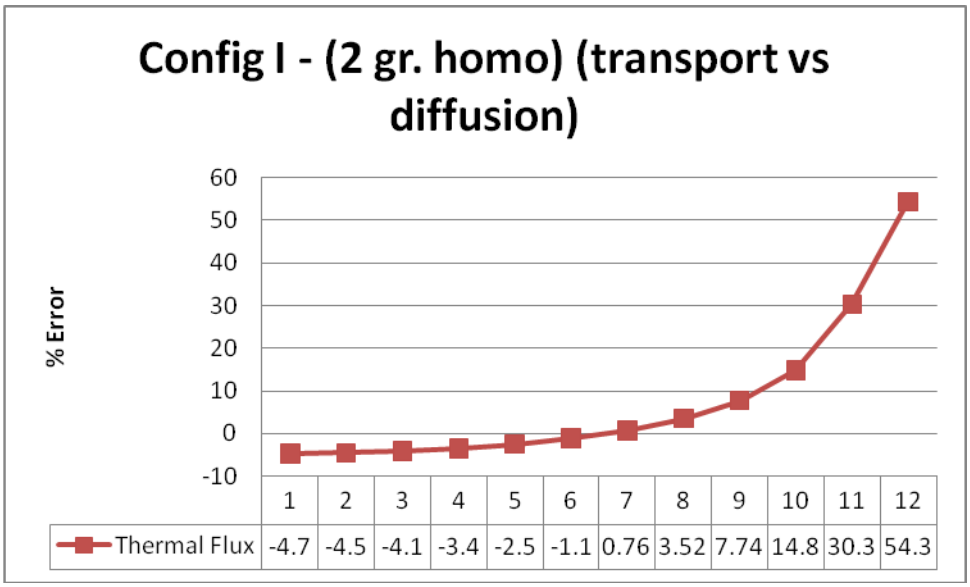

Figure 3.12 – Configuration I, Thermal Flux, Error

Fission Rate

Fission Rate	1	2	3	4	5	6
69 gr. Detailed Transport	1.36E+00	1.34E+00	1.30E+00	1.25E+00	1.17E+00	1.08E+00
2 gr. Detailed Transport	1.37E+00	1.35E+00	1.31E+00	1.25E+00	1.17E+00	1.08E+00
2 gr. Homo. Transport	1.41E+00	1.38E+00	1.34E+00	1.27E+00	1.19E+00	1.08E+00
2 gr. Homo. Diffusion	1.34E+00	1.32E+00	1.29E+00	1.23E+00	1.16E+00	1.07E+00

Fission Rate	7	8	9	10	11
69 gr. Detailed Transport	9.71E-01	8.47E-01	7.09E-01	5.60E-01	4.11E-01
2 gr. Detailed Transport	9.66E-01	8.39E-01	7.00E-01	5.51E-01	4.04E-01
2 gr. Homo. Transport	9.61E-01	8.23E-01	6.72E-01	5.10E-01	3.54E-01
2 gr. Homo. Diffusion	9.68E-01	8.52E-01	7.24E-01	5.86E-01	4.61E-01

Table 3.6 – Configuration I, Fission Rate

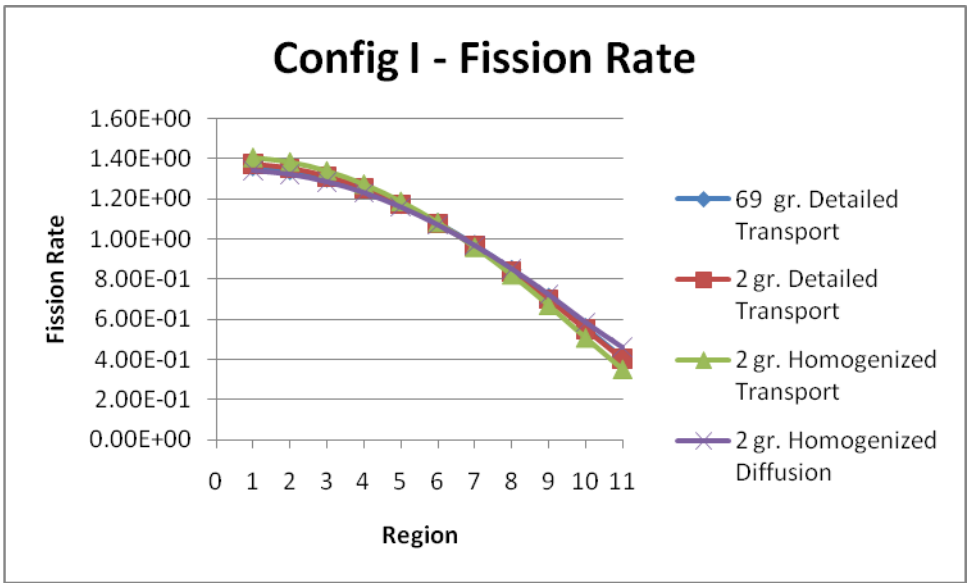

Figure 3.13 – Configuration I, Fission Rate

Error (%)

Nodes	1	2	3	4	5	6
Transport vs. Diffusion %	-4.70	-4.53	-4.13	-3.43	-2.50	-1.17
Nodes	7	8	9	10	11	
Transport vs. Diffusion %	0.74	3.51	7.73	14.83	30.29	

Root Mean Square (%)

10.83 %

Table 3.7 – Configuration I, Fission Rate, Error

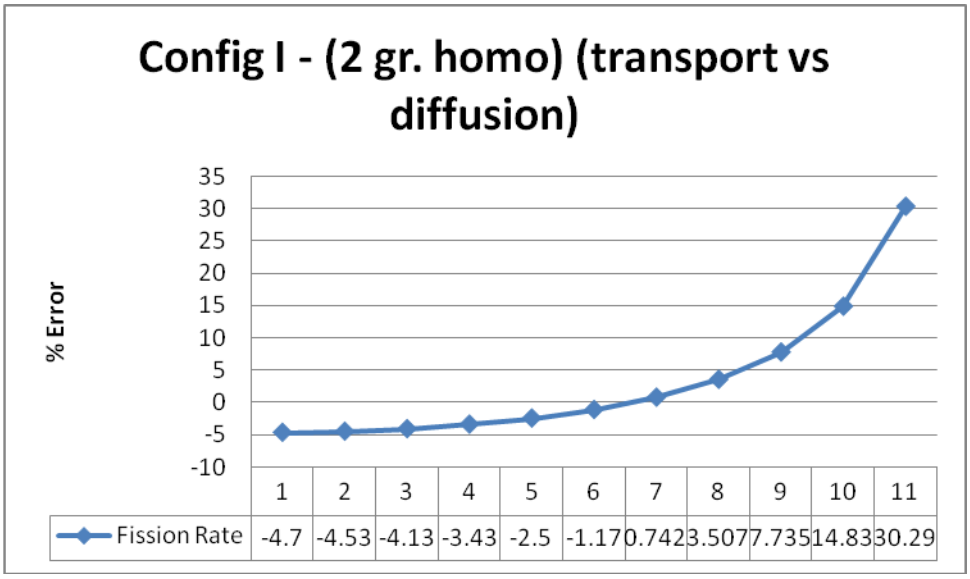

Figure 3.14 – Configuration I, Fission Rate, Error

3.4.2 Configuration II

Fast Flux

Fast Flux	1	2	3	4	5	6
69 gr. Detailed Transport	8.70E+02	5.42E+02	3.83E+02	2.84E+02	2.11E+02	1.57E+02
2 gr. Detailed Transport	8.93E+02	5.51E+02	3.85E+02	2.83E+02	2.08E+02	1.52E+02
2 gr. Homo. Transport	9.89E+02	5.97E+02	3.86E+02	2.64E+02	1.81E+02	1.24E+02
2 gr. Homo. Diffusion	1.09E+03	6.28E+02	3.78E+02	2.40E+02	1.53E+02	9.68E+01

Fast Flux	7	8	9	10	11	12
69 gr. Detailed Transport	1.16E+02	8.57E+01	6.24E+01	4.43E+01	2.77E+01	1.99E+00
2 gr. Detailed Transport	1.11E+02	8.07E+01	5.78E+01	4.03E+01	2.47E+01	1.74E+00
2 gr. Homo. Transport	8.45E+01	5.73E+01	3.83E+01	2.49E+01	1.36E+01	1.02E+00
2 gr. Homo. Diffusion	6.15E+01	3.90E+01	2.48E+01	1.58E+01	9.27E+00	6.02E-01

Table 3.8 – Configuration II, Fast Flux

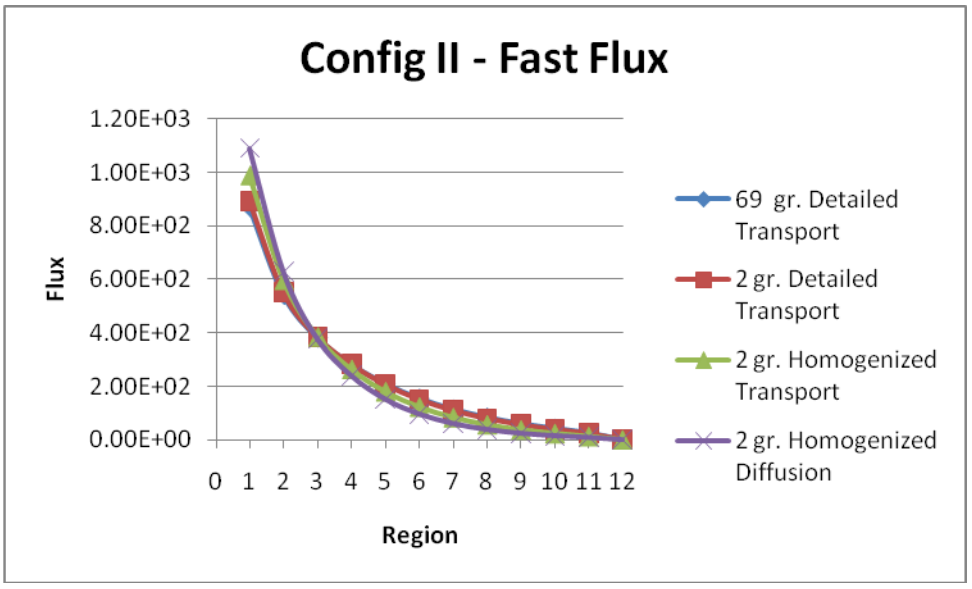

Figure 3.15 – Configuration II, Fast Flux

Error (%)

Nodes	1	2	3	4	5	6
Transport vs. Diffusion %	10.17	5.12	-2.02	-9.12	-15.81	-21.86
Nodes	7	8	9	10	11	12
Transport vs. Diffusion %	-27.28	-31.89	-35.28	-36.38	-32.03	-41.27

Root Mean Square (%)

25.83 %

Table 3.9 – Configuration II, Fast Flux, Error

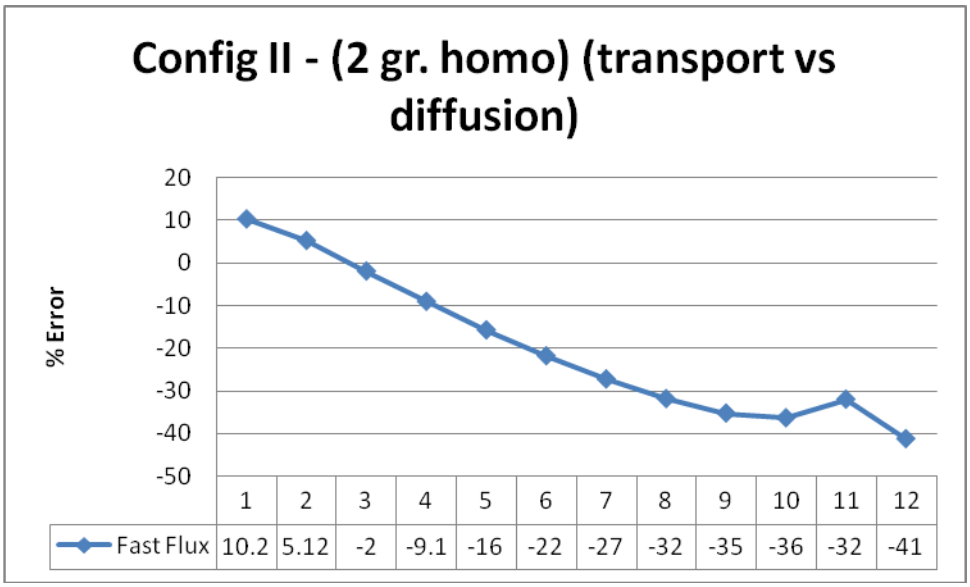

Figure 3.16 – Configuration II, Fast Flux, Error

Thermal Flux

Thermal Flux	1	2	3	4	5	6
69 gr. Detailed Transport	1.75E+03	1.50E+03	1.13E+03	8.40E+02	6.24E+02	4.63E+02
2 gr. Detailed Transport	1.75E+03	1.49E+03	1.12E+03	8.20E+02	6.02E+02	4.41E+02
2 gr. Homo. Transport	1.97E+03	1.61E+03	1.13E+03	7.73E+02	5.29E+02	3.62E+02
2 gr. Homo. Diffusion	2.18E+03	1.71E+03	1.11E+03	7.06E+02	4.48E+02	2.84E+02

Thermal Flux	7	8	9	10	11	12
69 gr. Detailed Transport	3.44E+02	2.53E+02	1.85E+02	1.31E+02	9.00E+01	4.86E+01
2 gr. Detailed Transport	3.22E+02	2.34E+02	1.67E+02	1.17E+02	7.89E+01	4.16E+01
2 gr. Homo. Transport	2.47E+02	1.67E+02	1.12E+02	7.24E+01	4.50E+01	2.18E+01
2 gr. Homo. Diffusion	1.80E+02	1.14E+02	7.27E+01	4.62E+01	3.08E+01	1.71E+01

Table 3.10 – Configuration II, Thermal Flux

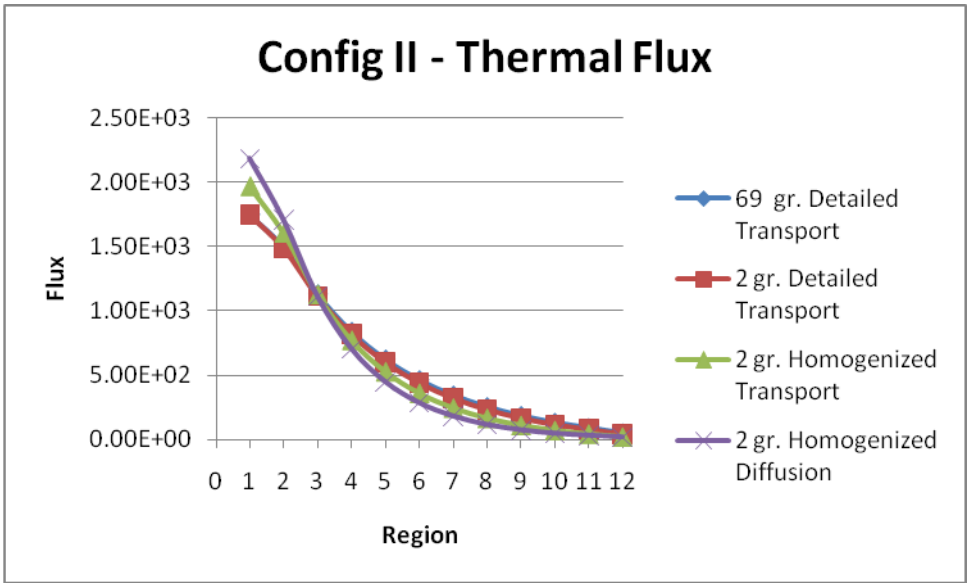

Figure 3.17 – Configuration II, Thermal Flux

Error (%)

Nodes	1	2	3	4	5	6
Transport vs. Diffusion %	10.98	6.28	-1.38	-8.75	-15.45	-21.56
Nodes	7	8	9	10	11	12
Transport vs. Diffusion %	-26.98	-31.61	-35.01	-36.18	-31.63	-21.33

Root Mean Square (%)

23.56 %

Table 3.11 – Configuration II, Thermal Flux, Error

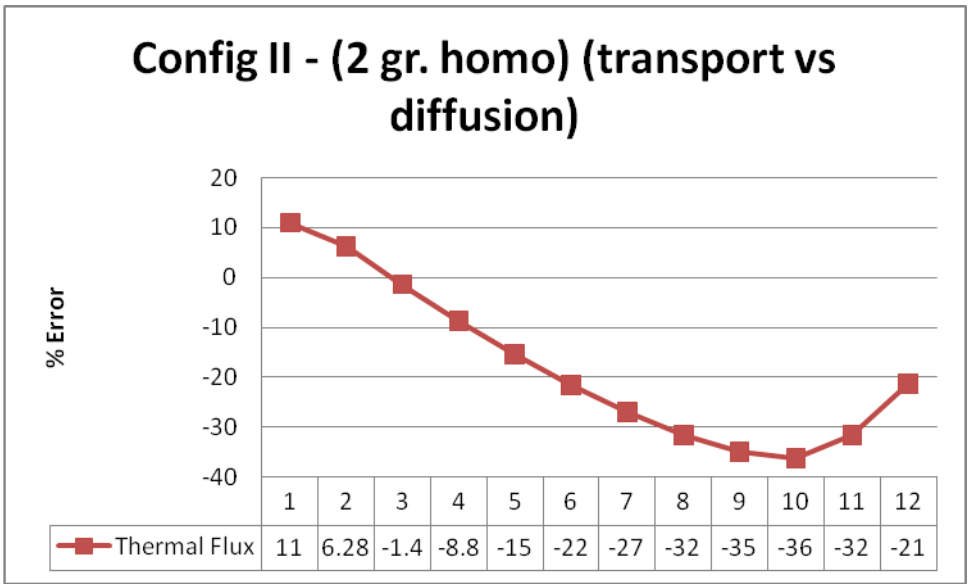

Figure 3.18 – Configuration II, Thermal Flux, Error

Fission Rate

Fission Rate	1	2	3	4	5	6
69 gr. Detailed Transport	3.67E+00	1.98E+00	1.49E+00	1.11E+00	8.21E-01	6.10E-01
2 gr. Detailed Transport	3.76E+00	2.01E+00	1.50E+00	1.10E+00	8.09E-01	5.93E-01
2 gr. Homo. Transport	4.22E+00	2.16E+00	1.52E+00	1.04E+00	7.11E-01	4.86E-01
2 gr. Homo. Diffusion	4.68E+00	2.30E+00	1.49E+00	9.47E-01	6.01E-01	3.81E-01

Fission Rate	7	8	9	10	11
69 gr. Detailed Transport	4.52E-01	3.34E-01	2.43E-01	1.73E-01	1.18E-01
2 gr. Detailed Transport	4.33E-01	3.14E-01	2.25E-01	1.57E-01	1.06E-01
2 gr. Homo. Transport	3.31E-01	2.25E-01	1.50E-01	9.73E-02	6.02E-02
2 gr. Homo. Diffusion	2.42E-01	1.54E-01	9.76E-02	6.21E-02	4.11E-02

Table 3.12 – Configuration II, Fission Rate

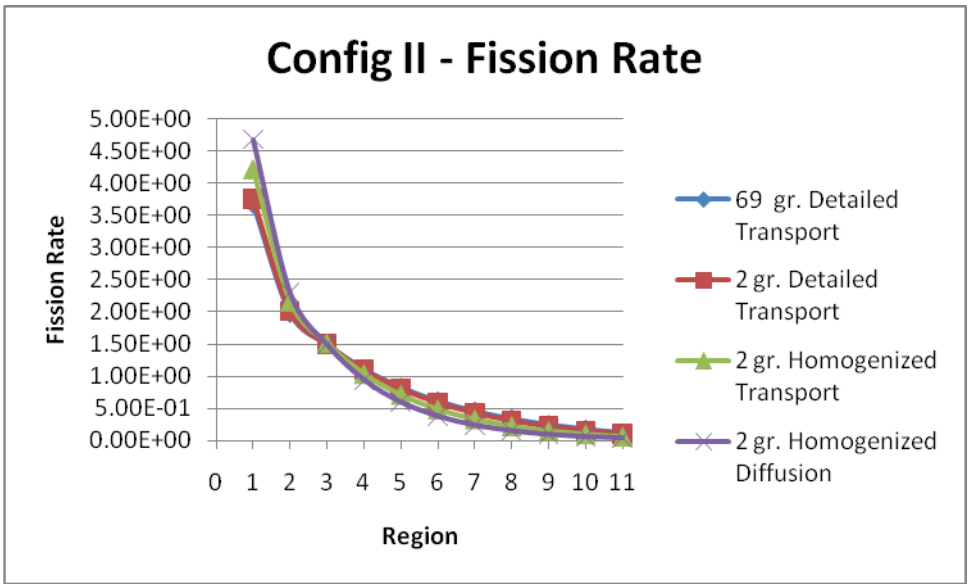

Figure 3.19 – Configuration II, Fission Rate

Error (%)

Nodes	1	2	3	4	5	6
Transport vs. Diffusion %	10.93	6.20	-1.47	-8.79	-15.48	-21.58
Nodes	7	8	9	10	11	
Transport vs. Diffusion %	-27.00	-31.61	-35.03	-36.19	-31.66	

Root Mean Square (%)

23.76 %

Table 3.13 – Configuration II, Fission Rate, Error

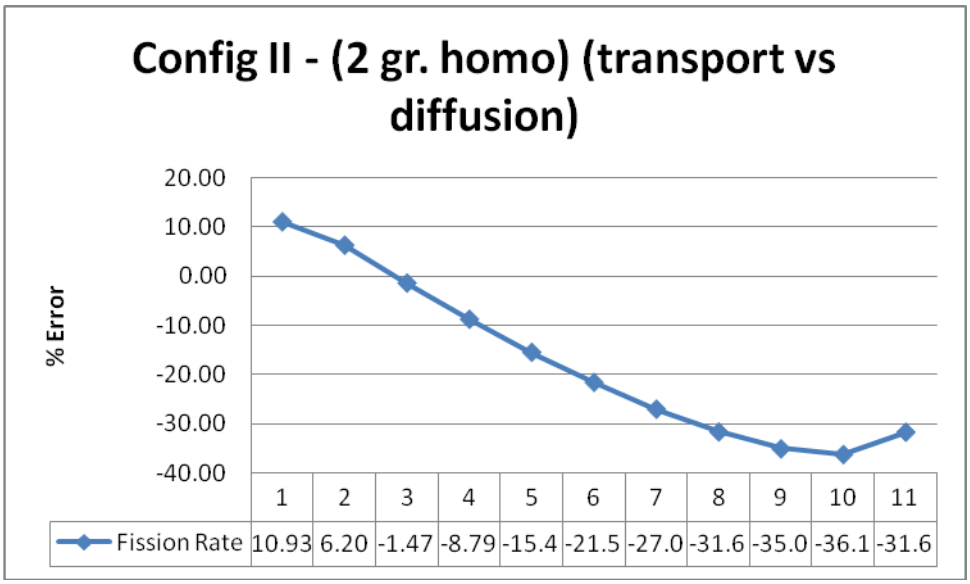

Figure 3.20 – Configuration II, Fission Rate, Error

3.4.3 Configuration III

Fast Flux

Fast Flux	1	2	3	4	5	6
69 gr. Detailed Transport	2.76E+02	2.75E+02	2.74E+02	2.73E+02	2.71E+02	2.69E+02
2 gr. Detailed Transport	2.74E+02	2.74E+02	2.73E+02	2.71E+02	2.70E+02	2.68E+02
2 gr. Homo. Transport	2.67E+02	2.67E+02	2.67E+02	2.67E+02	2.66E+02	2.66E+02
2 gr. Homo. Diffusion	9.18E+01	9.75E+01	1.09E+02	1.27E+02	1.54E+02	1.89E+02

Fast Flux	7	8	9	10	11	12
69 gr. Detailed Transport	2.65E+02	2.61E+02	2.56E+02	2.59E+02	2.78E+02	2.19E+01
2 gr. Detailed Transport	2.65E+02	2.62E+02	2.58E+02	2.64E+02	2.85E+02	2.22E+01
2 gr. Homo. Transport	2.66E+02	2.65E+02	2.65E+02	2.76E+02	2.78E+02	2.50E+01
2 gr. Homo. Diffusion	2.36E+02	2.98E+02	3.77E+02	5.04E+02	6.32E+02	5.03E+01

Table 3.14 – Configuration III, Fast Flux

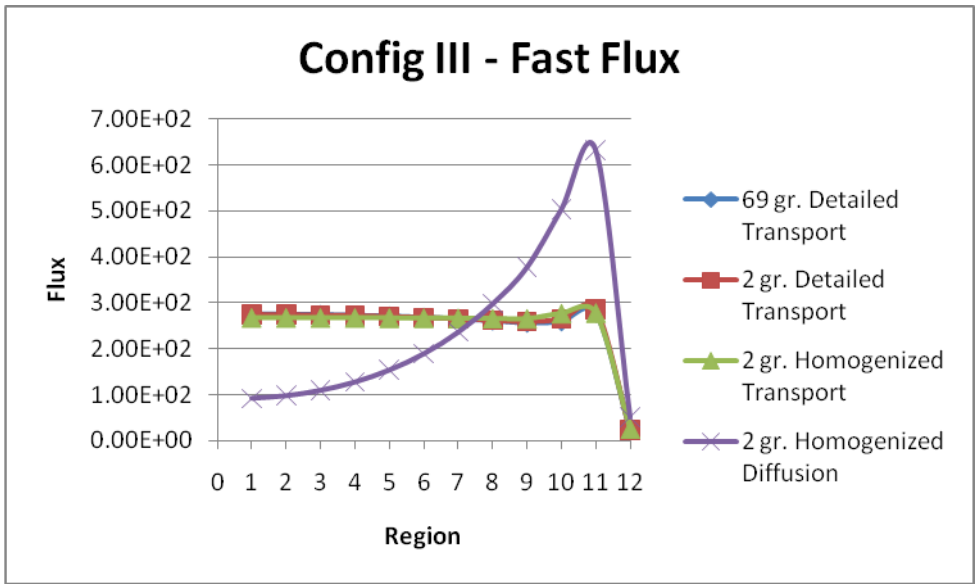

Figure 3.21 – Configuration III, Fast Flux

Error (%)

Nodes	1	2	3	4	5	6
Transport vs. Diffusion %	-65.61	-63.49	-59.11	-52.23	-42.39	-28.99
Nodes	7	8	9	10	11	12
Transport vs. Diffusion %	-11.2	12.16	42.56	82.51	127.78	101.53

Root Mean Square (%)

66.28 %

Table 3.15 – Configuration III, Fast Flux, Error

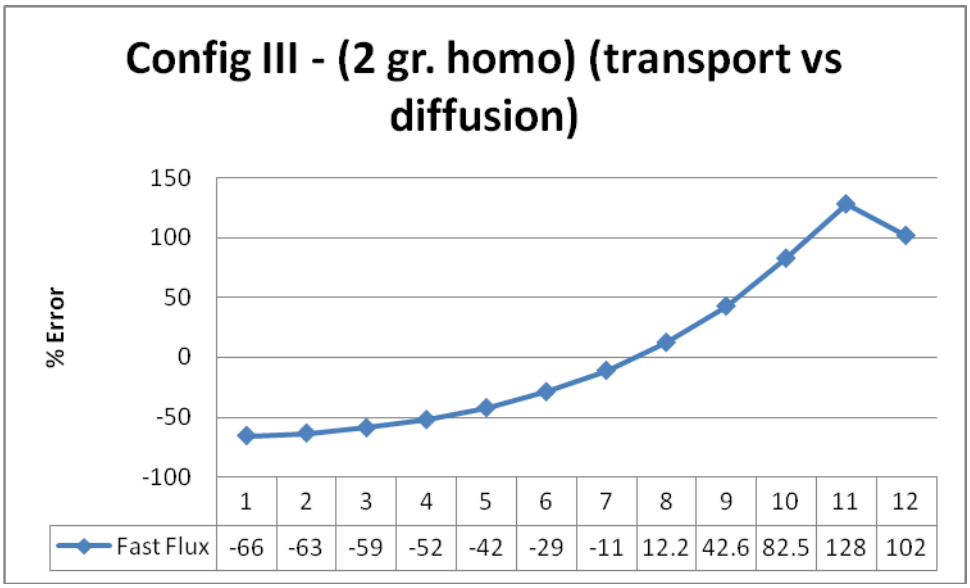

Figure 3.22 – Configuration III, Fast Flux, Error

Thermal Flux

Thermal Flux	1	2	3	4	5	6
69 gr. Detailed Transport	7.61E+02	7.60E+02	7.57E+02	7.54E+02	7.49E+02	7.42E+02
2 gr. Detailed Transport	7.39E+02	7.38E+02	7.36E+02	7.32E+02	7.27E+02	7.21E+02
2 gr. Homo. Transport	7.21E+02	7.21E+02	7.20E+02	7.20E+02	7.19E+02	7.18E+02
2 gr. Homo. Diffusion	2.53E+02	2.68E+02	3.00E+02	3.51E+02	4.23E+02	5.20E+02

Thermal Flux	7	8	9	10	11	12
69 gr. Detailed Transport	7.33E+02	7.21E+02	7.08E+02	6.82E+02	5.90E+02	3.73E+02
2 gr. Detailed Transport	7.14E+02	7.06E+02	6.96E+02	6.75E+02	5.92E+02	3.72E+02
2 gr. Homo. Transport	7.17E+02	7.16E+02	7.14E+02	6.98E+02	6.08E+02	3.63E+02
2 gr. Homo. Diffusion	6.50E+02	8.19E+02	1.04E+03	1.29E+03	1.41E+03	1.02E+03

Table 3.16 – Configuration III, Thermal Flux

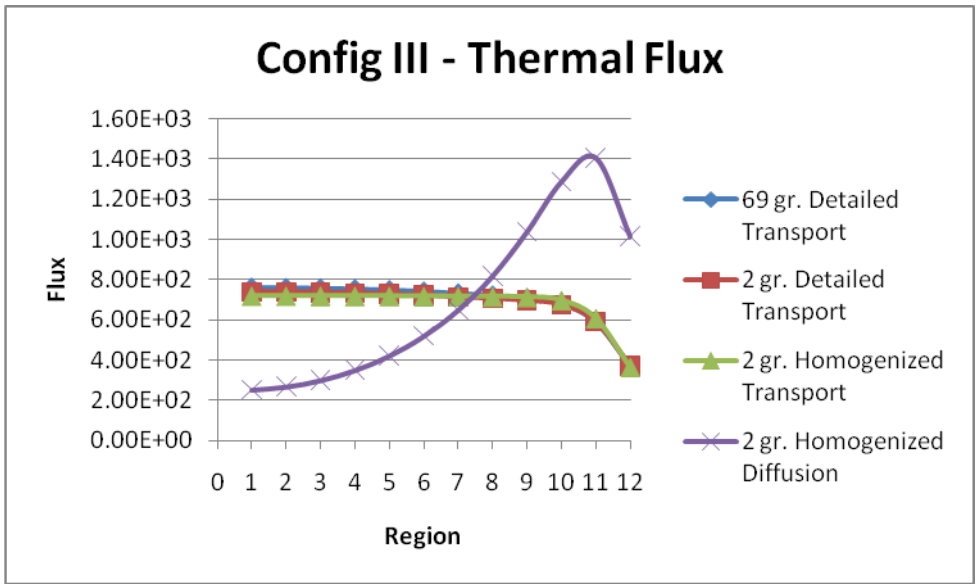

Figure 3.23 – Configuration III, Thermal Flux

Error (%)

Nodes	1	2	3	4	5	6
Transport vs. Diffusion %	-64.92	-62.75	-58.31	-51.28	-41.26	-27.57
Nodes	7	8	9	10	11	12
Transport vs. Diffusion %	-9.4	14.43	45.45	84.47	131.47	180.34

Root Mean Square (%)

79.56 %

Table 3.17 – Configuration III, Thermal Flux, Error

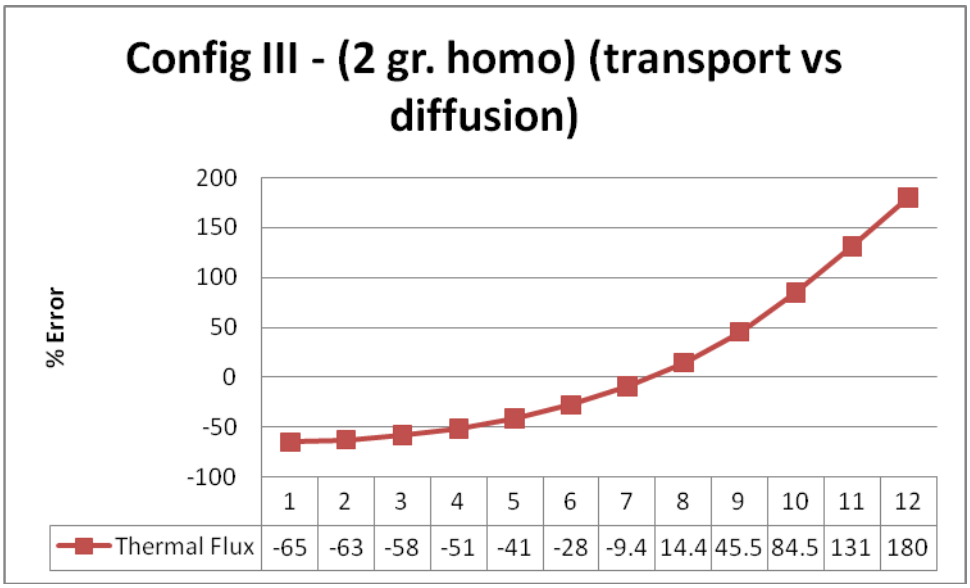

Figure 3.24 – Configuration III, Thermal Flux, Error

Fission Rate

Fission Rate	1	2	3	4	5	6
69 gr. Detailed Transport	1.01E+00	1.01E+00	1.00E+00	9.99E-01	9.92E-01	9.83E-01
2 gr. Detailed Transport	1.00E+00	9.99E-01	9.96E-01	9.91E-01	9.85E-01	9.76E-01
2 gr. Homo. Transport	9.75E-01	9.75E-01	9.75E-01	9.74E-01	9.73E-01	9.72E-01
2 gr. Homo. Diffusion	3.42E-01	3.63E-01	4.06E-01	4.74E-01	5.71E-01	7.03E-01

Fission Rate	7	8	9	10	11
69 gr. Detailed Transport	9.71E-01	9.56E-01	9.38E-01	9.05E-01	1.24E+00
2 gr. Detailed Transport	9.67E-01	9.56E-01	9.42E-01	9.16E-01	1.27E+00
2 gr. Homo. Transport	9.71E-01	9.69E-01	9.67E-01	9.48E-01	1.30E+00
2 gr. Homo. Diffusion	8.78E-01	1.11E+00	1.40E+00	1.75E+00	3.01E+00

Table 3.18 – Configuration III, Fission Rate

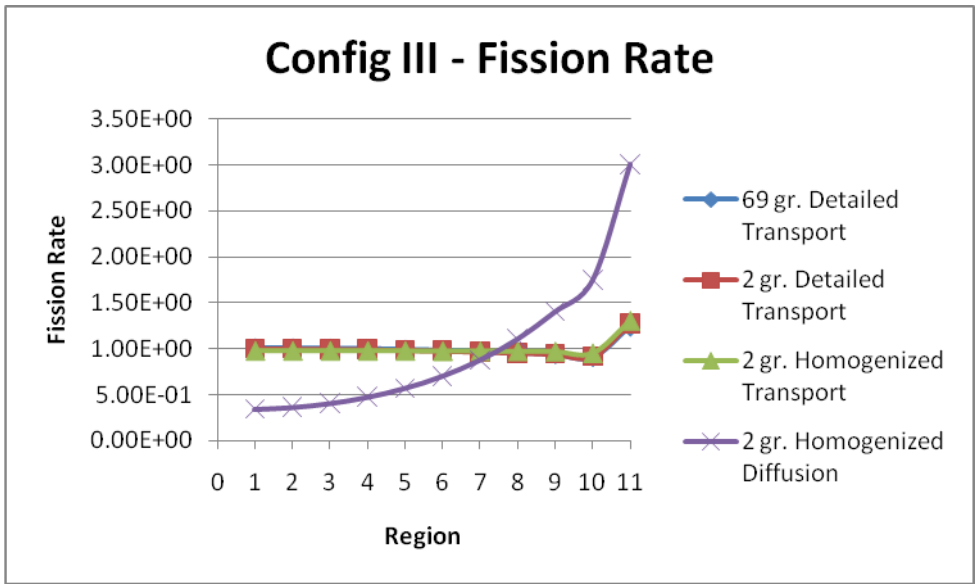

Figure 3.25 - Configuration III, Fission Rate

Error (%)

Nodes	1	2	3	4	5	6
Transport vs. Diffusion %	-64.98	-62.82	-58.37	-51.37	-41.35	-27.69
Nodes	7	8	9	10	11	12
Transport vs. Diffusion %	-9.54	14.24	45.23	84.38	131.15	

Root Mean Square (%)

62.78 %

Table 3.19 – Configuration III, Fission Rate, Error

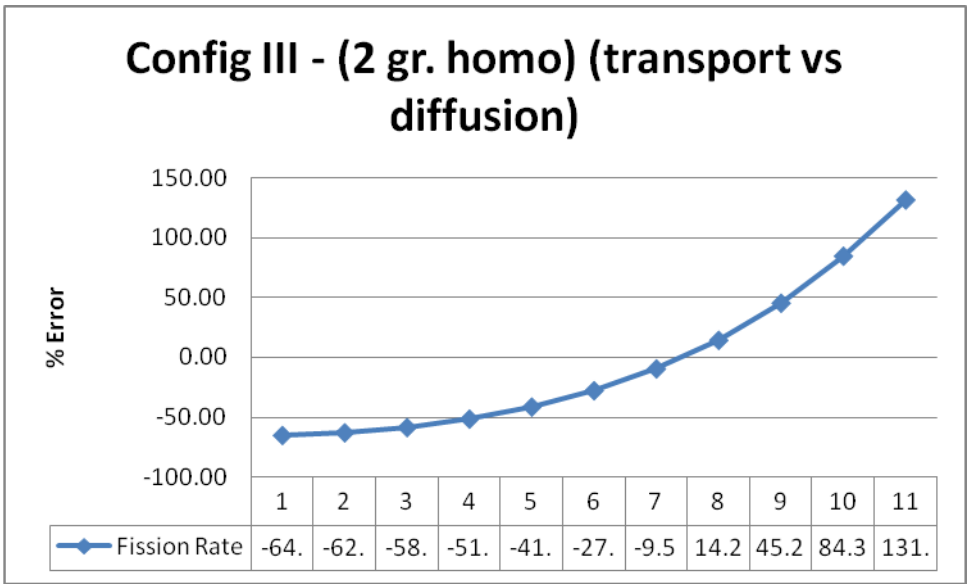

Figure 3.26 – Configuration III, Fission Rate, Error

3.5 Objective

Numerical calculations reveal that the largest error is incurred when going from two-energy-group node-homogenized transport approximation to two-energy-group-node-homogenized diffusion approximation. The work presented here is concerned with reducing the loss in accuracy by appropriately adjusting the values of the diffusion coefficients.

Diffusion theory (as well as the underlying Fick's law) is not valid in the vicinity of a surface or in the presence of a reflector. Assumptions made about the angular flux tend to break down at the fuel-reflector interface. Since diffusion theory is not accurate, this inaccuracy serves as a motivation for coming up with a method that reduces the discrepancy between diffusion and transport. There is a distinct possibility that diffusion theory does not appropriately account for the leakage term. The diffusion term comes into play when deriving the simplified diffusion equation from the transport equation.

4.0 METHOD

"The more complicated and restricted the method, the less the opportunity for expression of one's original sense of freedom. Though they play an important role in the early stage, the techniques should not be too mechanical, complex or restrictive." (Bruce Lee)

To reduce the difference between homogenized-node two-group transport and diffusion results the approach is to manipulate the leakage term with the expectation that one can match diffusion derived results with transport derived results.

4.1 Equating the transport and diffusion leakage terms

For CANDU reactors, because of the small fuel-to-moderator/coolant ratio and the relatively small discharge burnup [~7,500 kWd/kg(U)], the two-group diffusion coefficients vary only approximately 1% with burnup and only approximately 5% between a homogenized fuel node and a moderator-only node. It is therefore reasonable to attempt to use a constant group diffusion coefficient throughout the reactor. In that case the two-group diffusion equations become (with standard notations):

$$
\begin{aligned}
&-D_1\nabla^2\Phi_1(\vec{r})+(\Sigma_{a1}(\vec{r})+\Sigma_{1\to2}(\vec{r}))\Phi_1(\vec{r})-\Sigma_{2\to1}(\vec{r})\Phi_1(\vec{r}) \\
&=\frac{1}{k_{eff}}\chi_1(\nu\Sigma_{f1}(\vec{r})\Phi_1(\vec{r})+\nu\Sigma_{f2}(\vec{r})\Phi_2(\vec{r})) \\
&-D_2\nabla^2\Phi_2(\vec{r})+(\Sigma_{a2}(\vec{r})+\Sigma_{2\to1}(\vec{r}))\Phi_2(\vec{r})-\Sigma_{1\to2}(\vec{r})\Phi_1(\vec{r}) \\
&=\frac{1}{k_{eff}}\chi_2(\nu\Sigma_{f1}(\vec{r})\Phi_1(\vec{r})+\nu\Sigma_{f2}(\vec{r})\Phi_2(\vec{r}))
\end{aligned}
\qquad 4.1
$$

The validity of the constant-diffusion-coefficient approximation is ultimately determined by how close the solution of the set of equations (4.1) is to the solution of the two-group transport equations.

Assuming that the two-group transport integral flux, $\begin{bmatrix} \Phi_1^{tr} \\ \Phi_2^{tr} \end{bmatrix}$ is known, and that it is sufficiently close to the diffusion integral flux in Eq. 4.1, "empirical" diffusion coefficients can be calculated [4] as ratios between the weighted integral of the leakage term and the weighted integral of the Laplacian of the flux:

$$D_1 = \frac{\left\{ \begin{array}{l} \int w_1(\vec{r})[(\Sigma_{a1}(\vec{r}) + \Sigma_{1\to 2}(\vec{r}))\Phi_1{}^{tr}(\vec{r}) - \Sigma_{2\to 1}(\vec{r})\Phi_1{}^{tr}(\vec{r})]d^3r \\ -\frac{1}{k_{eff}^{tr}} \int w_1(\vec{r})[\chi_1(\nu\Sigma_{f1}(\vec{r})\Phi_1{}^{tr}(\vec{r}) + \nu\Sigma_{f2}(\vec{r})\Phi_2{}^{tr}(\vec{r}))]d^3r \end{array} \right\}}{\int w_1(\vec{r})\nabla^2\Phi_1{}^{tr}(\vec{r})d^3r} \qquad 4.2$$

$$D_2 = \frac{\left\{ \begin{array}{l} \int w_2(\vec{r})[(\Sigma_{a2}(\vec{r}) + \Sigma_{2\to 1}(\vec{r}))\Phi_2(\vec{r}) - \Sigma_{1\to 2}(\vec{r})\Phi_1(\vec{r})]d^3r \\ -\frac{1}{k_{eff}^{tr}} \int w_2(\vec{r})[\chi_2(\nu\Sigma_{f1}(\vec{r})\Phi_1(\vec{r}) + \nu\Sigma_{f2}(\vec{r})\Phi_2(\vec{r}))]d^3r \end{array} \right\}}{\int w_2(\vec{r})\nabla^2\Phi_2{}^{tr}(\vec{r})d^3r}$$

The proposed method assumes that diffusion coefficients calculated using Eq. (4.2) for a model consisting entirely of fresh fuel nodes (and a reflector) can subsequently be used in any model, consisting of any combination of fuel and reflector nodes. The assumption stems from the expectation that variations in the "empirical" diffusion coefficients (with fresh and between fuel nodes and reflector nodes) are small, just like those in the "theoretical" (calculated as $\frac{1}{3\Sigma_{tr}}$) diffusion coefficients.

To work out the diffusion term in a one-dimensional case we need to use an approximation method to solve for the double derivatives. To obtain a solution a discretization method such as finite differences can be used. The convention used in this thesis is illustrated in Figure 2.3.

5.0 CALCULATIONS AND RESULTS

"Restlessness is discontent — and discontent is the first necessity of progress." (Thomas Edison)

5.1 Calculations

To test the validity of the proposed method, the same test model and fuel configurations as in the preliminary study were used.

The diffusion calculations are similar to the ones performed in chapter 3 except that the corrected diffusion coefficient, calculated using equations 4.1-4.2, is used instead of the traditional diffusion coefficient ($\frac{1}{3\Sigma_{tr}}$) . In Eqs. (4.2) all fuel nodes are assigned homogenized cross sections corresponding to fresh fuel. The weight function is chosen to be equal to unity everywhere except in meshes near boundaries, where it is chosen to be zero, to avoid results being skewed by the presence of boundaries.

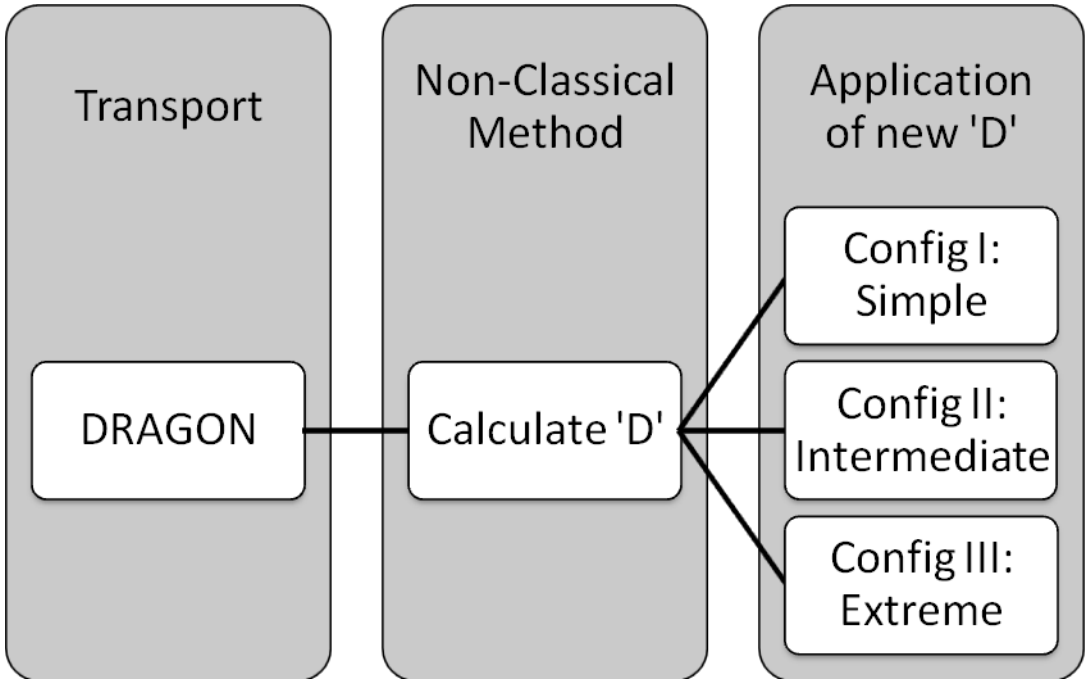

Figure 5.1 – Use of Empirical Diffusion Coefficient

5.2 Results

Section 5.3 represents the shift from step 3 to step 4 (Refer 1.0 – Introduction)

Section 5.4 represents the shift from step 1 to step 4 (Refer 1.0 – Introduction)

5.3 Comparison of two-group homogenized-node using diffusion (old, new) and transport

5.3.1 Configuration I

Fast Flux

Fast Flux	1	2	3	4	5	6
2 gr. Homo. Transport	3.01E+02	2.96E+02	2.86E+02	2.72E+02	2.54E+02	2.32E+02
2 gr. Homo. Diffusion	2.86E+02	2.82E+02	2.74E+02	2.62E+02	2.47E+02	2.28E+02
Corrected Diffusion	3.00E+02	2.95E+02	2.86E+02	2.72E+02	2.54E+02	2.31E+02

Fast Flux	7	8	9	10	11	12
2 gr. Homo. Transport	2.05E+02	1.76E+02	1.44E+02	1.09E+02	6.66E+01	5.20E+00
2 gr. Homo. Diffusion	2.07E+02	1.82E+02	1.55E+02	1.25E+02	8.63E+01	5.91E+00
Corrected Diffusion	2.05E+02	1.76E+02	1.44E+02	1.10E+02	6.74E+01	5.22E+00

Table 5.1 – Configuration I, Fast Flux

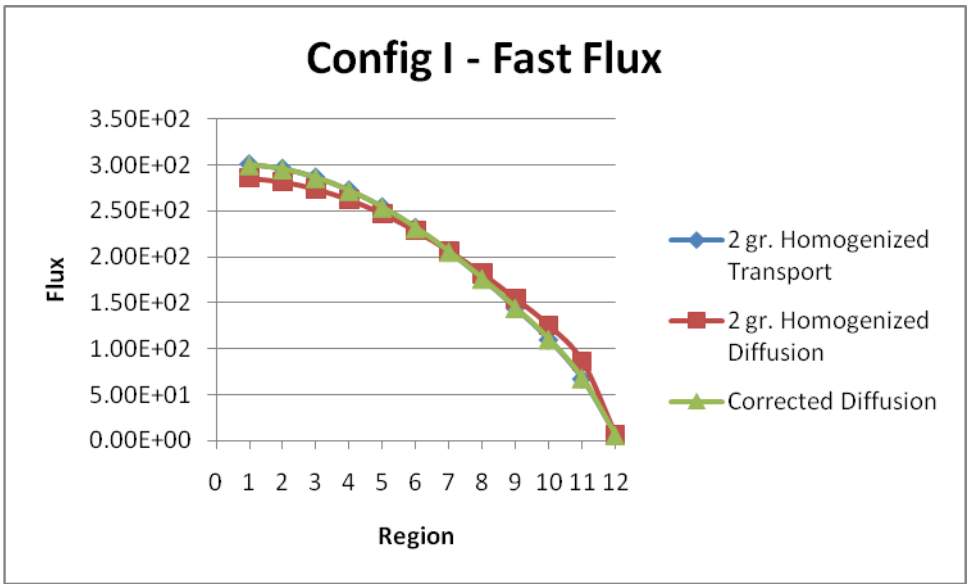

Figure 5.2 – Configuration I, Fast Flux

Error (%)

Nodes	1	2	3	4	5	6
Transport vs. Diffusion %	-4.92	-4.71	-4.32	-3.66	-2.71	-1.36
Transport vs. [C] Diffusion %	-0.17	-0.15	-0.13	-0.13	-0.11	-0.07

Nodes	7	8	9	10	11	12
Transport vs. Diffusion %	0.53	3.31	7.5	14.7	29.61	13.6
Transport vs. [C] Diffusion %	-0.01	0.07	0.26	0.6	1.27	0.3

Root Mean Square (%)

Original: 10.93 % | Corrected: 0.43 %

Table 5.2 – Configuration I, Fast Flux, Error

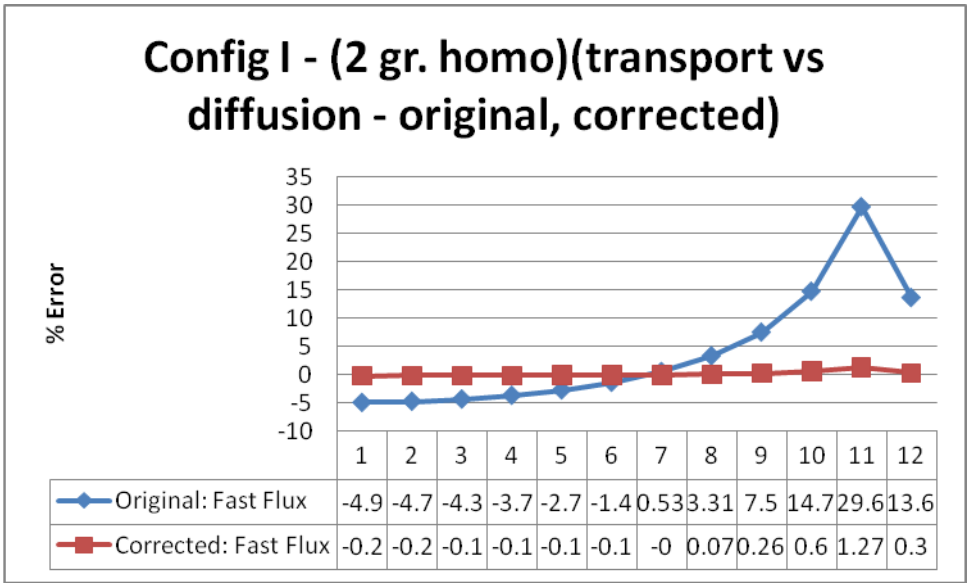

Figure 5.3 – Configuration I, Fast Flux, Error

Thermal Flux

Thermal Flux	1	2	3	4	5	6
2 gr. Homo. Transport	6.65E+02	6.54E+02	6.33E+02	6.02E+02	5.62E+02	5.12E+02
2 gr. Homo. Diffusion	6.33E+02	6.25E+02	6.07E+02	5.82E+02	5.48E+02	5.06E+02
Corrected Diffusion	6.64E+02	6.53E+02	6.32E+02	6.01E+02	5.61E+02	5.12E+02

Thermal Flux	7	8	9	10	11	12
2 gr. Homo. Transport	4.54E+02	3.89E+02	3.18E+02	2.41E+02	1.68E+02	8.92E+01
2 gr. Homo. Diffusion	4.58E+02	4.03E+02	3.42E+02	2.77E+02	2.19E+02	1.38E+02
Corrected Diffusion	4.54E+02	3.89E+02	3.19E+02	2.42E+02	1.70E+02	9.09E+01

Table 5.3 – Configuration I, Thermal Flux

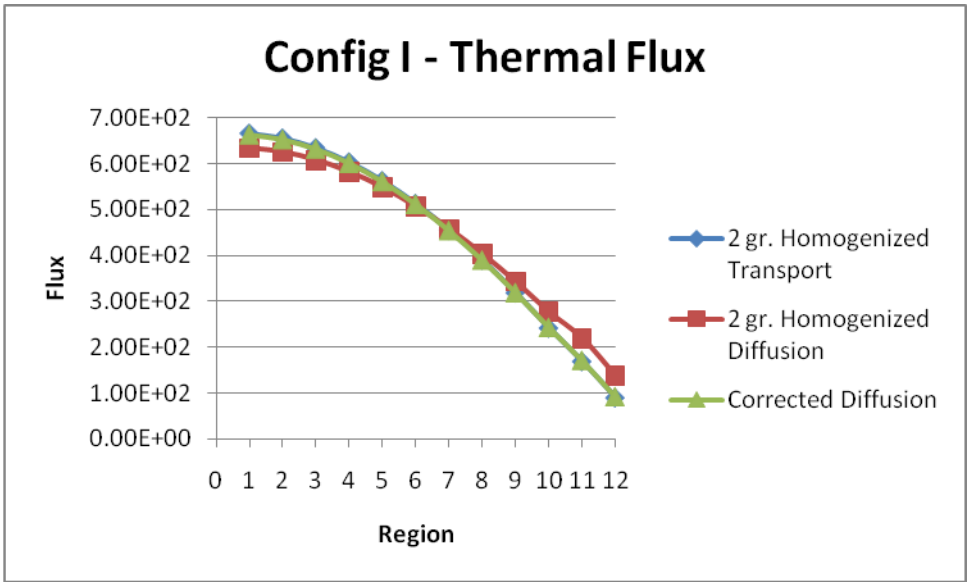

Figure 5.4 – Configuration I, Thermal Flux

Error (%)

Nodes	1	2	3	4	5	6
Transport vs. Diffusion %	10.17	5.12	-2.02	-9.12	-15.81	-21.86
Transport vs. [C] Diffusion %	-0.21	-0.01	0.05	0.11	0.2	0.25

Nodes	7	8	9	10	11	12
Transport vs. Diffusion %	-27.28	-31.89	-35.28	-36.38	-32.03	-41.27
Transport vs. [C] Diffusion %	0.31	0.36	0.45	0.66	1.3	0.32

Root Mean Square (%)

Original: 25.83 % | Corrected: 0.48 %

Table 5.4 – Configuration I, Thermal Flux, Error

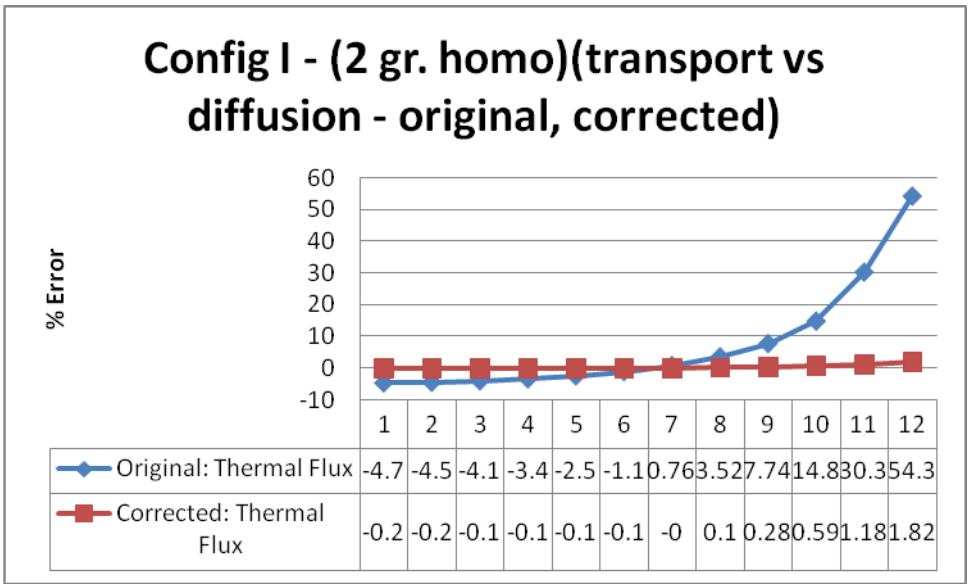

Figure 5.5 – Configuration I, Thermal Flux, Error

Fission Rate

Fission Rate	1	2	3	4	5	6
2 gr. Homo. Transport	1.41E+00	1.38E+00	1.34E+00	1.27E+00	1.19E+00	1.08E+00
2 gr. Homo. Diffusion	1.34E+00	1.32E+00	1.29E+00	1.23E+00	1.16E+00	1.07E+00
Corrected Diffusion	1.41E+00	1.38E+00	1.34E+00	1.27E+00	1.19E+00	1.08E+00

Fission Rate	7	8	9	10	11
2 gr. Homo. Transport	9.61E-01	8.23E-01	6.72E-01	5.10E-01	3.54E-01
2 gr. Homo. Diffusion	9.68E-01	8.52E-01	7.24E-01	5.86E-01	4.61E-01
Corrected Diffusion	9.61E-01	8.24E-01	6.74E-01	5.13E-01	3.58E-01

Table 5.5 – Configuration I, Fission Rate

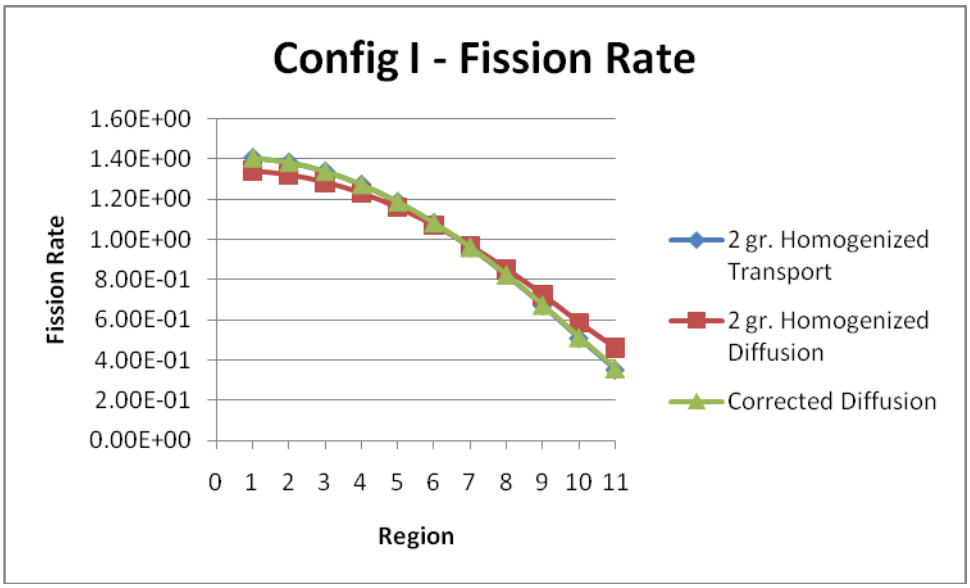

Figure 5.6 - Configuration I, Fission Rate

Error (%)

Nodes	1	2	3	4	5	6
Transport vs. Diffusion %	-4.70	-4.53	-4.13	-3.43	-2.50	-1.17
Transport vs. [C] Diffusion %	-0.15	-0.12	-0.18	-0.14	-0.14	-0.06

Nodes	7	8	9	10	11	
Transport vs. Diffusion %	0.74	3.51	7.73	14.83	30.29	
Transport vs. [C] Diffusion %	-0.01	0.11	0.27	0.58	1.16	

<u>Root Mean Square</u> (%)

Original: 10.83 % | Corrected: 0.41 %

Table 5.6 – Configuration I, Fission Rate, Error

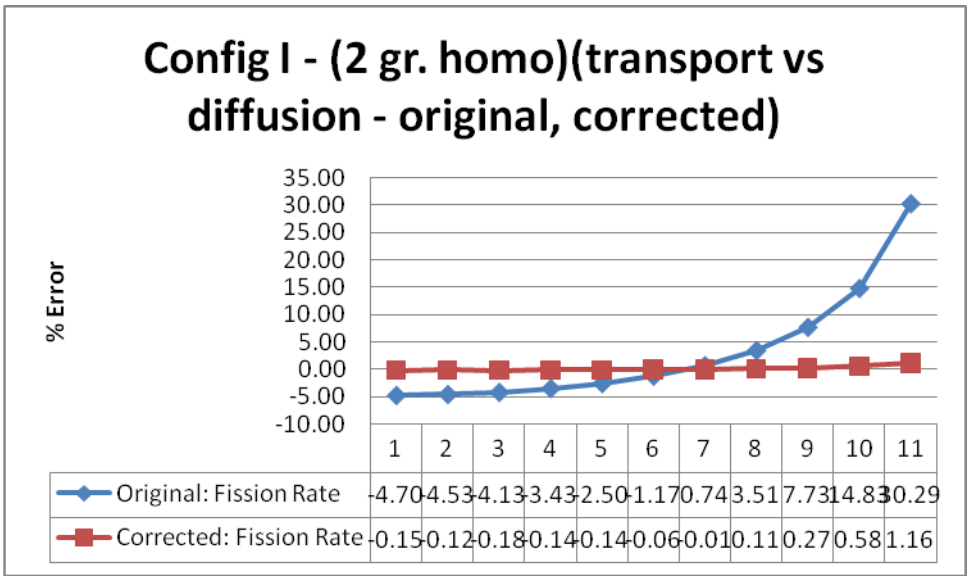

Figure 5.7 – Configuration I, Fission Rate, Error

5.3.2 Configuration II

Fast Flux

Fast Flux	1	2	3	4	5	6
2 gr. Homo. Transport	9.89E+02	5.97E+02	3.86E+02	2.64E+02	1.81E+02	1.24E+02
2 gr. Homo. Diffusion	1.09E+03	6.28E+02	3.78E+02	2.40E+02	1.53E+02	9.68E+01
Corrected Diffusion	9.87E+02	5.98E+02	3.86E+02	2.65E+02	1.82E+02	1.24E+02

Fast Flux	7	8	9	10	11	12
2 gr. Homo. Transport	8.45E+01	5.73E+01	3.83E+01	2.49E+01	1.36E+01	1.02E+00
2 gr. Homo. Diffusion	6.15E+01	3.90E+01	2.48E+01	1.58E+01	9.27E+00	6.02E-01
Corrected Diffusion	8.48E+01	5.75E+01	3.85E+01	2.50E+01	1.38E+01	1.03E+00

Table 5.7 – Configuration II, Fast Flux

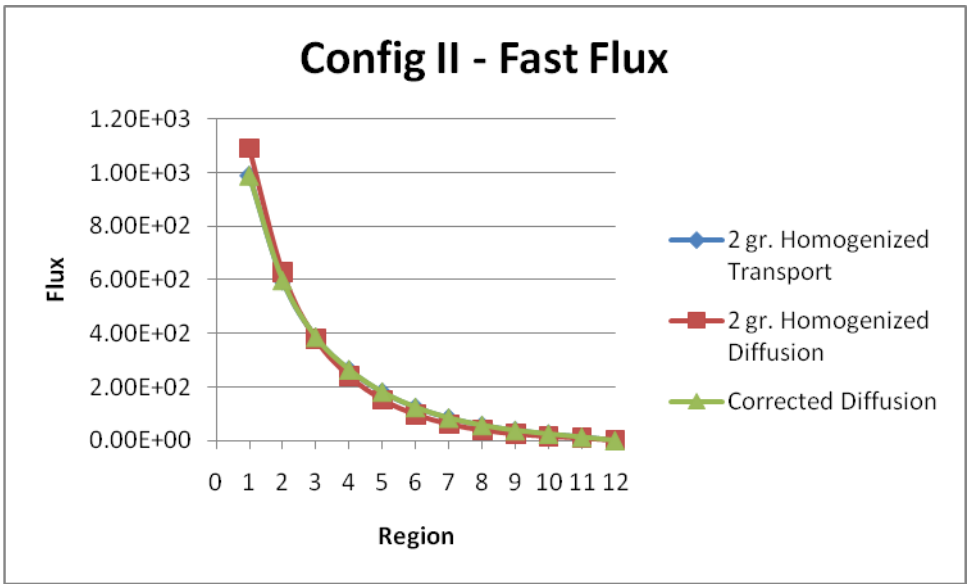

Figure 5.8 – Configuration II, Fast Flux

Error (%)

Nodes	1	2	3	4	5	6
Transport vs. Diffusion %	10.17	5.12	-2.02	-9.12	-15.81	-21.86
Transport vs. [C] Diffusion %	-0.21	-0.01	0.05	0.11	0.2	0.25

Nodes	7	8	9	10	11	12
Transport vs. Diffusion %	-27.28	-31.89	-35.28	-36.38	-32.03	-41.27
Transport vs. [C] Diffusion %	0.31	0.36	0.45	0.66	1.3	0.32

Root Mean Square (%)

Original: 25.83 % | Corrected: 0.48 %

Table 5.8 – Configuration II, Fast Flux, Error

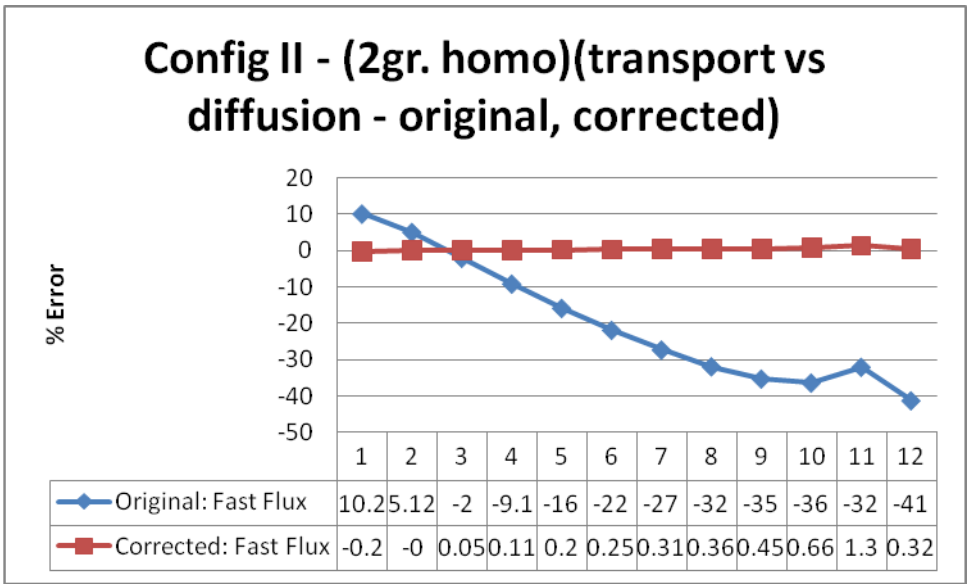

Figure 5.9 – Configuration II, Fast Flux, Error

Thermal Flux

Thermal Flux	1	2	3	4	5	6
2 gr. Homo. Transport	1.97E+03	1.61E+03	1.13E+03	7.73E+02	5.29E+02	3.62E+02
2 gr. Homo. Diffusion	2.18E+03	1.71E+03	1.11E+03	7.06E+02	4.48E+02	2.84E+02
Corrected Diffusion	1.97E+03	1.61E+03	1.13E+03	7.74E+02	5.30E+02	3.63E+02

Thermal Flux	7	8	9	10	11	12
2 gr. Homo. Transport	2.47E+02	1.67E+02	1.12E+02	7.24E+01	4.50E+01	2.18E+01
2 gr. Homo. Diffusion	1.80E+02	1.14E+02	7.27E+01	4.62E+01	3.08E+01	1.71E+01
Corrected Diffusion	2.48E+02	1.68E+02	1.12E+02	7.29E+01	4.56E+01	2.22E+01

Table 5.9 – Configuration II, Thermal Flux

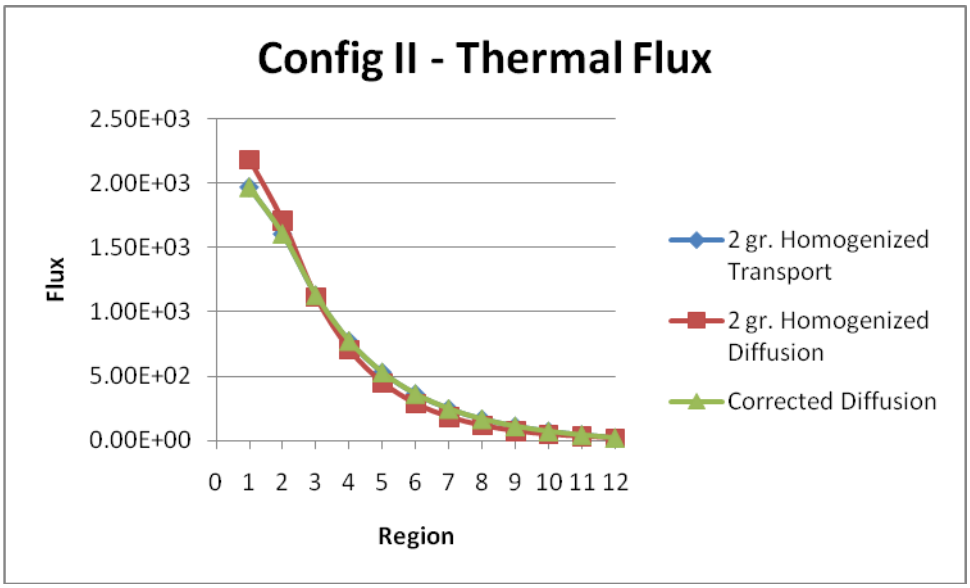

Figure 5.10 – Configuration II, Thermal Flux

Error (%)

Nodes	1	2	3	4	5	6
Transport vs. Diffusion %	10.98	6.28	-1.38	-8.75	-15.45	-21.56
Transport vs. [C] Diffusion %	-0.14	-0.07	0.04	0.1	0.18	0.24

Nodes	7	8	9	10	11	12
Transport vs. Diffusion %	-26.98	-31.61	-35.01	-36.18	-31.63	-21.33
Transport vs. [C] Diffusion %	0.28	0.38	0.43	0.67	1.2	1.86

<u>Root Mean Square</u> (%)

Original: 23.56 % | Corrected: 0.70 %

Table 5.10 – Configuration II, Thermal Flux, Error

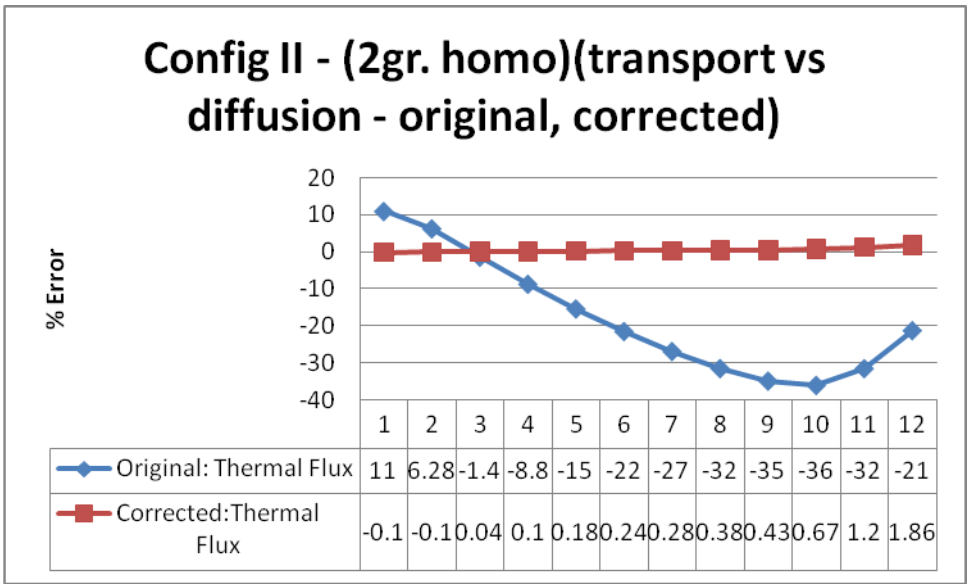

Figure 5.11 – Configuration II, Thermal Flux, Error

Fission Rate

Fission Rate	1	2	3	4	5	6
2 gr. Homo. Transport	4.22E+00	2.16E+00	1.52E+00	1.04E+00	7.11E-01	4.86E-01
2 gr. Homo. Diffusion	4.68E+00	2.30E+00	1.49E+00	9.47E-01	6.01E-01	3.81E-01
Corrected Diffusion	4.22E+00	2.16E+00	1.52E+00	1.04E+00	7.12E-01	4.87E-01

Fission Rate	7	8	9	10	11
2 gr. Homo. Transport	3.31E-01	2.25E-01	1.50E-01	9.73E-02	6.02E-02
2 gr. Homo. Diffusion	2.42E-01	1.54E-01	9.76E-02	6.21E-02	4.11E-02
Corrected Diffusion	3.32E-01	2.25E-01	1.51E-01	9.79E-02	6.09E-02

Table 5.11 – Configuration II, Fission Rate

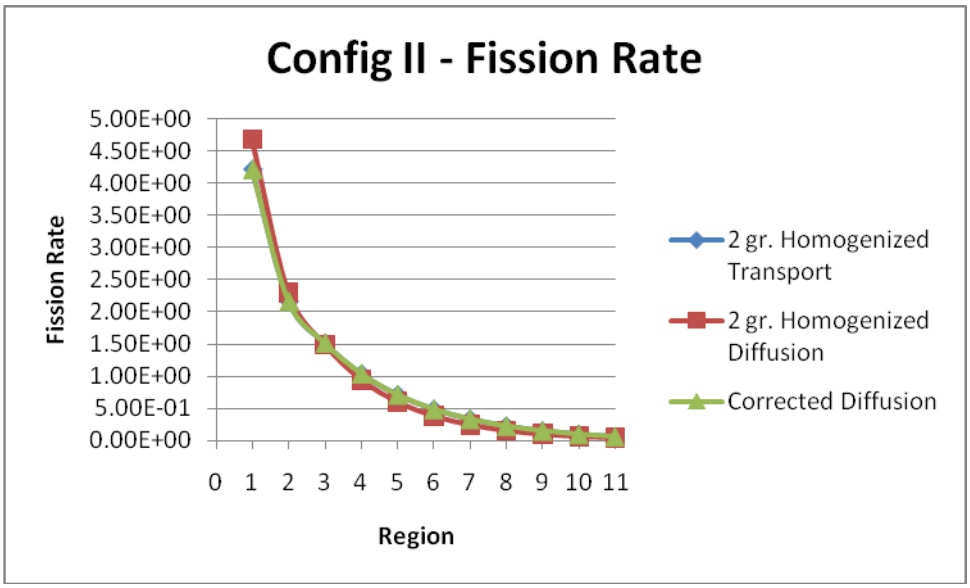

Figure 5.12 - Configuration II, Fission Rate

Error (%)

Nodes	1	2	3	4	5	6
Transport vs. Diffusion %	10.93	6.20	-1.47	-8.79	-15.48	-21.58
Transport vs. [C] Diffusion %	-0.16	-0.04	0.05	0.08	0.18	0.24

Nodes	7	8	9	10	11	
Transport vs. Diffusion %	-27.00	-31.61	-35.03	-36.19	-31.66	
Transport vs. [C] Diffusion %	0.31	0.36	0.43	0.68	1.21	

Root Mean Square (%)

Original: 23.76 % | Corrected: 0.47 %

Table 5.12 – Configuration II, Fission Rate, Error

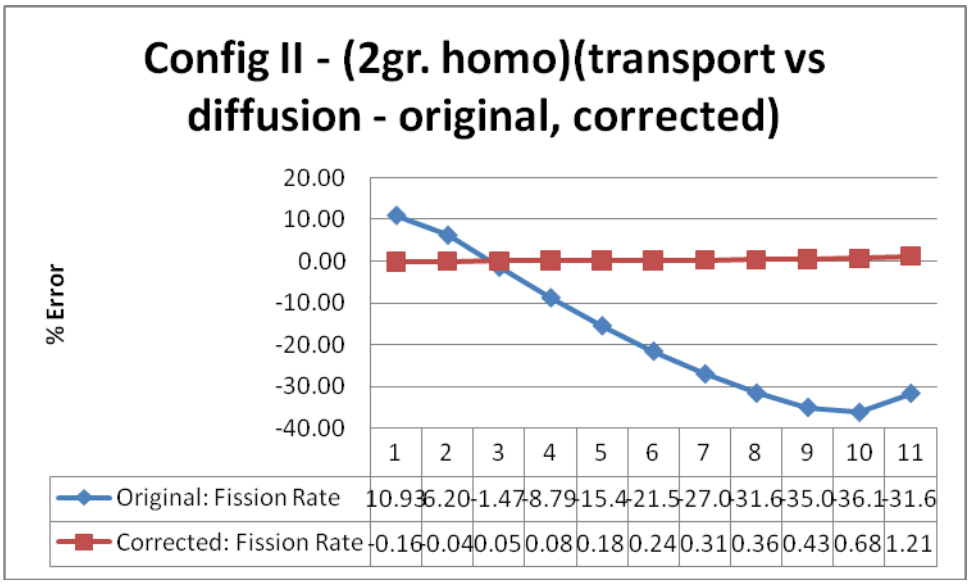

Figure 5.13 – Configuration II, Fission Rate, Error

5.3.3 Configuration III

Fast Flux

Fast Flux	1	2	3	4	5	6
2 gr. Homo. Transport	2.67E+02	2.67E+02	2.67E+02	2.67E+02	2.66E+02	2.66E+02
2 gr. Homo. Diffusion	9.18E+01	9.75E+01	1.09E+02	1.27E+02	1.54E+02	1.89E+02
Corrected Diffusion	2.63E+02	2.63E+02	2.64E+02	2.64E+02	2.64E+02	2.65E+02

Fast Flux	7	8	9	10	11	12
2 gr. Homo. Transport	2.66E+02	2.65E+02	2.65E+02	2.76E+02	2.78E+02	2.50E+01
2 gr. Homo. Diffusion	2.36E+02	2.98E+02	3.77E+02	5.04E+02	6.32E+02	5.03E+01
Corrected Diffusion	2.66E+02	2.66E+02	2.67E+02	2.81E+02	2.84E+02	2.53E+01

Table 5.13 – Configuration III, Fast Flux

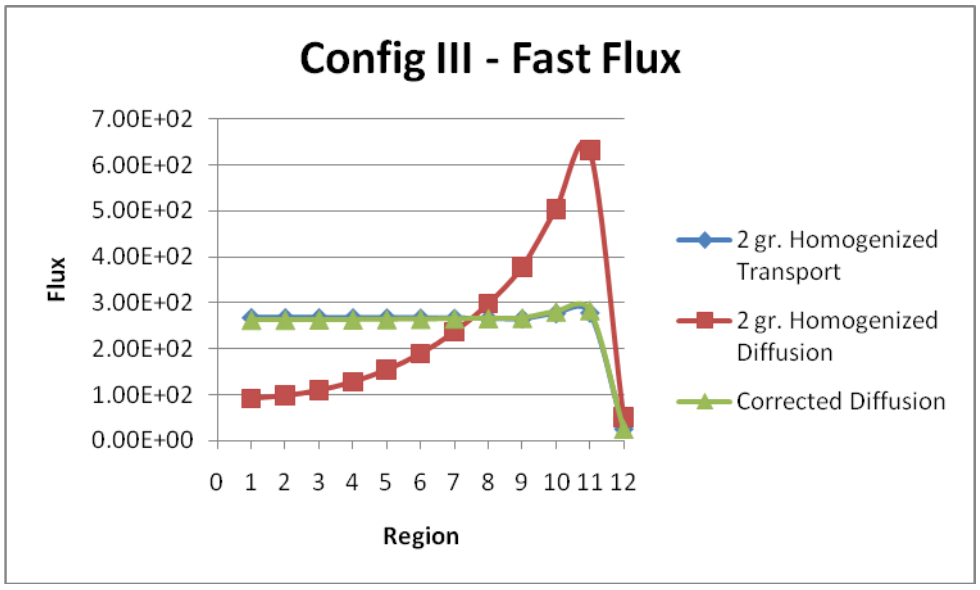

Figure 5.14 – Configuration III, Fast Flux

Error (%)

Nodes	1	2	3	4	5	6
Transport vs. Diffusion %	-65.61	-63.49	-59.11	-52.23	-42.39	-28.99
Transport vs. [C] Diffusion %	-1.45	-1.4	-1.25	-1.09	-0.81	-0.48

Nodes	7	8	9	10	11	12
Transport vs. Diffusion %	-11.2	12.16	42.56	82.51	127.78	101.53
Transport vs. [C] Diffusion %	-0.06	0.44	1.01	1.78	2.41	1.42

Root Mean Square (%)

Original: 66.28 % | Corrected: 1.29 %

Table 5.14 – Configuration III, Fast Flux, Error

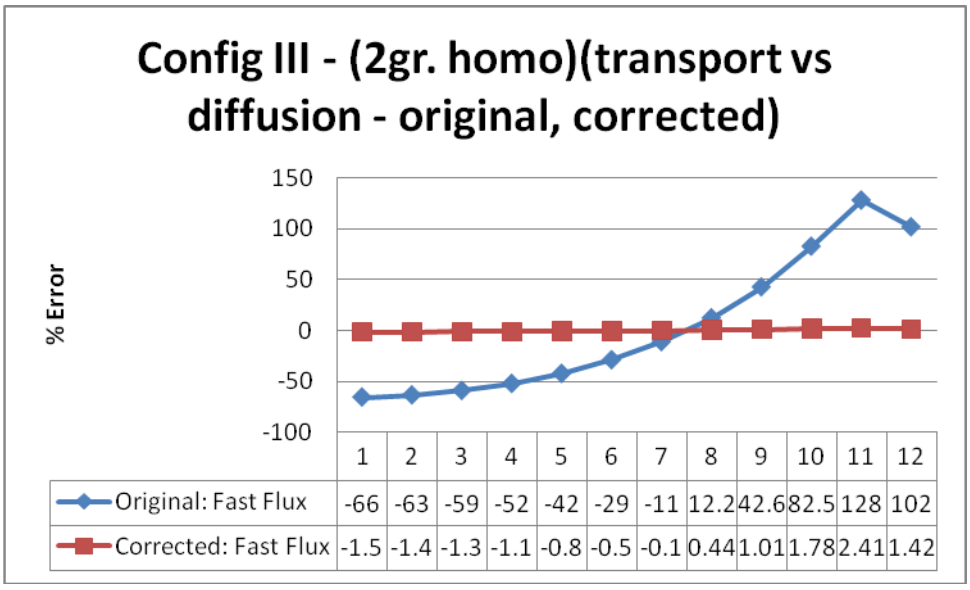

Figure 5.15 – Configuration III, Fast Flux, Error

Thermal Flux

Thermal Flux	1	2	3	4	5	6
2 gr. Homo. Transport	7.21E+02	7.21E+02	7.20E+02	7.20E+02	7.19E+02	7.18E+02
2 gr. Homo. Diffusion	2.53E+02	2.68E+02	3.00E+02	3.51E+02	4.23E+02	5.20E+02
Corrected Diffusion	7.10E+02	7.11E+02	7.11E+02	7.12E+02	7.14E+02	7.15E+02

Thermal Flux	7	8	9	10	11	12
2 gr. Homo. Transport	7.17E+02	7.16E+02	7.14E+02	6.98E+02	6.08E+02	3.63E+02
2 gr. Homo. Diffusion	6.50E+02	8.19E+02	1.04E+03	1.29E+03	1.41E+03	1.02E+03
Corrected Diffusion	7.17E+02	7.20E+02	7.22E+02	7.10E+02	6.22E+02	3.74E+02

Table 5.15 – Configuration III, Thermal Flux

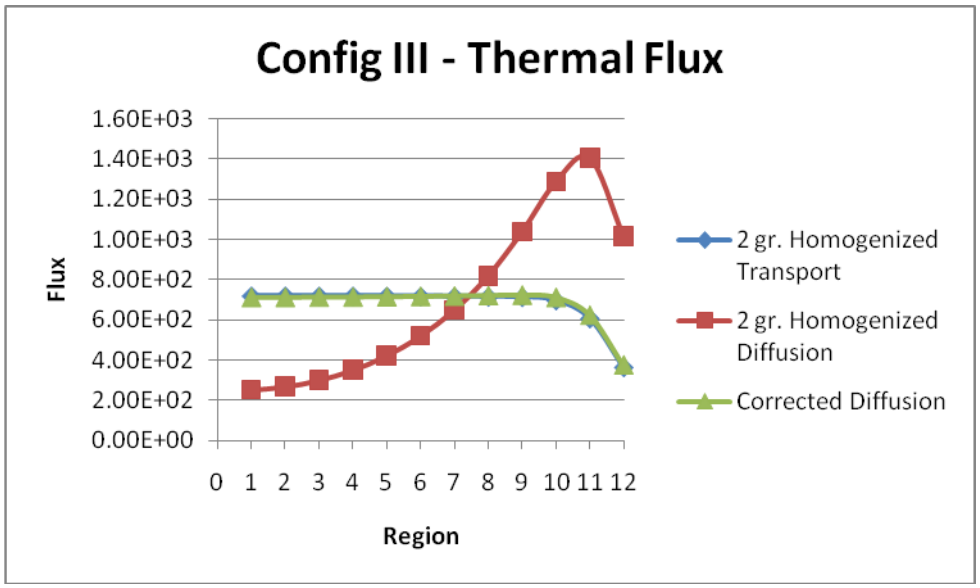

Figure 5.16 – Configuration III, Thermal Flux

Error (%)

Nodes	1	2	3	4	5	6
Transport vs. Diffusion %	-64.92	-62.75	-58.31	-51.28	-41.26	-27.57
Transport vs. [C] Diffusion %	-1.43	-1.37	-1.24	-1.04	-0.77	-0.43

Nodes	7	8	9	10	11	12
Transport vs. Diffusion %	-9.4	14.43	45.45	84.47	131.47	180.34
Transport vs. [C] Diffusion %	-0.02	0.48	1.06	1.7	2.34	3.02

Root Mean Square (%)

Original: 79.56 % | Corrected: 1.48 %

Table 5.16 – Configuration III, Thermal Flux, Error

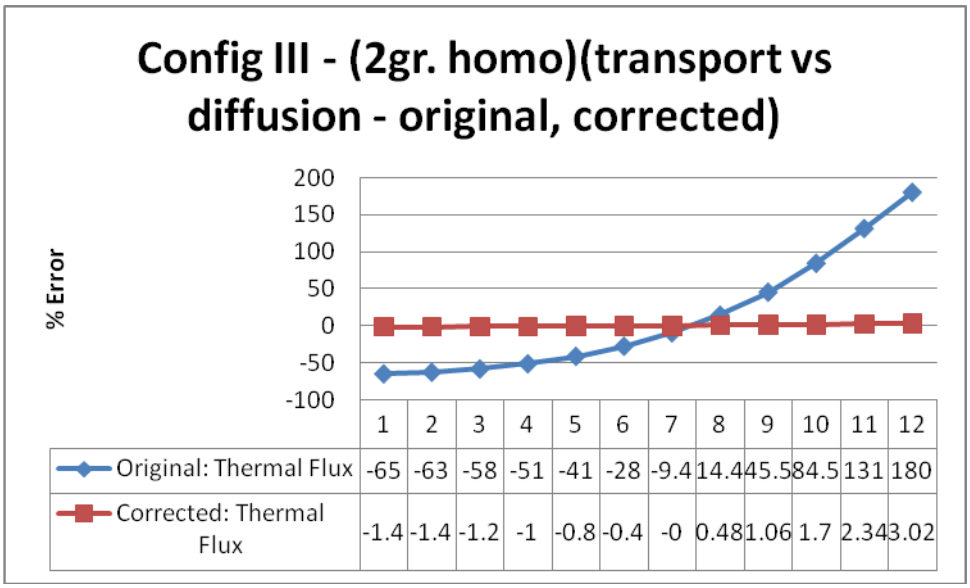

Figure 5.17 – Configuration III, Thermal Flux, Error

Fission Rate (s^{-1})

Fission Rate	1	2	3	4	5	6
2 gr. Homo. Transport	9.75E-01	9.75E-01	9.75E-01	9.74E-01	9.73E-01	9.72E-01
2 gr. Homo. Diffusion	3.42E-01	3.63E-01	4.06E-01	4.74E-01	5.71E-01	7.03E-01
Corrected Diffusion	9.61E-01	9.62E-01	9.63E-01	9.64E-01	9.66E-01	9.68E-01

Fission Rate	7	8	9	10	11
2 gr. Homo. Transport	9.71E-01	9.69E-01	9.67E-01	9.48E-01	1.30E+00
2 gr. Homo. Diffusion	8.78E-01	1.11E+00	1.40E+00	1.75E+00	3.01E+00
Corrected Diffusion	9.71E-01	9.74E-01	9.77E-01	9.64E-01	1.33E+00

Table 5.17 – Configuration III, Fission Rate

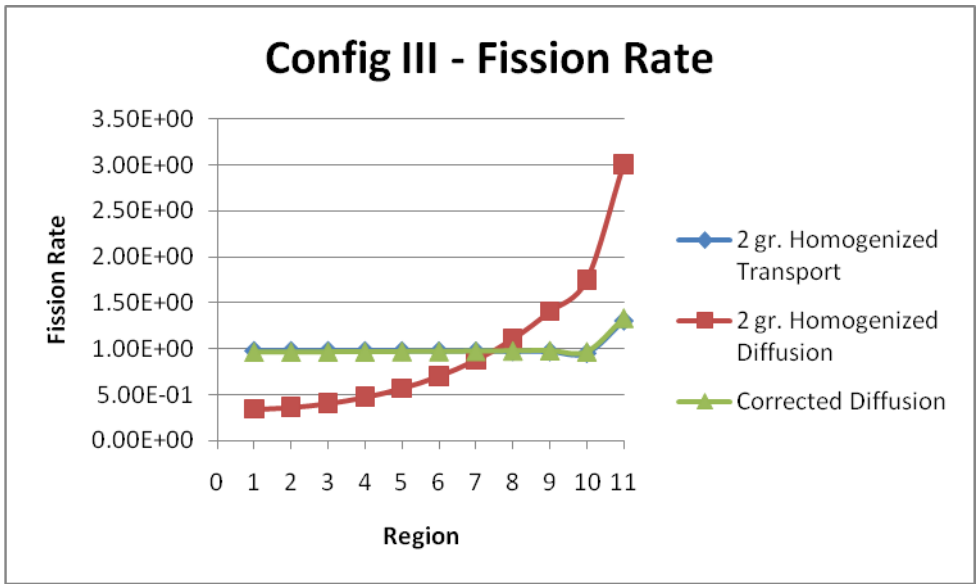

Figure 5.18 - Configuration III, Fission Rate

Error (%)

Nodes	1	2	3	4	5	6
Transport vs. Diffusion %	-64.98	-62.82	-58.37	-51.37	-41.35	-27.69
Transport vs. [C] Diffusion %	-1.44	-1.37	-1.24	-1.04	-0.78	-0.43

Nodes	7	8	9	10	11	12
Transport vs. Diffusion %	-9.54	14.24	45.23	84.38	131.15	
Transport vs. [C] Diffusion %	-0.01	0.48	1.05	1.70	2.35	

Root Mean Square (%)

Original: 62.78 % | Corrected: 1.25 %

Table 5.18 – Configuration III, Fission Rate, Error

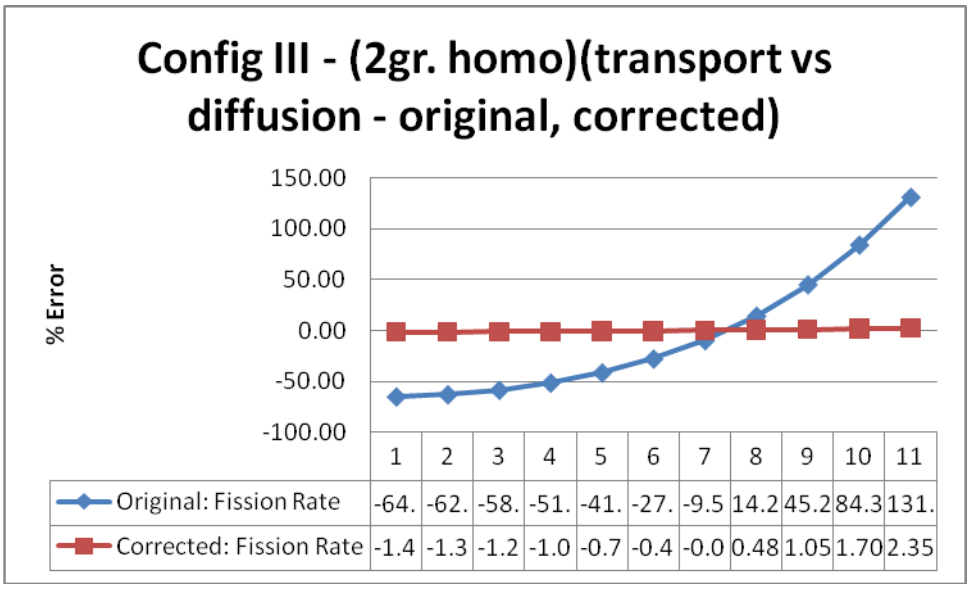

Figure 5.19 – Configuration III, Fission Rate, Error

5.4 Comparison of "exact" transport results with two-group homogenized node diffusion (old, new)

5.4.1 Configuration I

Fast Flux

Fast Flux	1	2	3	4	5	6
69 gr. Detailed Transport	2.90E+02	2.86E+02	2.78E+02	2.66E+02	2.50E+02	2.30E+02
2 gr. Homo. Diffusion	2.86E+02	2.82E+02	2.74E+02	2.62E+02	2.47E+02	2.28E+02
Corrected Diffusion	3.00E+02	2.95E+02	2.86E+02	2.72E+02	2.54E+02	2.31E+02

Fast Flux	7	8	9	10	11	12
69 gr. Detailed Transport	2.07E+02	1.81E+02	1.51E+02	1.19E+02	7.97E+01	5.81E+00
2 gr. Homo. Diffusion	2.07E+02	1.82E+02	1.55E+02	1.25E+02	8.63E+01	5.91E+00
Corrected Diffusion	2.05E+02	1.76E+02	1.44E+02	1.10E+02	6.74E+01	5.22E+00

Table 5.19 – Configuration I, Fast Flux

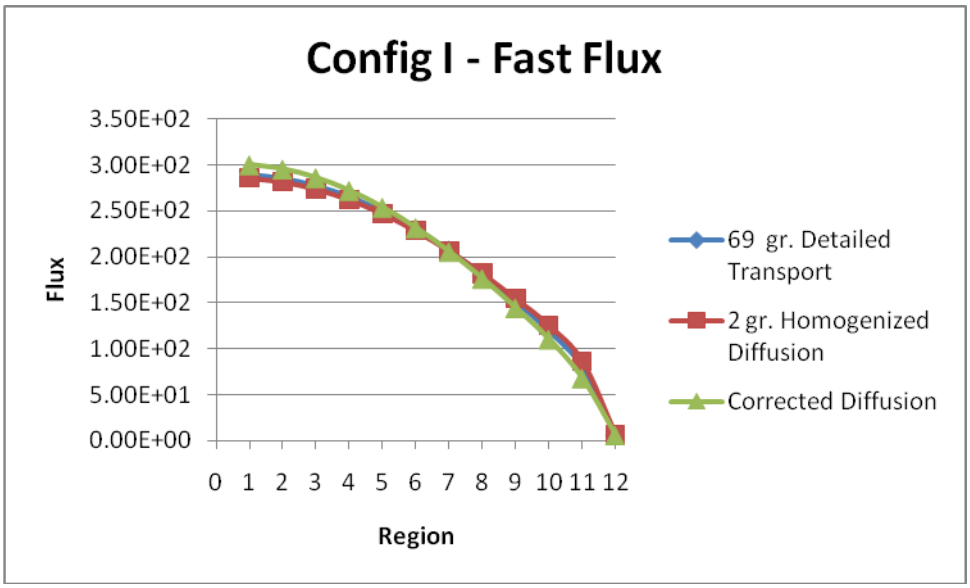

Figure 5.20 – Configuration I, Fast Flux

Error (%)

Nodes	1	2	3	4	5	6
Transport vs. Diffusion %	-1.37	-1.33	-1.36	-1.43	-1.17	-1.00
Transport vs. [C] Diffusion %	3.45	3.22	2.96	2.33	1.63	0.30

Nodes	7	8	9	10	11	12
Transport vs. Diffusion %	-0.06	0.74	2.48	4.79	8.22	1.72
Transport vs. [C] Diffusion %	-1.02	-2.58	-4.79	-7.78	-15.48	-10.16

Root Mean Square (%)

Original: 3.03 % | Corrected: 6.28 %

Table 5.20 – Configuration I, Fast Flux, Error

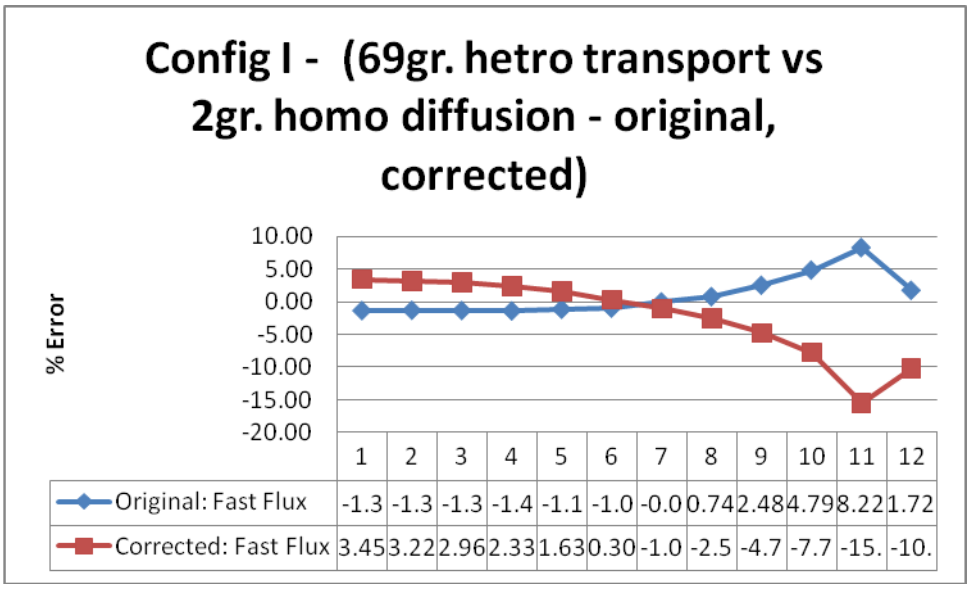

Figure 5.21 – Configuration I, Fast Flux, Error

Thermal Flux

Thermal Flux	1	2	3	4	5	6
69 gr. Detailed Transport	6.57E+02	6.47E+02	6.29E+02	6.02E+02	5.66E+02	5.22E+02
2 gr. Homo. Diffusion	6.33E+02	6.25E+02	6.07E+02	5.82E+02	5.48E+02	5.06E+02
Corrected Diffusion	6.64E+02	6.53E+02	6.32E+02	6.01E+02	5.61E+02	5.12E+02

Thermal Flux	7	8	9	10	11	12
69 gr. Detailed Transport	4.69E+02	4.09E+02	3.43E+02	2.70E+02	1.99E+02	1.15E+02
2 gr. Homo. Diffusion	4.58E+02	4.03E+02	3.42E+02	2.77E+02	2.19E+02	1.38E+02
Corrected Diffusion	4.54E+02	3.89E+02	3.19E+02	2.42E+02	1.70E+02	9.09E+01

Table 5.21 – Configuration I, Thermal Flux

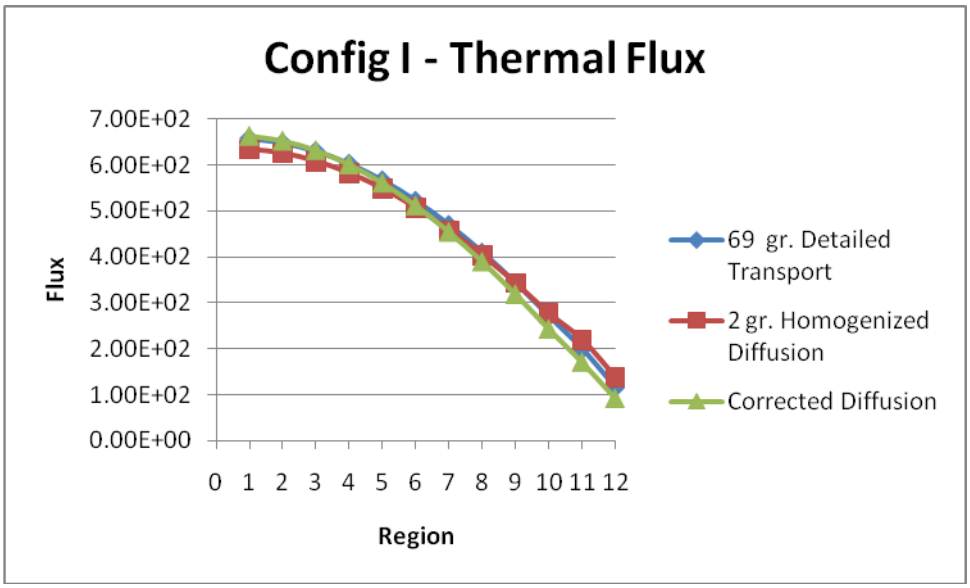

Figure 5.22 – Configuration I, Thermal Flux

Error (%)

Nodes	1	2	3	4	5	6
Transport vs. Diffusion %	-3.60	-3.46	-3.52	-3.32	-3.19	-3.00
Transport vs. [T] Diffusion %	1.12	0.87	0.45	-0.17	-0.89	-1.85

Nodes	7	8	9	10	11	12
Transport vs. Diffusion %	-2.38	-1.53	-0.18	2.49	9.97	19.88
Transport vs. [T] Diffusion %	-3.24	-4.95	-6.89	-10.46	-14.63	-21.04

Root Mean Square (%)

Original: 6.93 % | Corrected: 8.44 %

Table 5.22 – Configuration I, Thermal Flux, Error

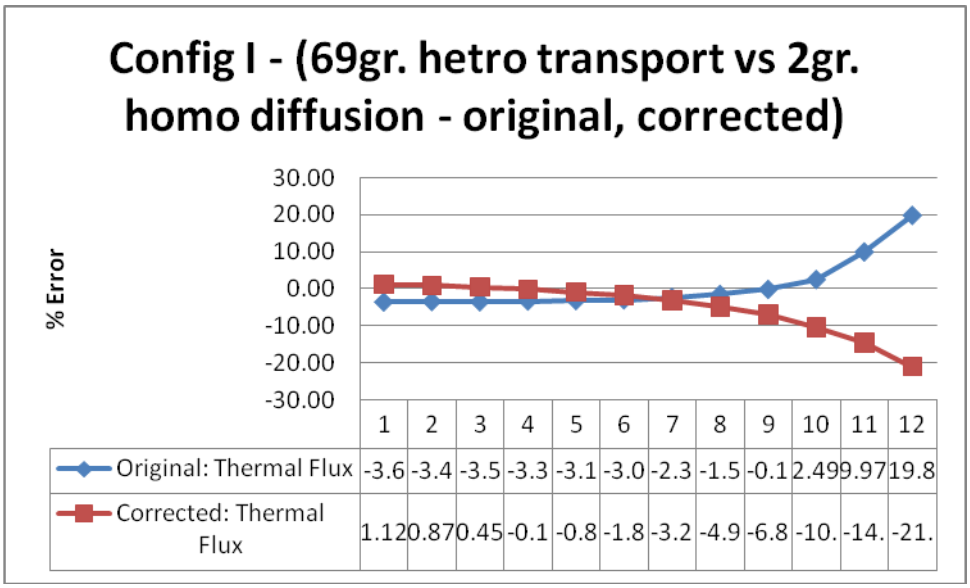

Figure 5.23 – Configuration I, Thermal Flux, Error

Fission Rate (s^{-1})

Fission Rate	1	2	3	4	5	6
69 gr. Detailed Transport	1.36E+00	1.34E+00	1.30E+00	1.25E+00	1.17E+00	1.08E+00
2 gr. Homo. Diffusion	1.34E+00	1.32E+00	1.29E+00	1.23E+00	1.16E+00	1.07E+00
Corrected Diffusion	1.41E+00	1.38E+00	1.34E+00	1.27E+00	1.19E+00	1.08E+00

Fission Rate	7	8	9	10	11
69 gr. Detailed Transport	9.71E-01	8.47E-01	7.09E-01	5.60E-01	4.11E-01
2 gr. Homo. Diffusion	9.68E-01	8.52E-01	7.24E-01	5.86E-01	4.61E-01
Corrected Diffusion	9.61E-01	8.24E-01	6.74E-01	5.13E-01	3.58E-01

Table 5.23 – Configuration I, Fission Rate

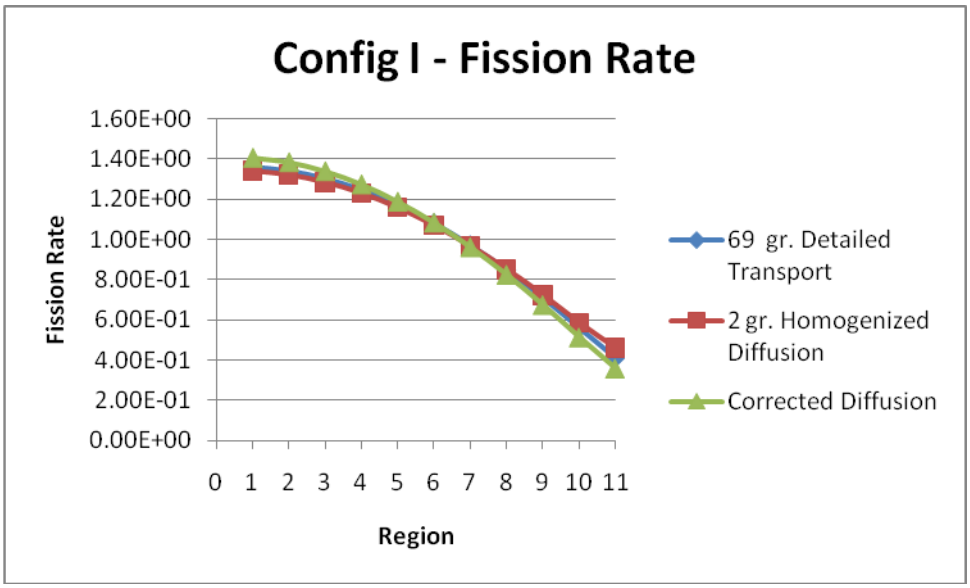

Figure 5.24 – Configuration I, Fission Rate

Error (%)

Nodes	1	2	3	4	5	6
Transport vs. Diffusion %	-1.37	-1.37	-1.36	-1.25	-1.11	-0.84
Transport vs. [C] Diffusion %	3.33	3.18	2.71	2.12	1.27	0.27

Nodes	7	8	9	10	11	
Transport vs. Diffusion %	-0.32	0.58	2.09	4.68	12.17	
Transport vs. [C] Diffusion %	-1.06	-2.73	-4.98	-8.32	-12.91	

Root Mean Square (%)

Original: 4.09 % | Corrected: 5.26 %

Table 5.24 – Configuration I, Fission Rate, Error

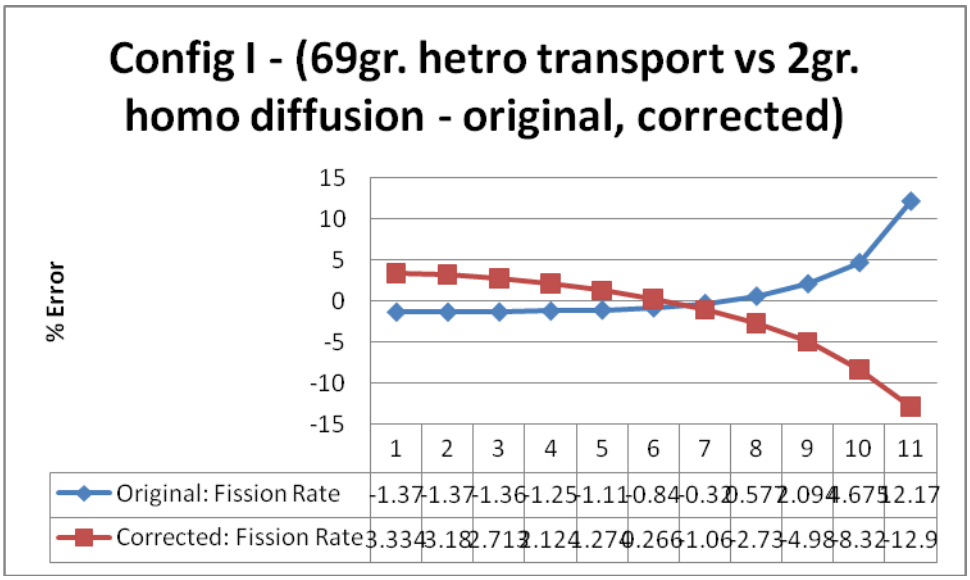

Figure 5.25– Configuration I, Fission Rate, Error

5.4.2 Configuration II

Fast Flux

Fast Flux	1	2	3	4	5	6
69 gr. Detailed Transport	8.70E+02	5.42E+02	3.83E+02	2.84E+02	2.11E+02	1.57E+02
2 gr. Homo. Diffusion	1.09E+03	6.28E+02	3.78E+02	2.40E+02	1.53E+02	9.68E+01
Corrected Diffusion	9.87E+02	5.98E+02	3.86E+02	2.65E+02	1.82E+02	1.24E+02

Fast Flux	7	8	9	10	11	12
69 gr. Detailed Transport	1.16E+02	8.57E+01	6.24E+01	4.43E+01	2.77E+01	1.99E+00
2 gr. Homo. Diffusion	6.15E+01	3.90E+01	2.48E+01	1.58E+01	9.27E+00	6.02E-01
Corrected Diffusion	8.48E+01	5.75E+01	3.85E+01	2.50E+01	1.38E+01	1.03E+00

Table 5.25 – Configuration II, Fast Flux

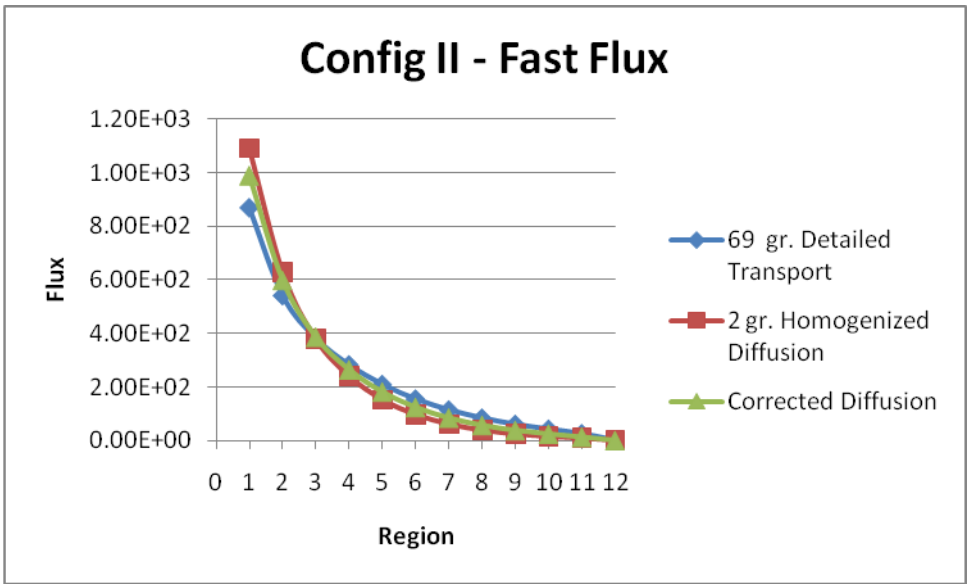

Figure 5.26 – Configuration II, Fast Flux

Error (%)

Nodes	1	2	3	4	5	6
Transport vs. Diffusion %	25.32	15.79	-1.34	-15.52	-27.47	-38.21
Transport vs. [C] Diffusion %	13.47	10.26	0.75	-6.72	-13.73	-20.85

Nodes	7	8	9	10	11	12
Transport vs. Diffusion %	-47.05	-54.47	-60.26	-64.31	-66.50	-69.73
Transport vs. [C] Diffusion %	-26.99	-32.88	-38.31	-43.52	-50.14	-48.20

Root Mean Square (%)

Original: 46.17 % | Corrected: 30.23 %

Table 5.26 – Configuration II, Fast Flux, Error

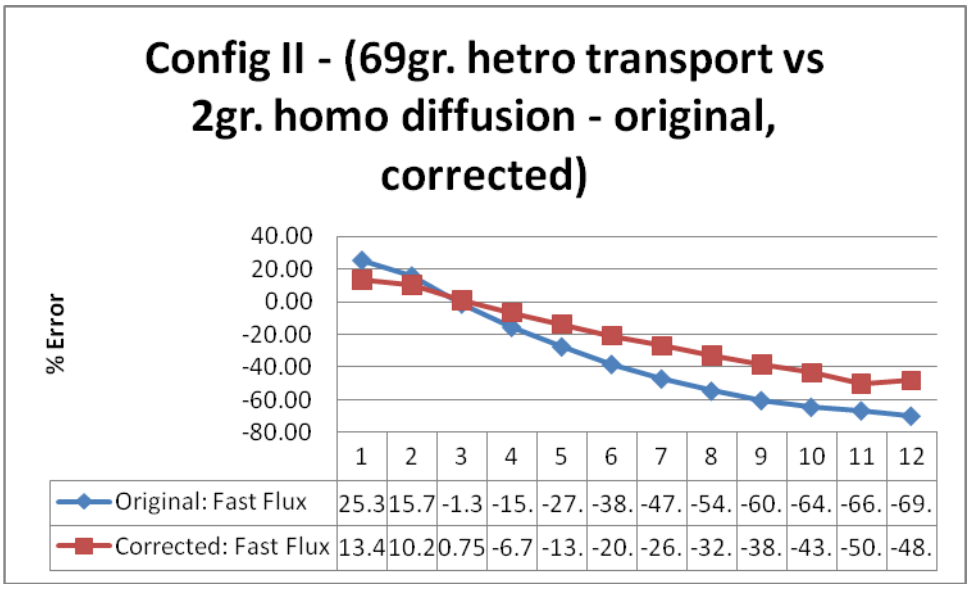

Figure 5.27 – Configuration II, Fast Flux, Error

Thermal Flux

Thermal Flux	1	2	3	4	5	6
69 gr. Detailed Transport	1.75E+03	1.50E+03	1.13E+03	8.40E+02	6.24E+02	4.63E+02
2 gr. Homo. Diffusion	2.18E+03	1.71E+03	1.11E+03	7.06E+02	4.48E+02	2.84E+02
Corrected Diffusion	1.97E+03	1.61E+03	1.13E+03	7.74E+02	5.30E+02	3.63E+02

Thermal Flux	7	8	9	10	11	12
69 gr. Detailed Transport	3.44E+02	2.53E+02	1.85E+02	1.31E+02	9.00E+01	4.86E+01
2 gr. Homo. Diffusion	1.80E+02	1.14E+02	7.27E+01	4.62E+01	3.08E+01	1.71E+01
Corrected Diffusion	2.48E+02	1.68E+02	1.12E+02	7.29E+01	4.56E+01	2.22E+01

Table 5.27 – Configuration II, Thermal Flux

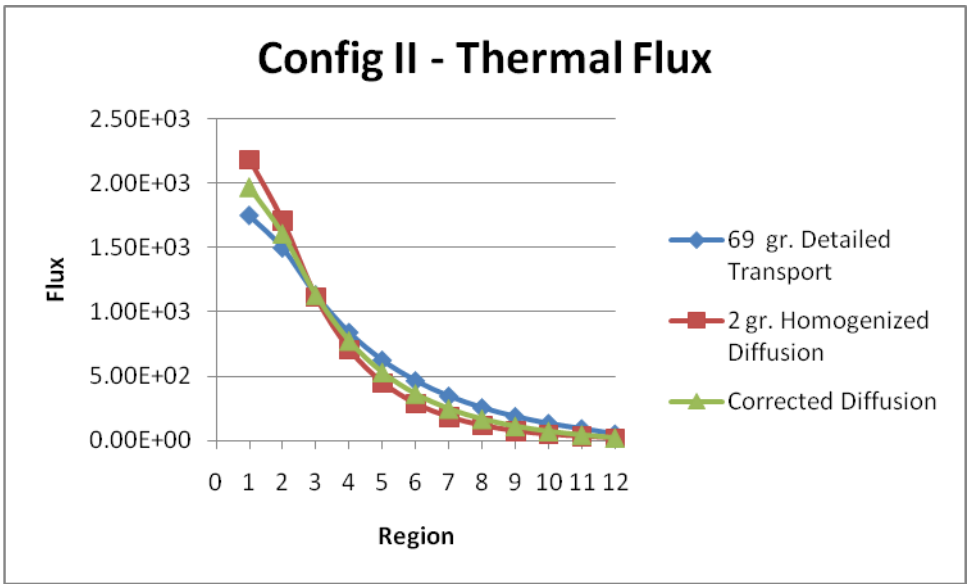

Figure 5.28 – Configuration II, Thermal Flux

Error (%)

Nodes	1	2	3	4	5	6
Transport vs. Diffusion %	24.45	14.10	-1.93	-15.96	-28.19	-38.70
Transport vs. [C] Diffusion %	12.46	7.43	-0.16	-7.87	-15.04	-21.65

Nodes	7	8	9	10	11	12
Transport vs. Diffusion %	-47.61	-55.02	-60.63	-64.76	-65.79	-64.82
Transport vs. [C] Diffusion %	-27.82	-33.72	-39.35	-44.39	-49.35	-54.33

Root Mean Square (%)

Original: 45.68 % | Corrected: 31.34 %

Table 5.28 – Configuration II, Thermal Flux, Error

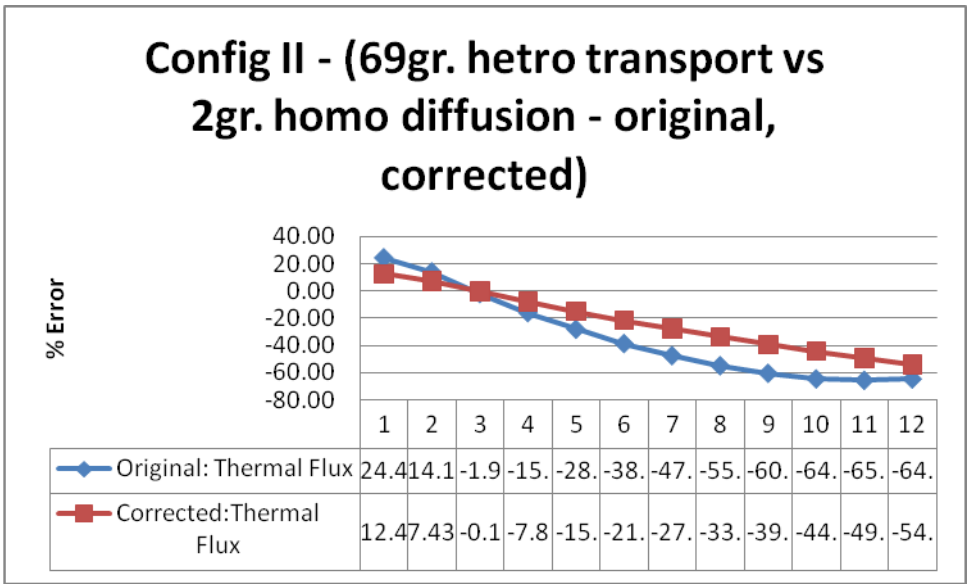

Figure 5.29 – Configuration II,Thermal Flux, Error

Fission Rate (s^{-1})

Fission Rate	1	2	3	4	5	6
69 gr. Detailed Transport	3.67E+00	1.98E+00	1.49E+00	1.11E+00	8.21E-01	6.10E-01
2 gr. Homo. Diffusion	4.68E+00	2.30E+00	1.49E+00	9.47E-01	6.01E-01	3.81E-01
Corrected Diffusion	4.22E+00	2.16E+00	1.52E+00	1.04E+00	7.12E-01	4.87E-01

Fission Rate	7	8	9	10	11
69 gr. Detailed Transport	4.52E-01	3.34E-01	2.43E-01	1.73E-01	1.18E-01
2 gr. Homo. Diffusion	2.42E-01	1.54E-01	9.76E-02	6.21E-02	4.11E-02
Corrected Diffusion	3.32E-01	2.25E-01	1.51E-01	9.79E-02	6.09E-02

Table 5.29 – Configuration II, Fission Rate

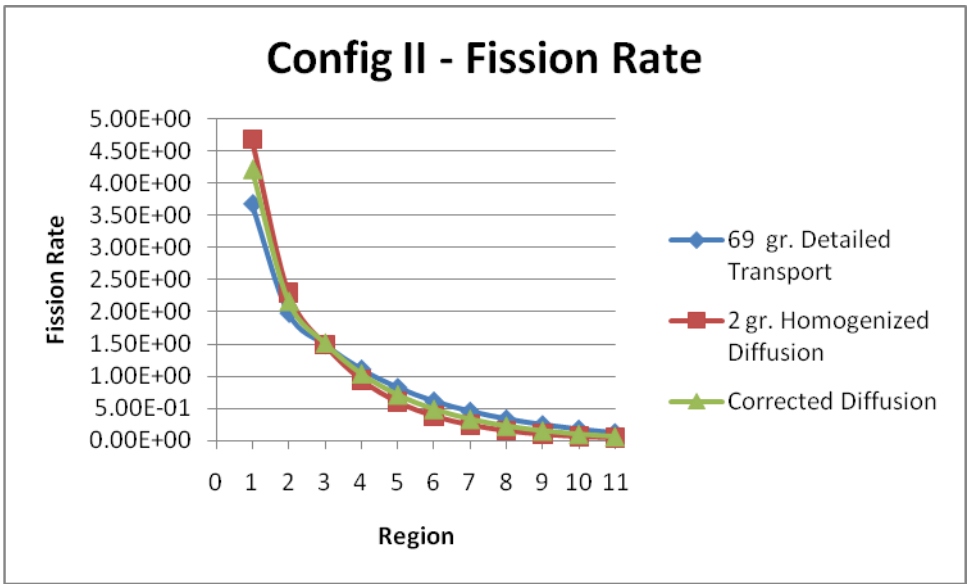

Figure 5.30 – Configuration II, Fission Rate

Error (%)

Nodes	1	2	3	4	5	6
Transport vs. Diffusion %	27.44	16.23	0.20	-14.39	-26.87	-37.52
Transport vs. [C] Diffusion %	14.71	9.41	1.74	-6.06	-13.32	-20.15

Nodes	7	8	9	10	11	
Transport vs. Diffusion %	-46.52	-53.97	-59.89	-64.05	-65.24	
Transport vs. [C] Diffusion %	-26.52	-32.46	-37.99	-43.27	-48.52	

Root Mean Square (%)

Original: 43.04 % | Corrected: 27.56 %

Table 5.30 – Configuration II, Fission Rate, Error

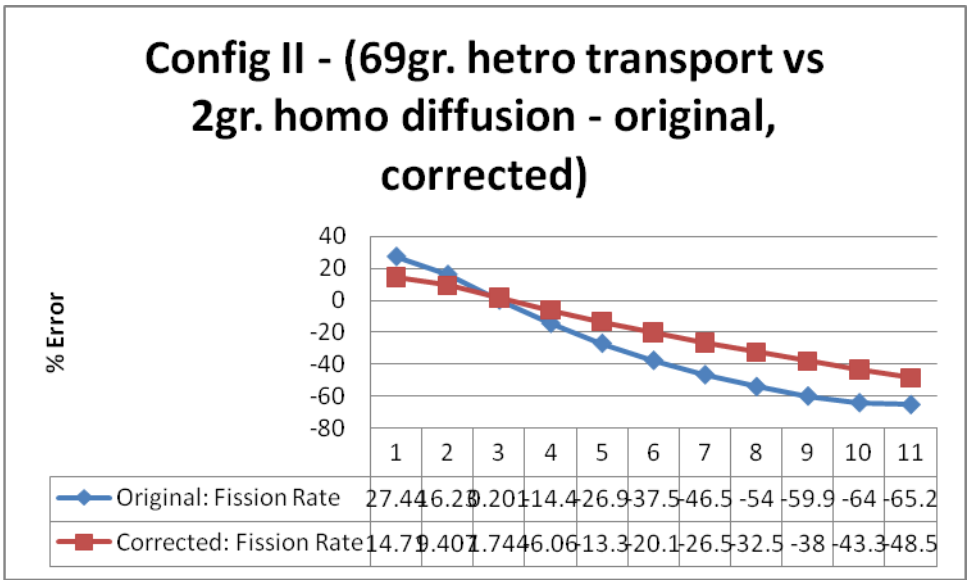

Figure 5.31 – Configuration II, Fission Rate, Error

5.4.3 Configuration III

Fast Flux

Fast Flux	1	2	3	4	5	6
69 gr. Detailed Transport	2.76E+02	2.75E+02	2.74E+02	2.73E+02	2.71E+02	2.69E+02
2 gr. Homo. Diffusion	9.18E+01	9.75E+01	1.09E+02	1.27E+02	1.54E+02	1.89E+02
Corrected Diffusion	2.63E+02	2.63E+02	2.64E+02	2.64E+02	2.64E+02	2.65E+02

Fast Flux	7	8	9	10	11	12
69 gr. Detailed Transport	2.65E+02	2.61E+02	2.56E+02	2.59E+02	2.78E+02	2.19E+01
2 gr. Homo. Diffusion	2.36E+02	2.98E+02	3.77E+02	5.04E+02	6.32E+02	5.03E+01
Corrected Diffusion	2.66E+02	2.66E+02	2.67E+02	2.81E+02	2.84E+02	2.53E+01

Table 5.31 – Configuration III, Fast Flux

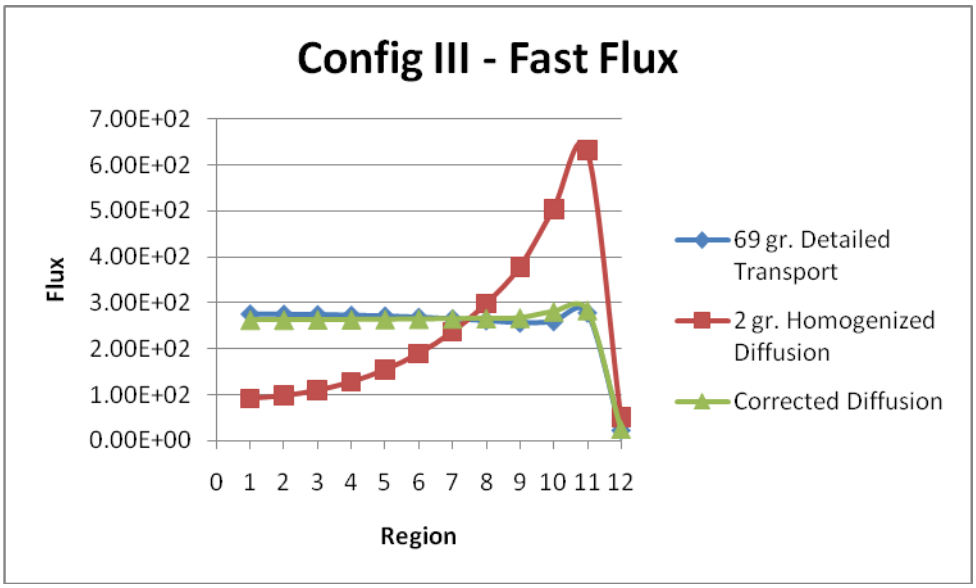

Figure 5.32 – Configuration III, Fast Flux

Error (%)

Nodes	1	2	3	4	5	6
Transport vs. Diffusion %	-66.70	-64.56	-60.26	-53.47	-43.19	-29.62
Transport vs. [C] Diffusion %	-4.59	-4.40	-3.75	-3.28	-2.61	-1.32

Nodes	7	8	9	10	11	12
Transport vs. Diffusion %	-11.04	14.08	47.05	94.24	127.18	129.20
Transport vs. [C] Diffusion %	0.27	1.83	4.14	8.30	2.09	15.28

Root Mean Square (%)

Original: 71.96 % | Corrected: 5.78 %

Table 5.32 – Configuration III, Fast Flux, Error

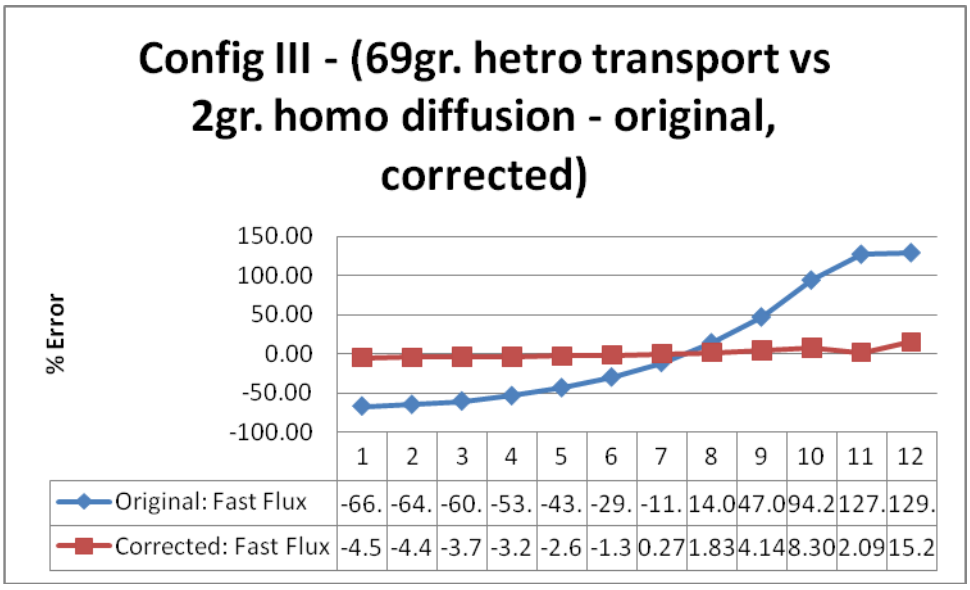

Figure 5.33 – Configuration III, Fast Flux, Error

Thermal Flux

Thermal Flux	1	2	3	4	5	6
69 gr. Detailed Transport	7.61E+02	7.60E+02	7.57E+02	7.54E+02	7.49E+02	7.42E+02
2 gr. Homo. Diffusion	2.53E+02	2.68E+02	3.00E+02	3.51E+02	4.23E+02	5.20E+02
Corrected Diffusion	7.10E+02	7.11E+02	7.11E+02	7.12E+02	7.14E+02	7.15E+02

Thermal Flux	7	8	9	10	11	12
69 gr. Detailed Transport	7.33E+02	7.21E+02	7.08E+02	6.82E+02	5.90E+02	3.73E+02
2 gr. Homo. Diffusion	6.50E+02	8.19E+02	1.04E+03	1.29E+03	1.41E+03	1.02E+03
Corrected Diffusion	7.17E+02	7.20E+02	7.22E+02	7.10E+02	6.22E+02	3.74E+02

Table 5.33 – Configuration III, Thermal Flux

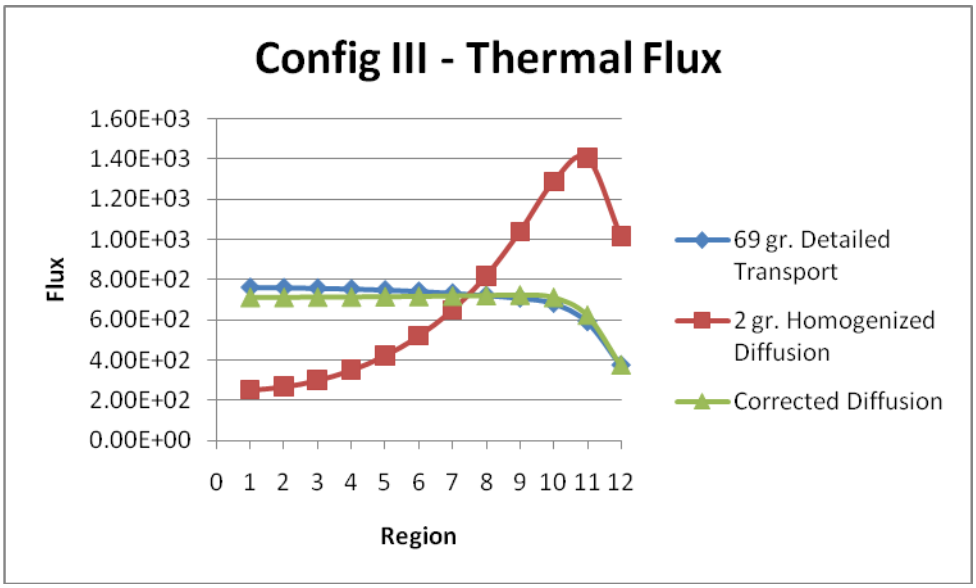

Figure 5.34 – Configuration III, Thermal Flux

Error (%)

Nodes	1	2	3	4	5	6
Transport vs. Diffusion %	-66.75	-64.72	-60.39	-53.43	-43.49	-29.88
Transport vs. [T] Diffusion %	-6.70	-6.41	-6.12	-5.53	-4.61	-3.58

Nodes	7	8	9	10	11	12
Transport vs. Diffusion %	-11.28	13.52	46.96	89.19	138.94	173.10
Transport vs. [T] Diffusion %	-2.13	-0.20	2.02	4.13	5.41	0.14

Root Mean Square (%)

Original: 80.45 % | Corrected: 4.50 %

Table 5.34 – Configuration III, Thermal Flux, Error

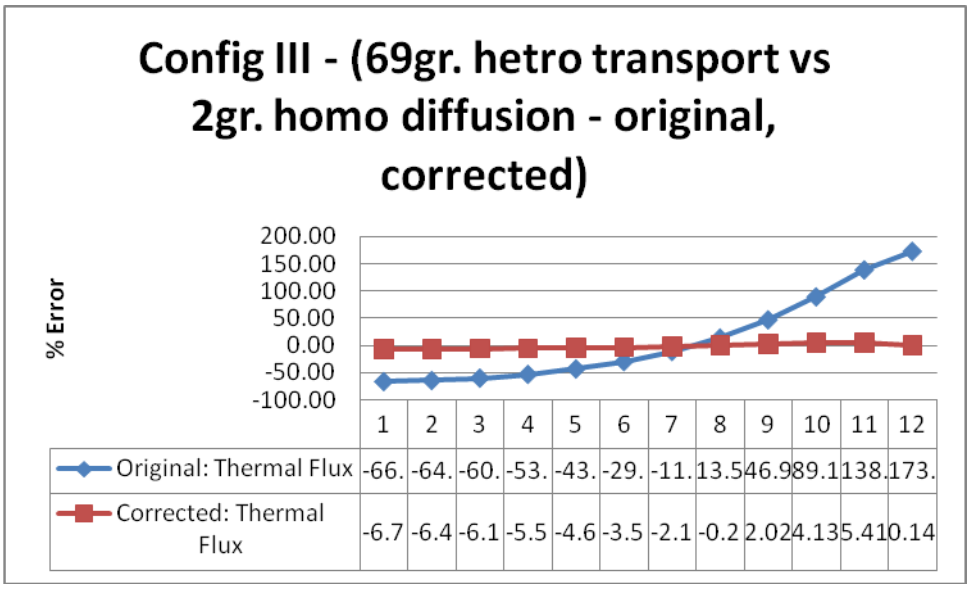

Figure 5.35 – Configuration III, Thermal Flux, Error

Fission Rate (s^{-1})

Fission Rate	1	2	3	4	5	6
69 gr. Detailed Transport	1.01E+00	1.01E+00	1.00E+00	9.99E-01	9.92E-01	9.83E-01
2 gr. Homo. Diffusion	3.42E-01	3.63E-01	4.06E-01	4.74E-01	5.71E-01	7.03E-01
Corrected Diffusion	9.61E-01	9.62E-01	9.63E-01	9.64E-01	9.66E-01	9.68E-01

Fission Rate	7	8	9	10	11
69 gr. Detailed Transport	9.71E-01	9.56E-01	9.38E-01	9.05E-01	1.24E+00
2 gr. Homo. Diffusion	8.78E-01	1.11E+00	1.40E+00	1.75E+00	3.01E+00
Corrected Diffusion	9.71E-01	9.74E-01	9.77E-01	9.64E-01	1.33E+00

Table 5.35 – Configuration III, Fission Rate

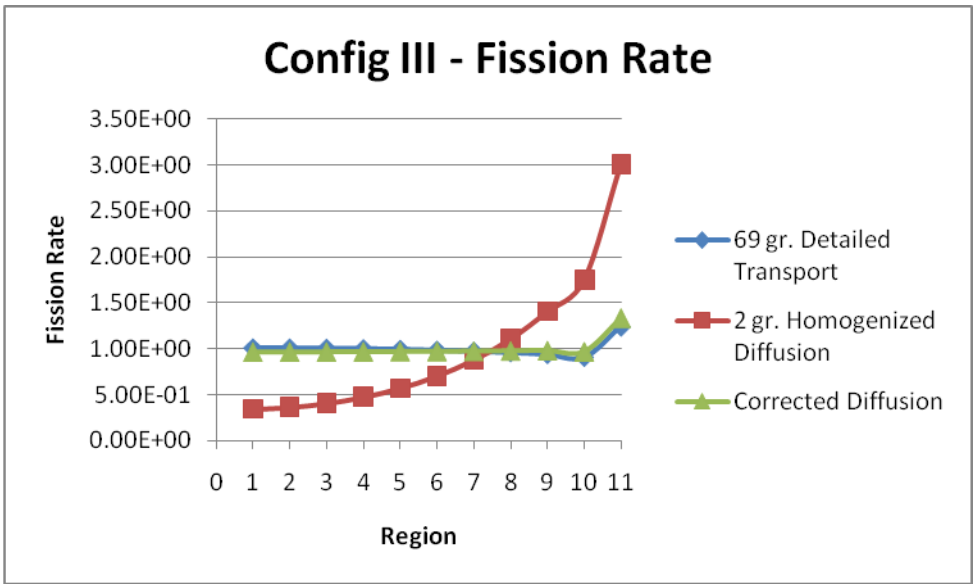

Figure 5.36 – Configuration III, Fission Rate

Error (%)

Nodes	1	2	3	4	5	6
Transport vs. Diffusion %	-66.12	-63.98	-59.56	-52.56	-42.44	-28.45
Transport vs. [T] Diffusion %	-4.66	-4.45	-4.06	-3.46	-2.62	-1.48

Nodes	7	8	9	10	11	
Transport vs. Diffusion %	-9.54	15.81	49.73	93.09	142.60	
Transport vs. [T] Diffusion %	-0.01	1.85	4.18	6.51	7.42	

Root Mean Square (%)

Original: 66.88 % | Corrected: 4.23 %

Table 5.36 – Configuration III, Fission Rate, Error

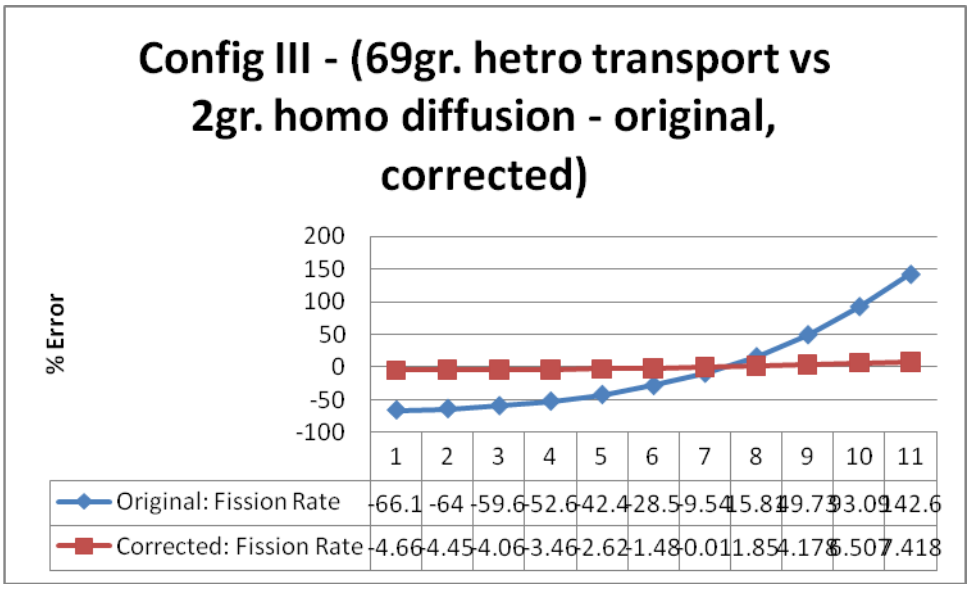

Figure 5.37 – Configuration III, Fission Rate, Error

6.0 INTERPRETATION OF RESULTS

"If your experiment needs statistics, you ought to have done a better experiment." (Ernest Rutherford)

6.1 Interpretation

Comparison between detailed-geometry many energy group transport, detailed-geometry few energy group transport, homogenized-geometry few energy group transport and few group homogenized-cell diffusion for a model involving a few CANDU lattice cells and reflector was performed. During this development it was found that detailed geometry transport and homogenized transport results are very close. Emphasis was shifted to comparing homogenized transport with homogenized-cell diffusion. While diffusion (before correcting) is a promising computational alternative to transport (Chapter 3), imperfections in the results necessitated improvements to the diffusion approximation.

Results show that diffusion theory is insufficiently accurate when using the traditional transport-derived diffusion coefficient $\frac{1}{3\Sigma_{tr}}$. It was shown that correcting the diffusion coefficients (Chapter 5), to enforce the transport-derived neutron balance leads to substantial gains(Refer Tables 5.1-5.36) in accuracy for simple one-dimensional models.

7.0 FUTURE WORK

These preliminary results need to be confirmed for two-dimensional models. Additionally, developing an interpretation of the difference between theoretical and empirical diffusion coefficients is desirable.

With ongoing developments in reactor technologies, it would be interesting to apply this technique to a future generation of Canadian reactors.

REFERENCES

[1] A. Hébert, Advanced Reactor Physics, Presses Internationales Polytechnique, 2009

[2] G. Marleau, Dragon Theory Manual, IGE-236R1, 2001

[3] J. R. Lamarsh, Introduction to Nuclear Reactor Theory, ANS, 2002

[4] A. Patel, E. Nichita, Empirical Diffusion Coefficients for Natural-Uranium CANDU Lattices, Transactions, American Nuclear Society, 2010